論文 / 著書情報
Article / Book Information

題目(和文)	
Title(English)	Hydrogen-Bonding Structure Studies of Solid Peptides by ^15^N and ^17^O NMR Spectroscopy
著者(和文)	黒木重樹
Author(English)	SHIGEKI KUROKI
出典(和文)	学位:博士(工学), 学位授与機関:東京工業大学, 報告番号:甲第2745号, 授与年月日:1994年3月26日, 学位の種別:課程博士, 審査員:
Citation(English)	Degree:Doctor of Engineering, Conferring organization: , Report number:甲第2745号, Conferred date:1994/3/26, Degree Type:Course doctor, Examiner:
学位種別(和文)	博士論文
Type(English)	Doctoral Thesis

Hydrogen-Bonding Structure Studies of Solid Peptides by ^{15}N and ^{17}O NMR Spectroscopy

A Dissertation

by Shigeki Kuroki

Department of Polymer Chemistry

Tokyo Institute of Technology

1993

Contents

Chapter 1
Introduction

The conformations of polypeptides and proteins arise from the positions of internal rotation, dihedral angle (ϕ,ψ) of the amino acid residues which make up the backbone chain, and many of these conformations are ruled very improbable or impossible by steric factors. In addition, many conformations bring parts of the chain into favorable contact with one another. These favorable contacts, contributing on the order of several kilocalories of negative free energy, are called noncovalent bonds. One of the noncovalent interactions in polypeptides and proteins is "*hydrogen bond*", which plays very important role in forming the three dimensional structure. The α–helix and β-sheet forms provide popular illustrations of this principle. The hydrogen bond is an intermediate intra- or inter-molecular interaction between an electron-deficient hydrogen atom and an oxygen atom with high electron density. The nature of hydrogen bond has been widely studied by spectroscopic methods[1-12] such as IR, Raman and NMR spectroscopies and crystallographic methods[13-16] such as X-ray and neutron diffractions, and theoretical approaches[17-19]. However, many aspects of the hydrogen bonded structure are, as yet, imperfectly understood. For this, it is needed some new approach to clarify the nature of hydrogen bond. Solid-state-high-resolution NMR spectroscopy has been one of the most powerful tools for obtaining useful information about details of the structure and electronic state of hydrogen-bonding .

In biological molecules, the nuclei which can be observed by NMR are ^{1}H, ^{2}H, ^{13}C, ^{17}O, ^{14}N, ^{15}N, etc. ^{1}H(spin number I=1/2) is the most popular nucleus for solution-state NMR. But, in solids, there are

strong homonuclear dipole-dipole interactions between ^{1}H nuclei because of its large abundance, it is difficult to obtain high-resolution NMR spectra without using CRAMPS(combined rotation and multiple-pulse spectroscopy) method. $^{2}H(I=1)$ spectrum is useful to study molecular dynamics, but it is not suitable to study molecular structure. $^{14}N(I=1)$ resonance line is broaden by quadruple interactions, and at present it is difficult to obtain high-resolution ^{14}N spectrum. On the other hand, $^{13}C(I=1/2)$ natural abundance is 1.1 % so that there is few homonuclear dipole-dipole interactions, and we can obtain high-resolution ^{13}C NMR spectrum by combination of CP(cross-polarization) method, high power proton decoupling and magic angle spinning. As has been revealed in a series of ^{13}C CP/MAS NMR studies of synthetic and biological polypeptides, every amino acid residue in solid polypeptides has characteristic ^{13}C chemical shift values. Since this shift varies, depending on the conformation such as α-helix, β-sheet and 3_1-helix forms, it can be regard as an intrinsic probe of the secondary structure of peptides[20-29]. It was also clear from the experimental and theoretical studies that such a chemical shift change is not caused by the specific peptide sequence, but by the local conformation and intermolecular interactions. This implies that the ^{13}C chemical shift in the solid state grossly depends on very confined electronic structure around the nucleus under consideration. Ando et al[30]. have also measured ^{13}C CP/MAS NMR spectra of some oligopeptides containing glycine residues in the solid state, in order to obtain information about the relationship between the carbonyl carbon chemical shift and hydrogen bond length. It was found that the ^{13}C signals of the carbonyl carbons in the >C=O···H-N< type hydrogen bond form are linearly deshielded with a decrease in the hydrogen bond length but those in the $>C=O\cdots H\text{-}N^{+}<$ type hydrogen bond form are linearly

shielded with a decrease in the hydrogen bond length. They justified such experimental finding by quantum chemical calculations of ^{13}C shieldings for model compounds. In this way, solid-state ^{13}C NMR spectroscopy has offered some successful results to peptides and proteins structural study.

In this doctoral work, I am concerned with two kinds of NMR observable nuclei such as ^{15}N and ^{17}O. Though these nuclei are associated with hydrogen-bonding structure in peptides and proteins. Nevertheless, they have been significantly used for investigation of hydrogen-bonding structure in peptides and polypeptides.

Since ^{15}N(I=1/2) nucleus is very low natural abundance to be 0.37% and have very low gyromagnetic ratio : $\gamma = -2.7112 \times 10^{-7} T^{-1} s^{-1}$, it has weak sensitivity. But, ^{15}N NMR spectroscopy has demonstrated to provide useful information about structure and dynamics of synthetic polypeptides and proteins in solution[31-36]. It has been reported that ^{15}N nucleus is highly sensitive to structural and conformational changes of the molecules. Most recently, high-resolution solid-state ^{15}N NMR has been developed by means of the CP/MAS method, and has been applied to the conformational characterization of polypeptides and oligopeptides. It has been demonstrated that the ^{15}N chemical shifts in the peptide backbone of a variety of polypeptides exhibit a significant conformation-dependent change[37-39], the α_R-helix form(97.0-99.2 ppm) appears more upfield than that of the β-sheet form(99.5-107.0 ppm). On the other hand, if the exact principal values of ^{15}N chemical shift tensors(σ_{11}, σ_{22} and σ_{33}) are available, it provides more detailed information about the structure of polypeptides and oligopeptides, which are closely associated with electronic state compared with the isotropic chemical shift value ($\sigma_{iso} = (\sigma_{11}+\sigma_{22}+\sigma_{33})/3$) which is determined by MAS. Because a nitrogen

atom possesses lone-pair electrons, it is of interest to examine the effects of the lone-pair electrons on the isotropic ^{15}N chemical shift (σ_{iso}) and the principal values of the ^{15}N chemical shift tensors (σ_{11}, σ_{22} and σ_{33}).

On the other hand, the oxygen atom is one of important atoms constituting hydrogen-bonding structure in peptides and polypeptides. Nevertheless, solid-state ^{17}O NMR study for peptides and polypeptides has never been carried out. This is due to very weak sensitivity for solid-state ^{17}O NMR measurement which comes from two following reasons. One is that ^{17}O nucleus is very low natural abundance to be 0.037 %. Another is that ^{17}O nucleus because of I=5/2 is quadrupolar nucleus, and so ^{17}O signal is broaden by nuclear quadrupolar effects in solids. On the other hand, solution-state ^{17}O NMR spectroscopy has been successfully employed to elucidate a number of structural problems in organic chemistry[40-43], because ^{17}O signal becomes very sharp due to the vanishment of quadrupolar interaction by isotropic fast reorientation in solution. For example, as the oxygen atom is directly associated with the formation of hydrogen bond, the formation of hydrogen bond for the carbonyl group in various compounds often results in large upfield shifts of the carbonyl ^{17}O NMR signal[44,45]. From these experimental findings, the ^{17}O NMR chemical shift in solids can be expected to establish as a means for investigating the hydrogen-bonding structure. Another NMR parameter besides chemical shift obtained by ^{17}O NMR is the nuclear quadrupolar coupling constant. The nuclear quadrupolar coupling constant comes from the interaction of the nuclear quadrupolar moment eQ with the electric field gradient eq at the site of the nucleus. The field gradients (which involve nuclear and electric contributions) and the corresponding asymmetry parameters η_Q are sensitive to the electric

charge distributions in the vicinity of the nucleus. Several semi-empirical MO(molecular orbital) method has been used for calculating the nuclear quadrupolar coupling constant and for relating it to structure features and electronic distribution[46-52]. The nuclear quadrupolar coupling constant also seems to be useful to investigation of the hydrogen-bonding structure.

From such situations, it can be expected that solid-state ^{15}N and ^{17}O NMR provides deep insight for understanding hydrogen-bonding structure in solid peptides and polypeptides.

This dissertation goes as follows:

In Chapter 2, in order to obtain and accumulate knowledge of the hydrogen-bonding in peptides, ^{15}N CP/MAS NMR spectra of the glycylglycine(GlyGly) oligopeptides are measured in the solid state. To clarify the origin of the relationship between the ^{15}N chemical shift and the manner of the hydrogen bond, the ^{15}N shielding and tensor components of the glycine amide nitrogens are calculated by employing quantum-chemical methods.

In Chapter 3, as a continuation of ^{15}N NMR study of the hydrogen bond in oligopeptides, I attempt to measure isotropic ^{15}N chemical shifts and individual components of ^{15}N chemical shift tensors of the glycine(Gly) residue in a variety of oligopeptides with the tert-butyloxycarbonyl(Boc) group in the terminal, and to clarify the relationship between hydrogen bond length and isotropic chemical shifts and individual components of chemical shift tensors. The obtained results will be discussed in comparison with Chapter 2 about hydrogen bond. Further, to do a deep insight into the hydrogen bond, the ^{15}N chemical shift and tensor components of the glycine amide nitrogens are calculated by employing quantum chemical method.

In Chapter 4, high-resolution ^{17}O NMR spectra of solid polyglycine(PG) I, PG II, glycylglycine(GlyGly) and glycylglycine nitrate (GlyGly•HNO_3) are measured and three kinds of NMR parameters such as chemical shift(δ), quadrupolar coupling constant(e^2qQ/h) and asymmetric parameter(η_Q) are obtained by spectrum simulation, and the relationship between the hydrogen-bonding structure and these NMR parameters is discussed. To do deep discussion on such relationship, quantum chemical calculations are carried out.

In Chapter 5, quadrupolar coupling constant(e^2qQ/h) and chemical shielding versus the hydrogen-bonding structure were calculated by employing FPT-MNDO-PM3 method. Compared with experimental results obtained in the preceding chapter, the relationship between these NMR parameters and the hydrogen-bonding structure is deeply discussed by employing quantum chemical method.

In Chapter 6, the concluding remarks of the present investigation are described.

References

1) R.D.B.Frazer, *The Application of Infra-Red Spectroscopy to Biological Problems*, Ph.D. Thesis, Univ.of London.

2) W.E.Seeds, *Nature and Structure of Collagen* (J.T.Randall, ed.), Butterworths, London, p.250.

3) G.N.Ramachandran, V.Sasisekharan and Y.T.Thathachari, *Collagen* (N.Ramanathan, ed.), Wiley(Interscience), New York, p.81.

4) G.N.Ramachandran, C.Ramaceishnan and V.Sasisekharan, *J.Mol.Biol.*, **7** (1963) 95.

5) R.M.Badger and A.D.E.Pullin, *J.Chem.Phys.*, **22** (1954) 1142.

6) T.Miyazawa, *J.Mol.Spectrosc.*, **4** (1960) 155.

7) T.Miyazawa, *J.Mol.Spectrosc.*, **4** (1960) 168.

8) G.N.Ramachandran, V.Sasisekharan and Y.T.Thathachari, *Collagen* (N.Ramanathan, ed.), Wiley(Interscience), New York, p.147.

9) G.N.Ramachandran, *Int.Rev.Connect.Tissue Res.*, **1** (1963) 127.

10) G.N.Ramachandran, *Aspects of Protein Structure* (G.N.Ramachandran, ed.), Academic Press, New York 1963, p.39.

11) G.N.Ramachandran, C.Ramaceishnan and C.M.Venkatachalam, *Conformation of Biopolymers* (G.N.Ramachandran, ed.), **2**,Academic Press, New York, p.429.

12) A.Elliott, *Aspects of Protein Structure*(G.N.Ramachandran, ed.), Academic Press, New York, p.54.

13) R.Taylor and O.Kennard, *Acc.Chem.Res.*, **17**(1984) 320.

14) R.Taylor, O.Kennard and W.Versichel, *J.Am.Chem.Soc.*, **105** (1983) 5761

15) R.Taylor, O.Kennard and W.Versichel, *J.Am.Chem.Soc.*, **106**(1984) 224.

16) R.Taylor, O.Kennard and W.Versichel, *Acta Cryst.*, **B40** (1984) 280.

17) P.A.Kollman and L.C.Allen, *Chemical Reviews*, **72** (1972) 283.

18) K.Morokuma, *Accounts of Chemical Research*, **10** (1977) 294.

19) H.Umeyama and K.Morokuma, *J.Am.Chem.Soc.*, **99** (1977) 1316.

20) T.Taki, S.Yamashita, M.Satoh, A.Shibata, T.Yamashita, R.Tabeta and H.Saitô, *Chem.Lett.*, (1981) 1803.

21) H.Saitô, R.Tabeta, A.Shoji, T.Ozaki and I.Ando, *Macromolecules*, **16** (1983) 1050.

22) H.Saitô, R.Tabeta, I.Ando, T.Ozaki and A.Shoji, *Chem.Lett*, (1983) 1437.

23) H.Saitô, Y.Iwanaga, R.Tabeta, and T.Asakura, *Chem.Lett*, (1983) 427.
24) H.Saitô, R.Tabeta, T.Asakura, Y.Iwanaga, A.Shoji, T.Ozaki and I.Ando, *Macromolecules*, **17** (1984) 1405.
25) A.Shoji, T.Ozaki, H.Saitô, R.Tabeta and I.Ando, *Macromolecules*, **17** (1984) 1472.
26) H.Saitô, R.Tabeta, A.Shoji, T.Ozaki, I.Ando and T.Miyata, *Biopolymers*, **23** (1984) 2279.
27) H.R.Kricheldorf, M.Mutter, F.Mazer, D.Müller and D.Forster, *Biopolymers*, **22** (1983) 1357.
28) H.R.Kricheldorf and D.Müller, *Macromolecules*, **16**(1983) 615.
29) H.R.Kricheldorf and D.Müller and K.Ziegler, *Polymer Bull.*, **9** (1983) 284.
30) S.Ando, I.Ando, A.Shoji and T.Ozaki, *J.Am.Chem.Soc.*, **110** (1988) 3380.
31) G.C.Levy and R.L.Lichter, *Nitrogen-15 Nuclear Magnetic Resonance Spectroscopy,* Wiley, New York, 1979, Chap. 6.
32) K.Wüthrich, *Nuclear Magnetic Resonance in Biological Reserch: Peptides and Protains*, North-Holland, Amsterdam, 1976, Chap. 7.
33) G.A.Webb and M.Witanowski, *Proc. Indian Acad. Sci. (Chem. Sci.),* (1985) 241.
34) G.E.Hawkes, E.W.Randall and C.H.Bradley, *Nature,* **257** (1975) 767.
35) W.W.Bachovchin and J.D.Roberts, *J.Am.Chem.Soc.*, **100** (1978) 8041.
36) K.L.Williamson, L.G.Pease and J.D.Roberts, *J.Am.Chem.Soc.*, **101** (1979) 714.
37) A.Shoji, T.Ozaki,T.Fujito, K.Deguchi and I.Ando, *Macromolecules*, **20** (1987) 2441.
38) A.Shoji, T.Ozaki,T.Fujito, K.Deguchi, S.Ando and I.Ando, *Macromolecules*, **22** (1989) 2860.
39) A.Shoji, T.Ozaki,T.Fujito, K.Deguchi, S.Ando and I.Ando,*J.Am.Chem.Soc.*, **112** (1990) 4693.
40) D.W.Boykin ed., *^{17}O NMR Spectroscopy in Organic Chemistry*, CRC Press, Boca Raton, FL, 1991.
41) A.L.Baumstark and D.W.Boykin, *^{17}O NMR Spectroscopy: Applications to Structual problems in Organic Chmistry, in Advances in*

Oxygenated Powcesses, **Vol.III**, A.L.Baumstark ed., JAI Press, 1991, p.141.
42) W.G.Klemperer, *The Multinuclear Approach to NMR Spectroscopy*, J.B.Lambert and F.G.Riddell, Dordrecht, Holland, 1983, p.245.
43) J.P.Kintzinger, in *Newly Accessible Nuclei*, **Vol.2**, P.Laszlo, ed., Academic Press, New York, 1983, p.79.
44) D.W.Boykin and A.L.Baumstark, *New Journal of Chmistry*, **16** (1992) 357.
45) D.W.Boykin and A.Kumar, *J.Heterocyclic Chem.*, **29** (1992) 1.
46) E.A.C.Lucken, *Neuclear Quadrupole Coupling Constants.* Academic press, London-New York, 1969.
47) C.T.O'Konski, *Determination of Organic Structures by Physical Methods*, **Vol.2**, Chap.11. Academic Press, New York, 1962.
48) E.Scrocco, *Advances Chem. Physics,* **5** (1963) 318.
49) C.H.Townes and B.P.Dailey, *J.Chem.Physics.* **17** (1949) 782.
50) F.A.Cotton and C.B.Harris, *Proc.Nat.Acad.Sci.USA*, **56** (1966) 12.
51) E.A.C.Lucken, *Trans.Faraday Soc.*, **57** (1961) 729.
52) J.M.Sichel and M.A.Whitehead, *Thoret.Chim.Acta (Berl)*, **11** (1968) 263.

Chapter 2

Hydrogen-Bonding Structure and ^{15}N NMR Chemical Shifts of Peptides Containing Gly Residue in the Solid State I. XGlyGly

2.1 Introduction

Recently, high-resolution ^{15}N NMR spectroscopy has been increasingly applied to the investigation of peptides, polypeptides and proteins in the solid state[1-12]. Shoji et al.[13] demonstrated that the isotropic ^{15}N chemical shifts of a number of homopolypeptides in the solid state, as determined by the cross polarization / magic angle spinning (CP/MAS) NMR method are significantly displaced as much as 1.2-10.0 ppm, according to their particular conformations such as the α-helix and β-sheet forms[13]. Such a large chemical shift difference may come from changes in the hydrogen bond length and angles by through change in the dihedral angles (θ,ϕ).

Ando et al.[14] have also measured ^{13}C CP/MAS NMR spectra of some oligopeptides containing glycine residues in the solid state, in order to obtain information about the relationship between the carbonyl carbon chemical shift and hydrogen bond length. It was found that the ^{13}C signals of the carbonyl carbons in the >C=O···H-N< type hydrogen bond form are linearly deshielded with a decrease in the hydrogen bond length but those in the >C=O···H-N^{+}< type hydrogen bond form are linearly shielded with a decrease in the hydrogen bond length. Further, they performed quantum chemical calculations of ^{13}C shieldings for model compounds taking into account the hydrogen bond and conformational effects which explain reasonably the experimental results[14]. In this work, in order to obtain and accumulate further knowledge of the hydrogen bonding in peptides, I attempt to measure ^{15}N CP/MAS NMR

spectra of oligopeptides containing glycine residues in the solid state and to clarify the origin of the relationship between the ^{15}N chemical shift and the manner of the hydrogen bond the ^{15}N shielding tensor components of the glycine amide nitrogens were carried out by employing quantum-chemical methods.

2.2 Experimental

Materials: A series of oligopeptides containing glycine residues, except for sarcosylglycylglycine(Sar-Gly-Gly), were purchased from Sigma Co. and were recrystallized according to the same procedures as those used in the X-ray diffraction studies on them. Sar-Gly-Gly was synthesized by stepwise elongation of N-hydroxysuccinnimide active esters and amino acids[15]. The N-terminal of the active ester was protected by o-nitrophenylsukfenyl(Nps-) group. This sample was purified and recrystallized from aqueous solution. Glycylglycine nitrate (Gly-Gly•HNO_3) was obtained by slow evaporation from an equimolar mixture of glycylglycine and nitric acid in water. Glycylglycine monohydrochloride monohydrate (Gly-Gly•HCl•H_2O) was obtained by slow evaporation from an equimolar mixture of glycylglycine and hydrogen chloride in water.

Measurements: ^{15}N CP/MAS NMR spectra were recorded at room temperature and 27.3MHz with a JEOL GSX-270 NMR spectrometer equipped with a CP/MAS accessory. Field strength of the ^{1}H decoupling was 1.2mT. The contact time was 5 ms, and repetition time was 10s. Spectral width and data points were 20kHz and 8k, respectively. Sample was placed in a cylindrical rotor and spun at 4 -5kHz. Spectrum was usually accumulated 100 - 600 times to achieve a

reasonable signal-to-noise ratio. ^{15}N chemical shifts were calibrated indirectly through external glycine-^{15}N(δ=11.59 ppm; line width =17Hz) relative to saturated $^{15}NH_4NO_3$(δ=0 ppm) solution in H_2O.

Theoretical calculation: The finite perturbation theory(FPT) within the INDO framework for calculating the ^{15}N shieldings was used. The FPT-INDO theory has the advantage of permitting the calculation of the paramagnetic term without requiring explicit wavefunctions of the excited states and the one-electron excitation energies, which are difficult to obtain with high accuracy by the usual semi-empirical MO approximations. This approach reproduces reasonably the experimental ^{13}C chemical shifts of L-alanine residues in peptides[16]. According to the FPT-INDO framework[17-19], $\sigma^d_{\alpha\beta}(A)$ (diamagnetic term) and $\sigma^p_{\alpha\beta}(A)$ (paramagnetic term) are expressed by

$$\sigma^d_{\alpha\beta} = \frac{e^2}{2mc^2}\sum_\mu\sum_\nu P_{\mu\nu}(0)\left\langle x_\mu \left| \frac{r_\nu r_A \delta_{\alpha\beta} - r_{\nu A} r_{A\beta}}{|r_A|^3} \right| x_\nu \right\rangle \qquad (2.1)$$

$$\sigma^p_{\alpha\beta} = -\frac{eh}{mc} i \sum_\mu\sum_\nu \left(\frac{\partial P_{\mu\nu}(B_\alpha)}{\partial B_\alpha} \right)_{B=0} \left\langle x_\mu \left| \frac{(r_A \times \nabla)_\beta}{|r_A|^3} \right| x_\nu \right\rangle \qquad (2.2)$$

$$\alpha,\beta = x,y,z$$

where the gauge origin of the vector potential is set at the position of nucleus A. The vectors r_ν and r_A are the position vectors of electron considered from the nucleus of the atom containing the atomic orbital (AO)χ_ν and from the nucleus A, respectively. $P_{\mu\nu}(B)$ and $P_{\mu\nu}(0)$ are the elements of the density matrix with and without the perturbation due to the magnetic field, **B**, respectively. The ^{15}N shielding calculation was carried out by similar procedure to that reported previously for a ^{13}C shielding calculation[13]. In the calculation, N-acetyl-N'-methylglycine amide as a model compound was adopted. The bond lengths and bond angles proposed by Momany et al.[20] were used. A HITAC M780H

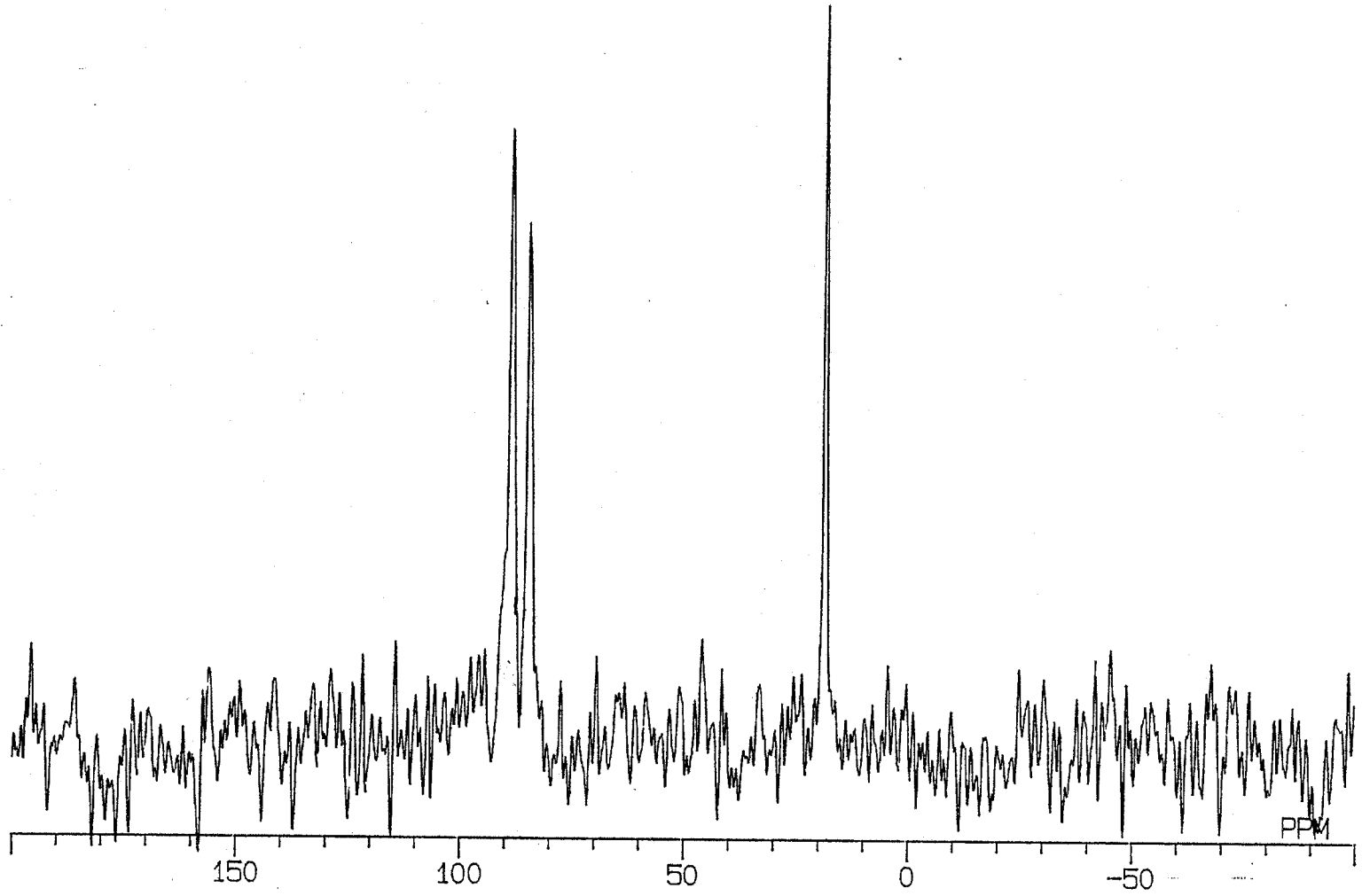

Fig.2.1 A typical 27.3 MHz ^{15}N CP/MAS NMR spectrum of L-alanylglycylglycine in the solid state.

Table 2.1 ^{15}N chemical shift of glycine residue amide nitrogens for oigopeptides containing glycine residue as determined by ^{15}N CP/MAS NMR (from $^{15}NH_4NO_3$) and their geometrical parameters of glycine residue amide nitrogen of Gly-Gly* peptides.

Sample	^{15}N chemical shift	Dihedral angle / degree		Hydrogen bond length and angle				ref.
				N···O	H···O	N-H	N-H···O	
	δ / ppm	φ	ψ	length(Å)	length(Å)	length(Å)	angle(deg.)	
GlyGly	95.3	157.1	10.7	2.94	1.97	1.02	158	23
GlyGly•HNO_3	89.4	165.6	176.9	3.12	2.38	0.76	165	24
GlyGly•H_2O•HCl	91.0	-79.6	3.8	3.30[a)]	2.30	0.79	162	25
AlaGlyGly	88.3	170.9	175.2	3.00	2.19	0.84	160	26
ValGlyGly	94.4	-146.6	-4.3	3.05	2.19	0.93	152	27
ProGlyGly	89.4	-110.5	175.1	2.89	2.07	0.85	165	28
SarGlyGly	89.0	-85.4	-177.5	3.06	2.23	0.85	167	29
TyrGlyGly	92.3	-103.9	-152.6	2.88	2.13	0.86	144	30
BocGlyGlyGlyOBzl	92.8[b)]	-77.8	-178.4	2.92	2.10	0.92	157	31

a) The Glycine Residue participates in H···Cl type hydrogen bond.
b) This value is converted to the $^{15}NH_4NO_3$ aq. reference from ref. 31.

computer at the Computer Center of the Tokyo Institute of Technology was used for calculation. The N-H bond length and N···O hydrogen bond length, optimized by ab initio STO-3G MO calculation, were determined for N-methylacetamides as a model compound. The calculations were performed on a HITAC M680H computer at the Computer Center of the Institute for Molecular Science, Okazaki.

2.3 Results and Discussion

^{15}N NMR chemical shifts of glycine amide nitrogen of peptides in the solid state: A 27.3 MHz ^{15}N CP/MAS NMR spectrum of L-alanylglycylglycine (L-Ala-Gly-Gly) in the solid state is shown as a typical example in Fig.2.1. ^{15}N CP/MAS spectra of the remaining samples were also obtained with similar resolutions. Signals were also assigned with reference to previous ^{15}N CP/MAS NMR and solution state ^{15}N NMR data[21].

Glycylglycine (X-Gly-Gly) sequence oligopeptides was used in this work. It is well known that the ^{15}N chemical shifts of peptides vary with the amino acid sequence[22]. For example, ^{15}N chemical shifts of the glycine residue depends upon the amino acid residue linked to the N-terminal of the glycine residue. Consequently, the glycylglycine sequence oligopeptides were used, in order to neglect the sequence-dependent ^{15}N chemical shifts.

All the ^{15}N chemical shift values of oligopeptides determined from the observed spectra are tabulated in Table2.1, together with the geometrical parameters obtained by X-ray diffraction studies. Some of the geometrical parameters were calculated by using the unit cell parameters and fractional coordinates given in the literature[23-31]. The ^{15}N chemical shifts and the geometrical parameters of tert-butyloxycarbonyl-

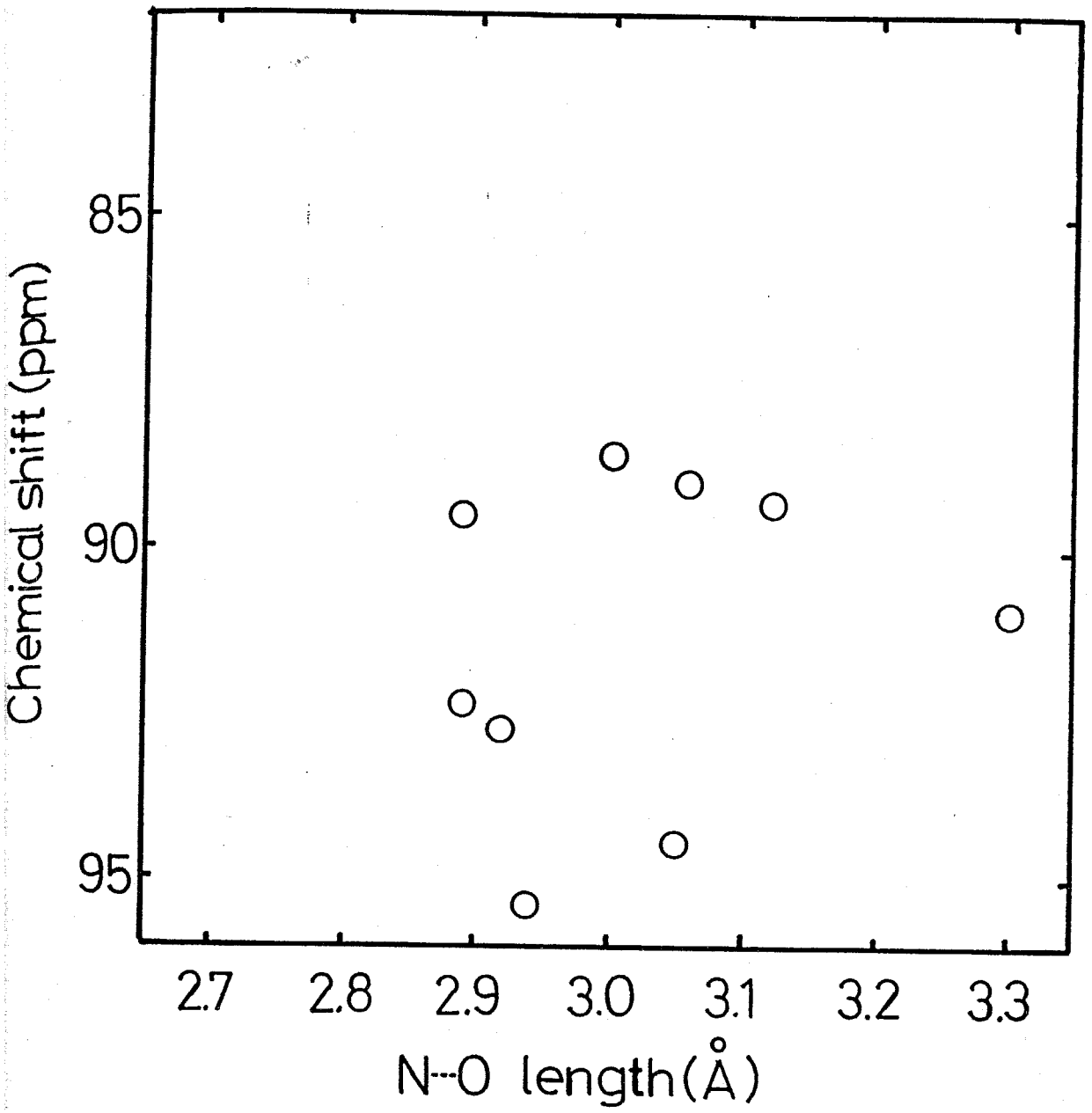

Fig.2.2 Plots of the observed ^{15}N chemical shift of oligopeptides in the solid state against the N···O hydrogen bond length($R_{N\cdots O}$).

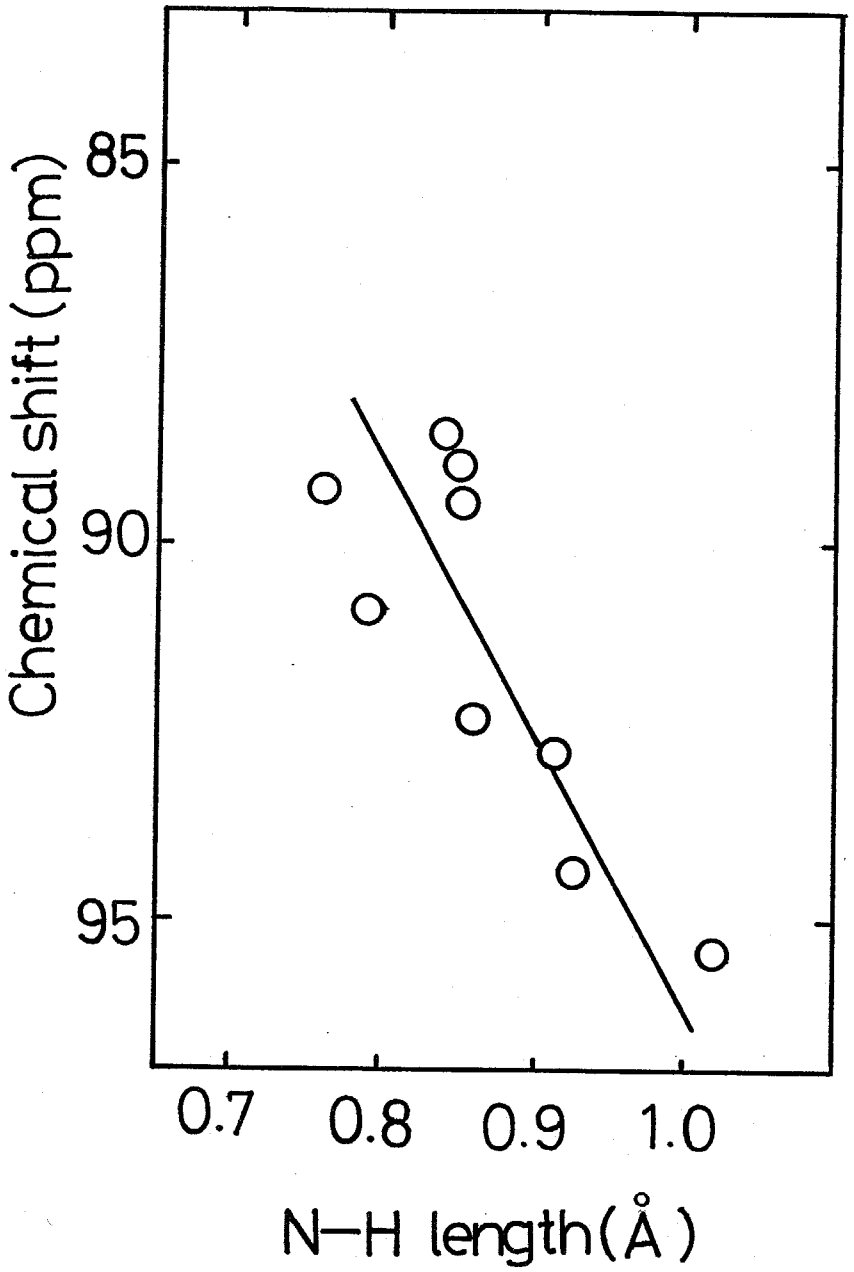

Fig.2.3 Plots of the observed ^{15}N chemical shift of oligopeptides in the solid state against the N-H bond length(R_{N-H}).

glycylglycylglycine-benzylester (Boc-Gly-Gly-Gly-OBzl) are inferred from the results of Hiyama et al[31].

Fig.2.2 shows the plot of the observed ^{15}N chemical shifts of Gly NH against the hydrogen bond length($R_{N\cdots O}$). However, it is found that there is no clear relationship between $R_{N\cdots O}$ and ^{15}N chemical shifts. This is different from the case of ^{13}C chemical shifts of the carbonyl carbons associated with the hydrogen bond, reported previously[14] where the ^{13}C signals of the carbonyl carbons are linearly deshielded with a decrease in $R_{N\cdots O}$.

Fig.2.3 shows the plot of the observed ^{15}N chemical shifts of the glycine residue in X-Gly-Gly against the N-H bond length(R_{N-H}) associated with hydrogen bond. It is found that there is a clear relationship between these parameters and the decrease of R_{N-H} leads to a linear increase in shielding. The expression for this relationship is

$$\sigma_{iso} = 39.32\, R_{N-H} + 57.73 \quad . \qquad (2.3)$$

Such a trend is very different from the obtained from ^{13}C NMR study. Amide ^{15}N chemical shifts are closely related to the length of the N-H bond but are not related to the N···O hydrogen bond length. This implies that the ^{15}N chemical shift value gives useful information about the N-H length in the hydrogen bond. It seems that the hydrogen bond angle (∠N-H···O) is also related to the ^{15}N chemical shift.

Ab initio calculation: relationship between the N-H bond length and the N···O hydrogen bond length: The structure of the two hydrogen-bonded N-methyl acetamides as a model system is shown in Fig.2.4. At first, the geometrical parameters of an N-methyl acetamide molecule were optimized using the ab initio STO-3G MO method. Next, for two hydrogen-bonded N-methyl acetamides, the bond length N-H was optimized as a function of the hydrogen bond length N···O. Fig.2.5

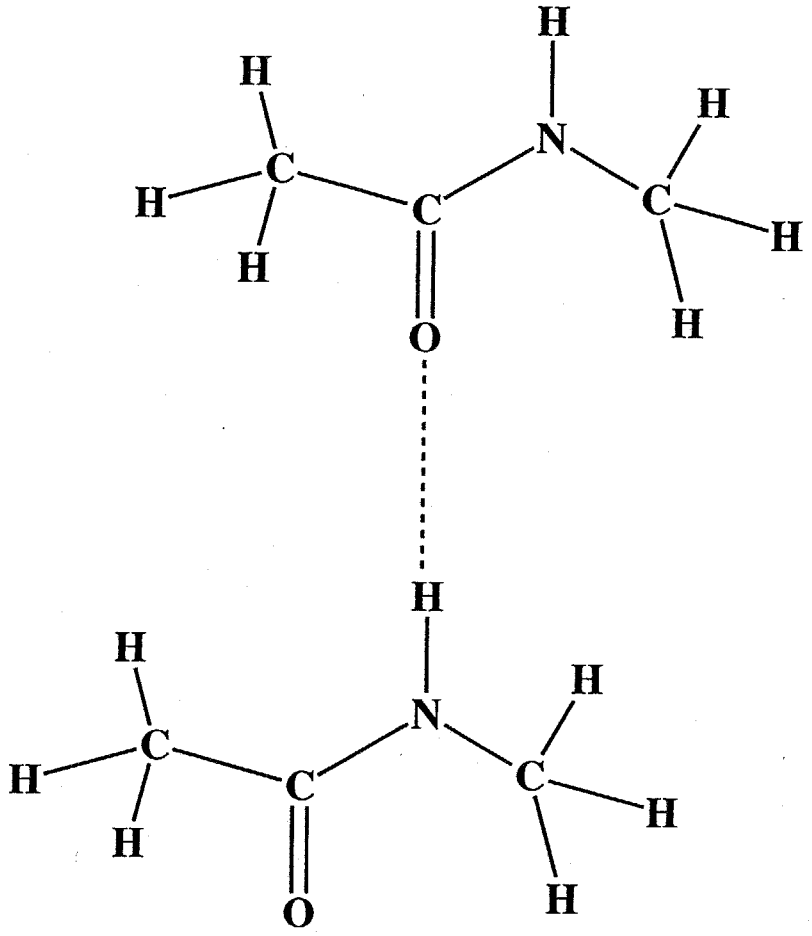

Fig.2.4 Structural model of the two hydrogen-bonded N-methylacetamides used as model compounds for STO-3G MO method.

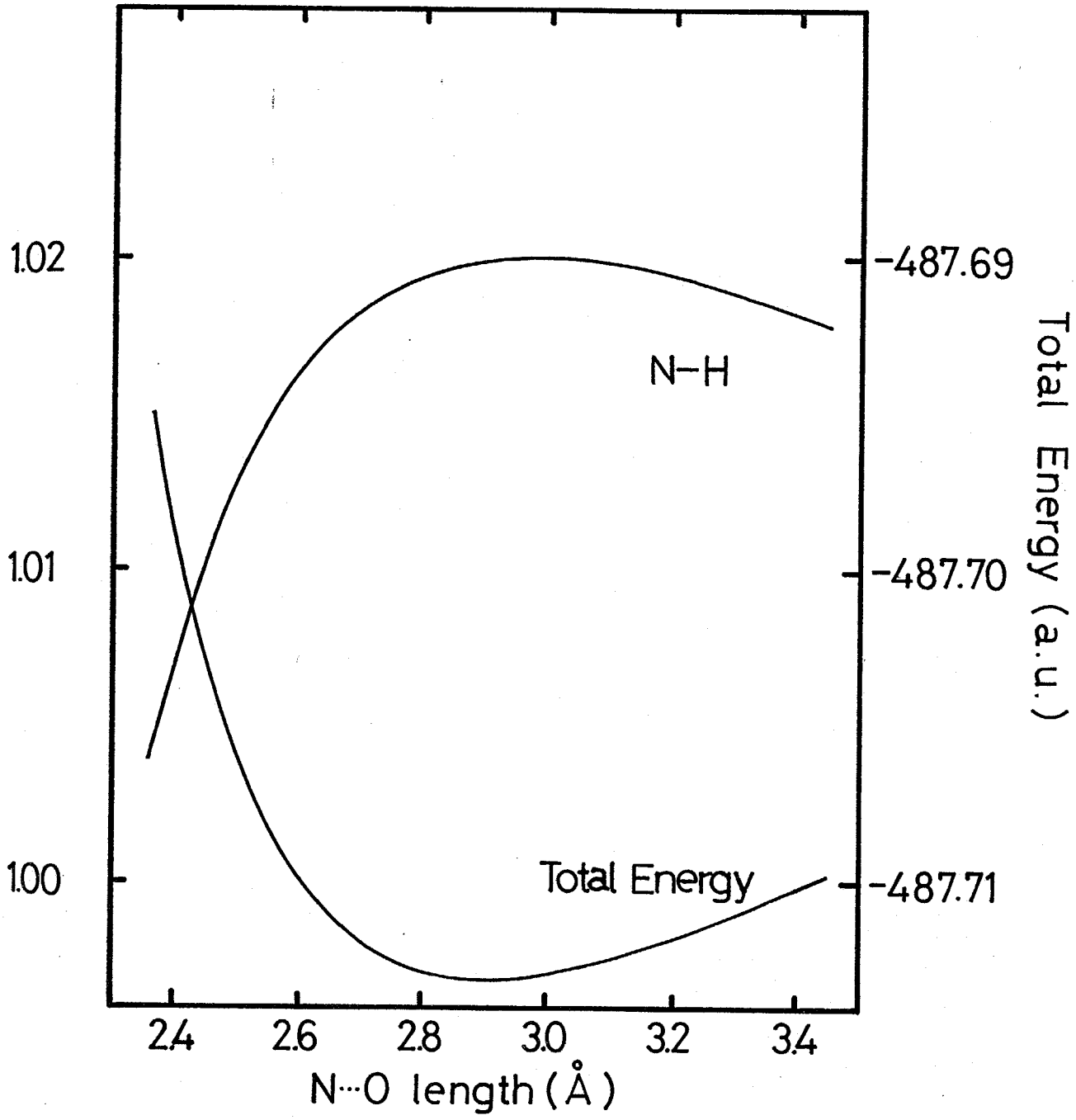

Fig.2.5 Plots of the calculation N-H bond length (R_{N-H}) and total energy against the hydrogen bond length($R_{N\cdots O}$).

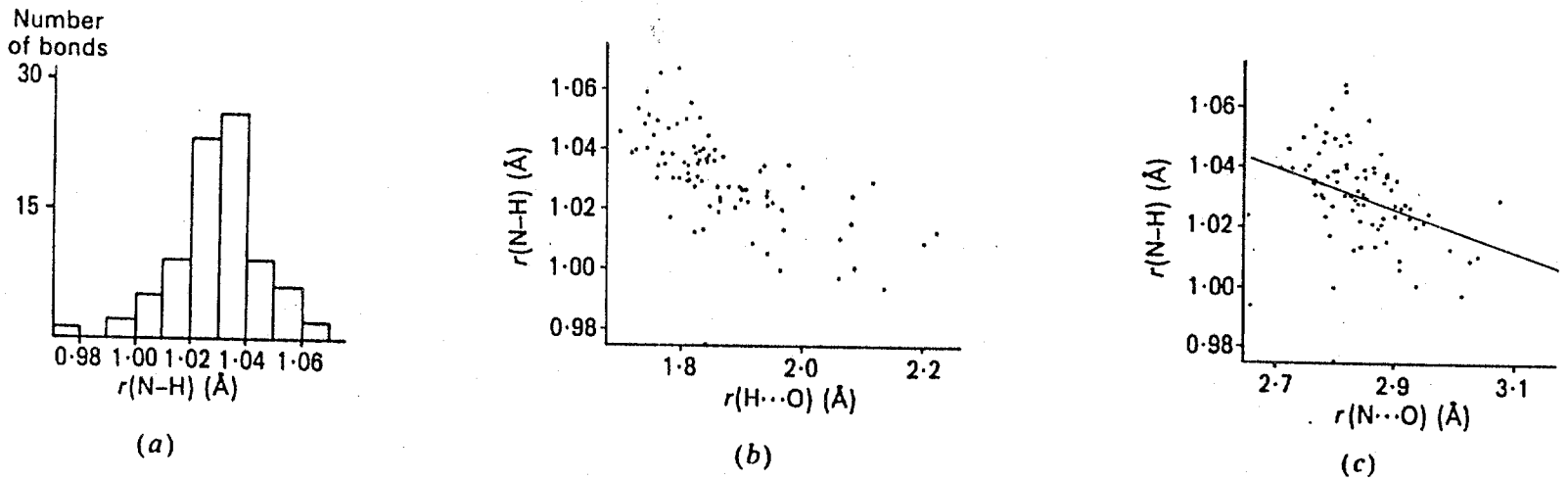

Fig.2.6 (*a*) Distribution of *r*(N–H) for the 83 bonds determined by neutron diffraction. (*b*) Scatterplot of *r*(N–H) against *r*(H···O). (*c*) Scatterplot of *r*(N–H) against *r*(N···O); least-squares regression line is also shown.

shows the relationship between the minimized bond length N-H or the total energy and the hydrogen bond length N···O, as determined by ab initio MO calculations.

It is shown that at $R_{N\cdots O} < 2.97$ Å, an increase of $R_{N\cdots O}$ leads to an increase of R_{N-H}. However, at $R_{N\cdots O} > 2.97$Å, an increase of $R_{N\cdots O}$ leads to a decrease of R_{N-H}. In the sample used in this work, the $R_{N\cdots O}$ values are between 2.85 and 3.30 Å. Therefore, it can be said that the R_{N-H} values decrease with an increase of $R_{N\cdots O}$.

On the other hand, X-ray diffraction studies, have shown that the R_{N-H} decrease with an increase of the $R_{N\cdots O}$ values(Fig.2.6)[32]. From the above results, it can be said that there is an apparent relationship between the hydrogen bond length $R_{N\cdots O}$ and the bond length R_{N-H}.

^{15}N shielding calculation: Figs.2.7 and 2.8 show the calculated isotropic shielding(σ_{iso}) and the paramagnetic terms of the tensor components (σ_{11}, σ_{22}, σ_{33}, from downfield to upfield) of Gly NH using the model compound N-acetyl-N'-methylglycineamide (Fig.2.9). The calculated values are all expressed in parts per million (ppm) with an opposite sign to those in Table 2.1. Note that the negative sign for the calculated shielding denotes deshielding, which is similar to the positive sign of the experimental chemical shift values. A shielding value, or tensor component, is usually represented as the sum of the diamagnetic and the paramagnetic terms. However, the anisotropic behavior of the shielding tensor can be predominantly explained by the paramagnetic term, since the diamagnetic term is isotropic.

Fig.2.7 shows the R_{N-H} dependence of the calculated isotropic ^{15}N shielding (σ_{iso}) of Gly NH. It is shown that a decrease of R_{N-H} leads to very large increase of σ_{iso}; for example, a decrease of 0.4 Å in R_{N-H} leads to a calculated shielding increase of about 30 ppm. This agree with

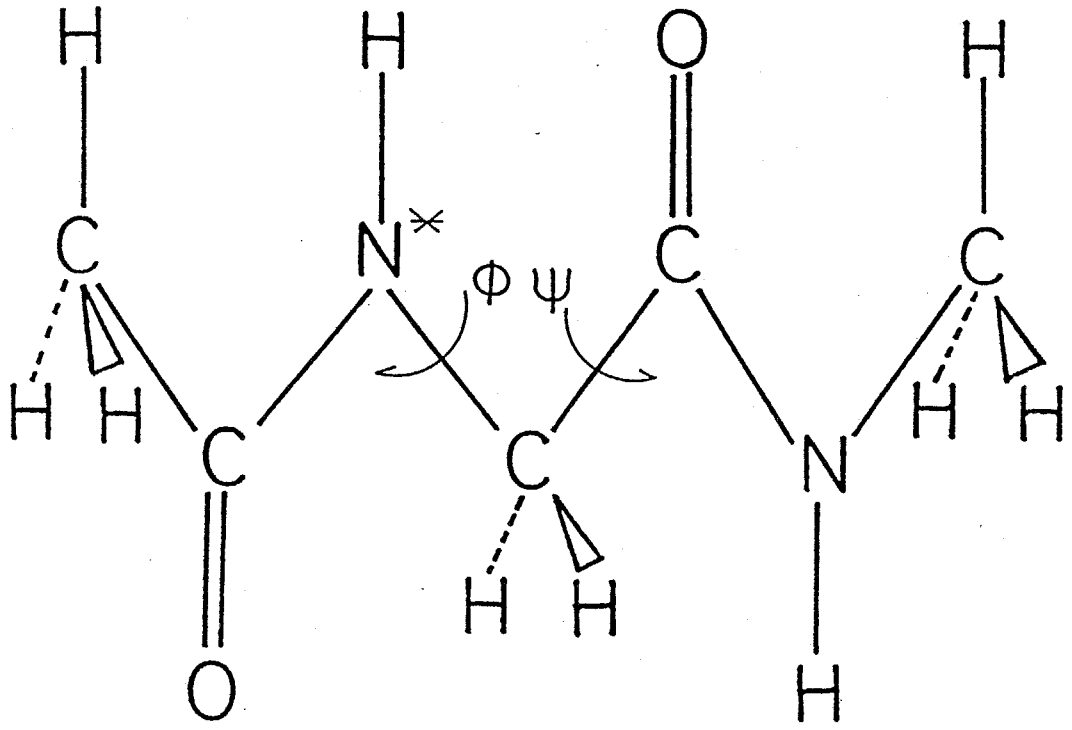

Fig.2.7 Molecular structure of N-acetyl-N'-methylglycine amide used as the model compound for FPT-INDO method.

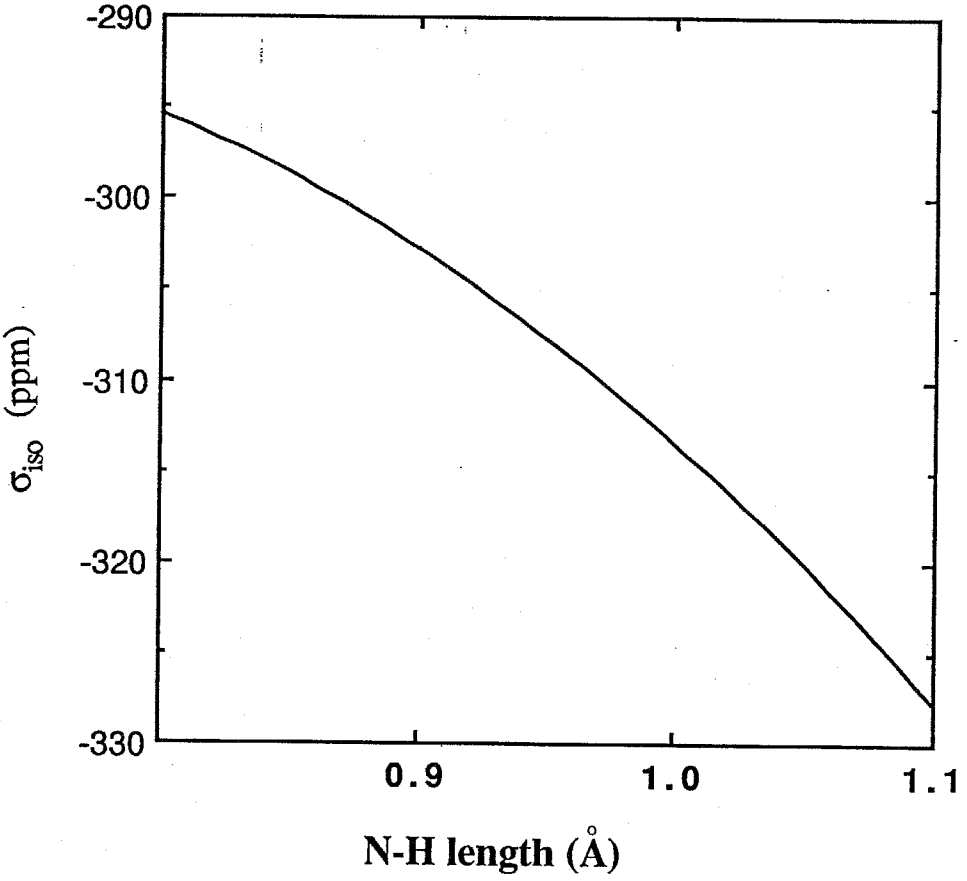

Fig.2.8 Plots of the calculated ^{15}N isotropic shielding the N-H bond length (R_{N-H}) from the FPT-INDO method.

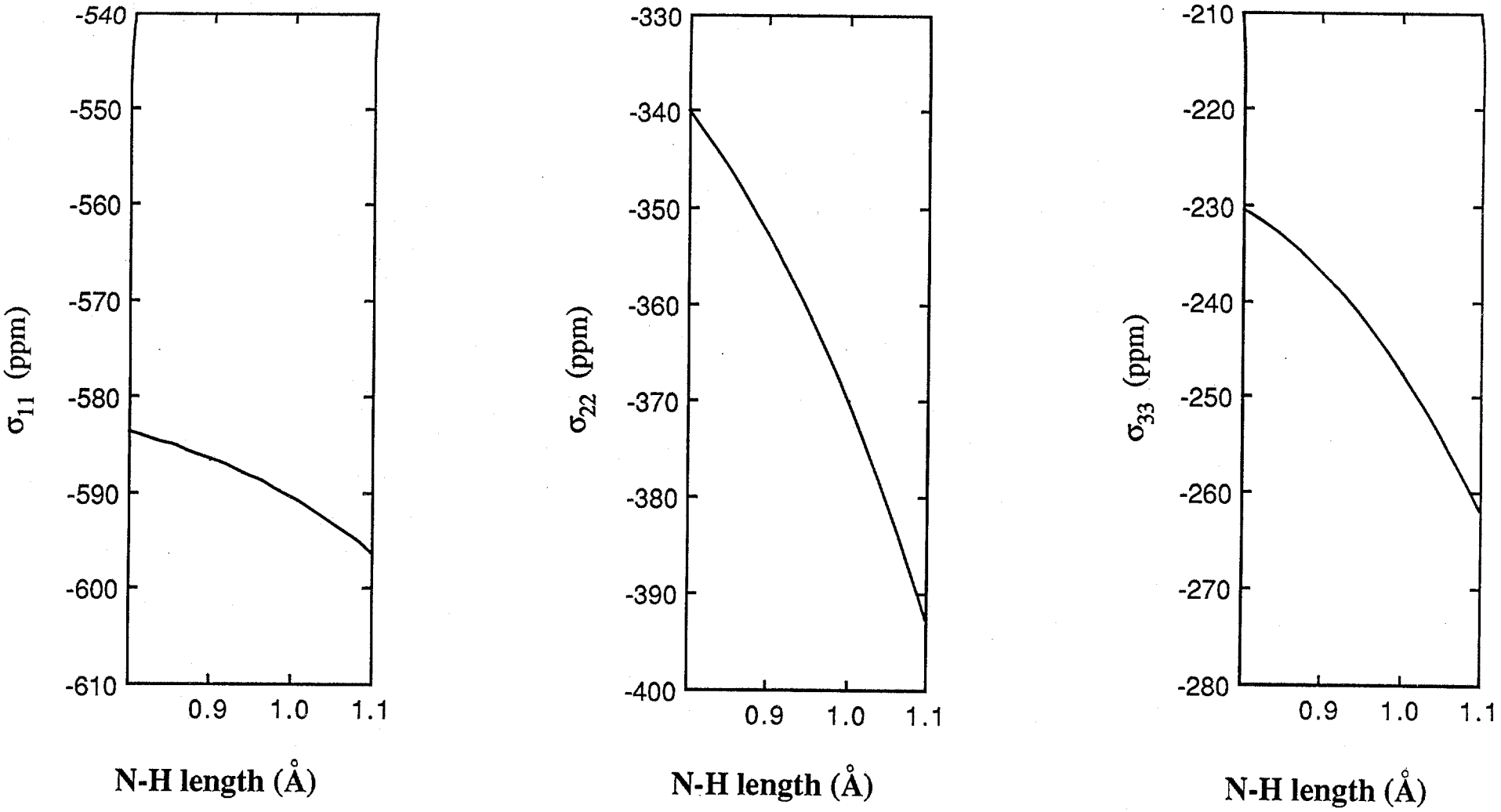

Fig.2.9 Plots of the calculated ^{15}N shielding tensor components against the N-H bond length (R_{N-H}) from the FPT-INDO method.

the observed results. This implies that the observed shielding increase is a consequence of the changes in the electronic state through a decrease of the N-H bond length.

Fig.2.8 shows the R_{N-H} of the calculated principal values of the ^{15}N shielding of the Gly NH. It is shown that a decrease of R_{N-H} leads to an increase in shielding of σ_{11}, σ_{22} and σ_{33}, respectively. The magnitudes for changes of the principal axes of the shielding occur in the order $\sigma_{22}>\sigma_{33}>\sigma_{11}$. The direction of the principal axes of the Gly NH ^{15}N shielding tensor components, as determined by the NMR study of a Boc-Gly-Gly-Gly-OBzl single crystal[31], are shown in Fig.2.10. The σ_{11} component lies approximately along the N-H bond, and the σ_{33} component lies approximately along the N-C' bond. The σ_{22} component is aligned in the direction perpendicular to the peptide plane. From this, it can be said that the σ_{22} and σ_{33} components, rather than the σ_{11} component, are sensitive to R_{N-H} changes. This may be due to the fact that the σ_{22} component lies approximately along the direction of the nitrogen lone-pair electrons and the electron density is very high in this direction. The σ_{33} component lies approximately along the N-C' bond into which lone-pair electrons of the nitrogen atom transfer, and so the bond order becomes very high. Consequently, The σ_{22} and σ_{33} components are sensitive to changes in R_{N-H}.

Finally, it can be concluded as follows: The observed ^{15}N shieldings of amide nitrogen increase linearly with a decrease of the N-H bond length associated with the hydrogen bond length; this can be justified by quantum chemical calculations. The ^{15}N shielding is applicable as a means for obtaining direct information about the nature of the hydrogen bond in the solid state, in addition to the ^{13}C shielding of the carbonyl carbons in the hydrogen bonds.

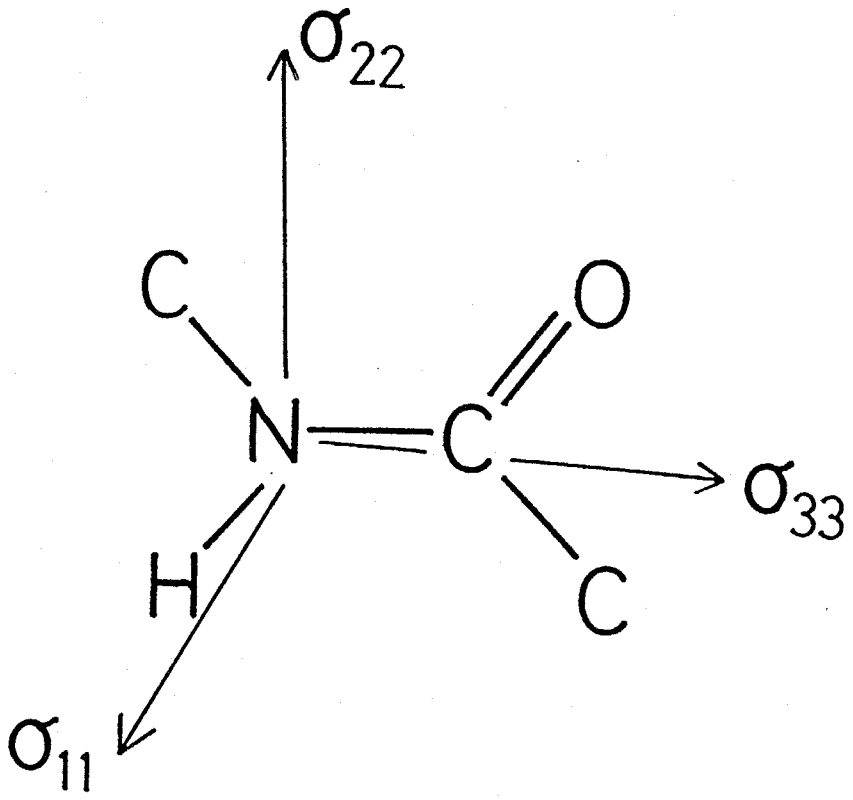

Fig.2.10 Orientation of the principal axes of the ^{15}N shielding tensors of the glycine residue amide nitrogen as determined in the literature 31.

References

1) G.A.Webb and M.Witanowski, *Proc.Indian Acad.Sci. (Chem.Sci.)*, **94** (1985) 241.

2) G.Harbisonm J.Herzfeld and R.J.Grriffin, *J.Am.Chem.Soc.*, **103** (1981) 4752.

3) T.A.Cross, J.A.Diverdi and S.T.Opella, *J.Am.Chem.Soc.*, **104** (1982) 1759.

4) T.A.Cross, M.H.Fray and S.T.Opella, *J.Am.Chem.Soc.*, **105** (1983) 7471.

5) H.G.Forster, D.Muller and H.R.Kricheldorf, *Int.J.Biol.Macromol.*, **5** (1983) 101.

6) T.H.Huang, W.W.Achovchin, R.G.Griffin and C.M.Dobson, *Biochemistry*, **23** (1984) 5933.

7) E.O.Stejeskal, J.Schaefer and R.A.MaKay, *J.Magn.Reson.*, **57** (1984) 471.

8) C.N.Matthews, R.Ludicky, J.Schaefer, E.O.Stejeskal and R.A.MaKay, *Origins Life*, **14** (1984) 243.

9) T.A.Cross and S.T.Opella, *J.Mol.Biol.*, **182** (1985) 367.

10) B.A.Choi, J.E.Roberts, J.N.S.Evans and M.F.Roberts, *Biochemistry*, **25** (1986) 557.

11) J.Schaefer, J.R.Garbow, G.E.Jacob, T.M.Forest and G.E.Willsin,Jr., *Biochem.Biophys.Res.Commun.*, **137** (1986) 736.

12) P.L.Stewart, K.G.Valentine and S.J.Opella, *J.Magn.Reson.*, **71** (1987) 45.

13) (a) A.Shoji, T.Ozaki, T.Fujito, K.Deguchi and I.Ando, *Macromolecules*, **20** (1987) 2441.

(b) A.Shoji, T.Ozaki, T.Fujito, K.Deguchi, S.Ando and I.Ando, *Macromolecules*, **22** (1989) 2860.

14) S.Ando, I.Ando, A.Shoji and T.Ozaki, *J.Am.Chem.Soc.*, **110** (1988) 3380.

15)(a) L.Zervas, D.Borovas and E.Gazis, *J.Am.Chem.Soc.*, **85** (1963) 3660.

(b) E.Wunsch, *Synthese von Prptidenm Teil 1 and 2*, Georg Thieme Verlag. Stuttgart, 1974.

(c) N.Izumiya, T.Kato, M.Ohno and H.Aoyagi, *Peptide Synthesis*, Maruzen, Tokyo, 1974.

16) I.Ando, H.Saito, R.Tabeta, A.Shoji and T.Ozaki, *Macromolecules*, **17** (1984) 457.
17) R.Ditchfield, D.P.Miller and J.A.Pople, *J.Chem.Phys.*, **54** (1971) 4186.
18) P.D.Eiliss, G.E.Maciel and J.M.McIver,Jr., *J.Am.Chem.Soc.*, **94** (1972) 4069.
19) I.Ando and G.A.Webb, *Theory of NMR Parameters*, Academic Press, London, 1983.
20) F.A.Momany, R.F.McGuire, J.F.Yan and H.A.Scheraga, *J.Phys.Chem.*, **75** (1971) 2286.
21) M.Witanowski, L.Stefaniak and G.A.Webb, *Annual Reports on NMR Spectroscopy*, Vol.18, Academic Press, London, 1986.
22) H.R.Kricheldorf, ,*Org.Magn.Reson,* **5(2)** (1981) 162.
23) A.B.Biswas, e.W.Hughes, B.D.Sharma and J.N.Willson, *Acta Cryst.* , **B24** (1968) 40.
24) T.F.Koetzle, w.C.Hamilton and R.Parthasarathy, *Acta Cryst.*, **B28** (1972) 2083.
25) S.N.Rao and R.Parthasarathy, *Acta Cryst.*, **B29** (1973) 2379.
26) V.L.Murali and E.Subramanian, *Int.J.Peptide Protein Res.*, **27** (1986) 472.
27) V.Lalitha, E.Subramanian and R.Parthasarathy, *Int.J.Peptide Protein Res.*, **27** (1986) 223.
28) V.Lalitha, E.Subramanian and J.Bordener, *Indian J.Pure Appl.Phys.*, **99(2)** (1977) 595.
29) J.P.Glusker, H.L.Carrell, H.M.Berman, B.Gallen and R.M.Peck, *J.Am.Chem.Soc.*, **110** (1988) 2378.
30) W.M.Carson and M.L.Hackert, *Acta Cryst.*, **B34** (1978) 1275.
31) Y.Hiyama, C.Niu, J.V.Silverton, A.Bavoso and D.A,Torchia, *J.Am.Chem.Soc.*, **110** (1988) 2378.
32) R.Taylor, O.Kennard and W.Versichel, *Acta Cryst.*, **B40** (1984) 280.

Chapter 3

Hydrogen-Bonding Structure and ^{15}N NMR Chemical Shifts of Peptides Containing Gly residue in the Solid State II. BocGlyX

3.1 Introduction

^{15}N NMR spectroscopy has demonstrated to provide useful information about structure and dynamics of synthetic polypeptides and natural proteins in solution[1-6]. It has been reported that the ^{15}N nucleus is highly sensitive to structural and conformational changes of the molecules. Most recently, high-resolution solid-state ^{15}N NMR has been developed by means of the cross polarization / magic angle spinning (CP/MAS) method, and has been applied to the conformational characterization of polypeptides and oligopeptides[7]. It has been demonstrated that the ^{15}N chemical shifts in the peptide backbone of a variety of polypeptides exhibit a significant conformation-dependent change[8-10] and the α_R-helix form(97.0-99.2 ppm) appears more upfield than that of the β-sheet form(99.5-107.0 ppm). On the other hand, if the exact principal values of ^{15}N chemical shift tensors(σ_{11}, σ_{22} and σ_{33}) are available, it provides more detailed information about the structure of polypeptides and oligopeptides, which are closely associated with electronic structure compared with the isotropic chemical shift value($\sigma_{iso} = (\sigma_{11}+\sigma_{22}+\sigma_{33})/3$) which is determined by MAS method. Because a nitrogen atom possesses lone-pair electrons, it is of interest to examine the effects of the lone-pair electrons on the isotropic ^{15}N chemical shift (σ_{iso}) and the principal values of the ^{15}N chemical shift tensors(σ_{11}, σ_{22} and σ_{33}). Further, the direction of the principal axes of the glycine residue ^{15}N shielding tensor components was experimentally determined by some investigators.[11] In preceding chapter[7], it was

described that in a variety of solid oligopeptides (X-GlyGly, where Gly is glycine residue and X is the other amino acid residue) the decrease of the N-H bond length in the >C=O···H-N< type hydrogen bond for the C-terminal Gly residue leads to a linear increase in ^{15}N shielding, but there is no clear relationship between the ^{15}N chemical shifts and N···O separation. The results that there is no relationship between them may come from the other amino acid (X) effect. For this, when details of the hydrogen bond through the ^{15}N chemical shift are studied, oligopeptides without the effect of X on the ^{15}N chemical shift of Gly residues must be chosen. If oligopeptides with tert-butyloxycarbonyl (Boc) group in the terminal are chosen, it can be expected that the oligopeptides do not have the effect of X on the ^{15}N chemical shift of Gly residue. (The Boc group is sometimes used as the terminal in oligopeptides.) As a continuation of ^{15}N NMR study of the hydrogen bond in oligopeptides, in this work I attempt to measure isotropic ^{15}N chemical shifts and individual components of ^{15}N chemical shift tensors of the glycine residue (Gly) in a variety of oligopeptides with the Boc group in the terminal, and to clarify the relationship between hydrogen bond length and isotropic chemical shifts and individual components of chemical shift tensors. The obtained results will be discussed in comparison with my previous NMR studies about hydrogen bond. Further, to do a deep insight into the hydrogen bond, the ^{15}N chemical shift and tensor components of the glycine amide nitrogen are calculated by employing quantum chemical method.

3.2 Experimental

Materials: A series of oligopeptides containing the ^{15}N labeled glycine residue (a ^{15}N purity of about 10 %) were prepared according to the

condensation reaction of Boc-glycine N-hydroxysuccinimide activated esters and amino acids[12]. The N-terminals of all the peptides considered here were protected by tert-butyloxycarbonyl (Boc) group using Boc-S (tert-butyl S-4,6-dimethylpyrimidin-2-ylthiocarbonate). A mixture of ^{15}N labeled glycine (Merck Inc., isotope purity 99 atom %) and glycine (Nihon-Rika Co) was used to obtain remarkably intense signals in the ^{15}N NMR spectra. The samples obtained were slowly recrystallized from ethyl acetate solution according to the procedure used in X-ray diffraction studies[13-17].

^{15}N NMR measurement: ^{15}N CP/MAS NMR spectra were recorded at room temperature with a JEOL GSX-270 spectrometer operating at 27.3 MHz equipped with a CP/MAS accessory. The field strength of ^{1}H decoupling was 1.2 mT. A contact time was 5 ms, and repetition time was 10 s. Spectral width and data points were 10 kHz and 8 k, respectively. Samples were placed in a cylindrical rotor and spun as fast as 4-5 kHz. Powder pattern spectra were recorded with the same instrument without magic angle spinning. Spectra were usually accumulated 100-2000 times to achieve a reasonable signal-to-noise ratio. ^{15}N chemical shifts Ire calibrated indirectly through external glycine- ^{15}N (δ=11.59 ppm ; line width=17 Hz) relative to saturated $^{15}NH_4NO_3$ solution(δ = 0 ppm) in H_2O. To obtain the three principal components of the shielding tensors (σ_{11}, σ_{22} and σ_{33}, from the downfield to upfield), a fitting was carried out by superimposing the theoretical powder pattern line shape with Lorentzian function (symmetrical broadening function) to the observed powder pattern as shown in Fig.3.1.

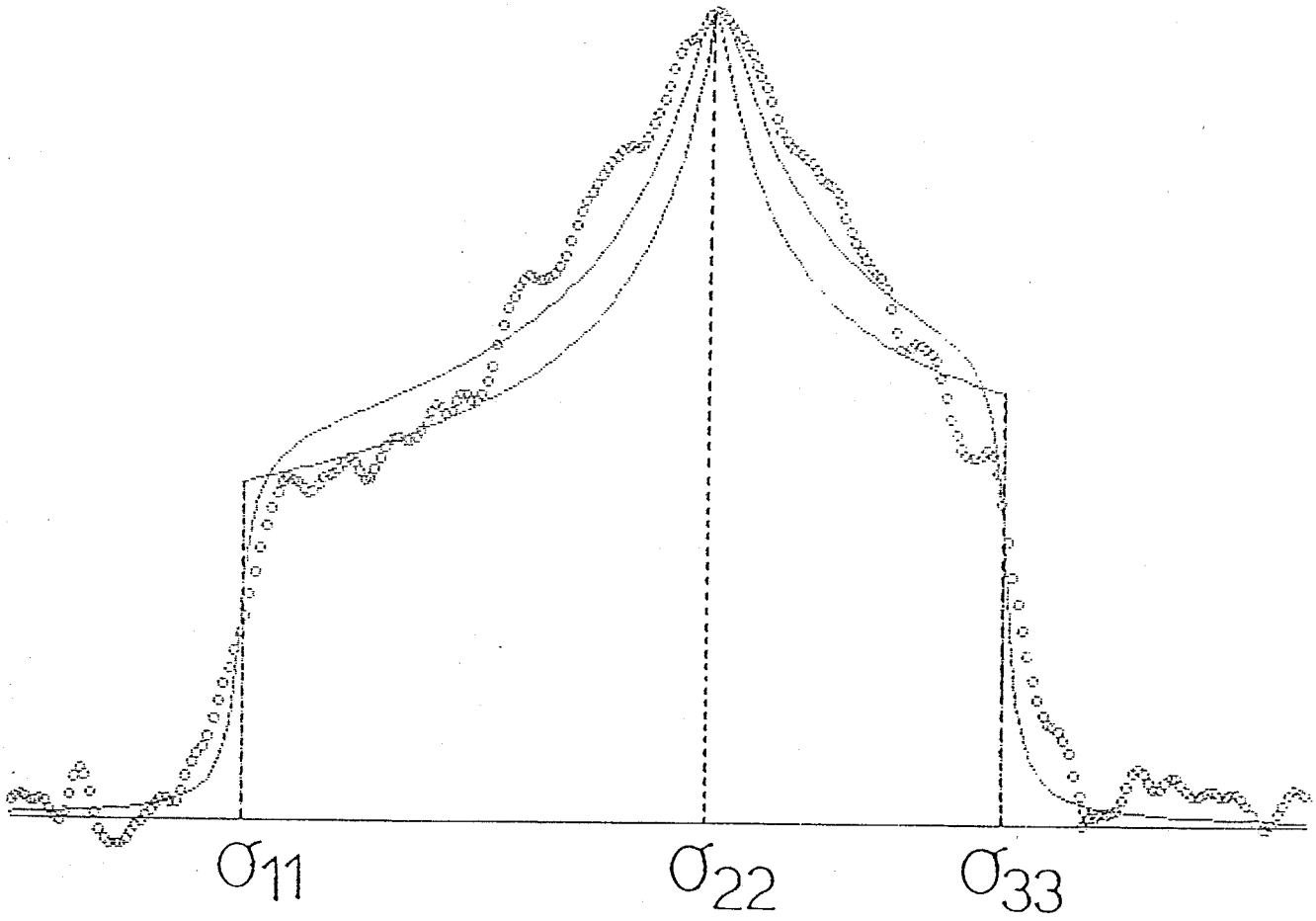

Fig.3.1 Schematic representations of experimental powder pattern and theoretical powder pattern convoluted with the Lorentzian function. The circles are the experimental data for BocGlyAla, σ_{11} = 121.5 ppm, σ_{22} = 52.2 ppm and σ_{33} = 11.1 ppm.

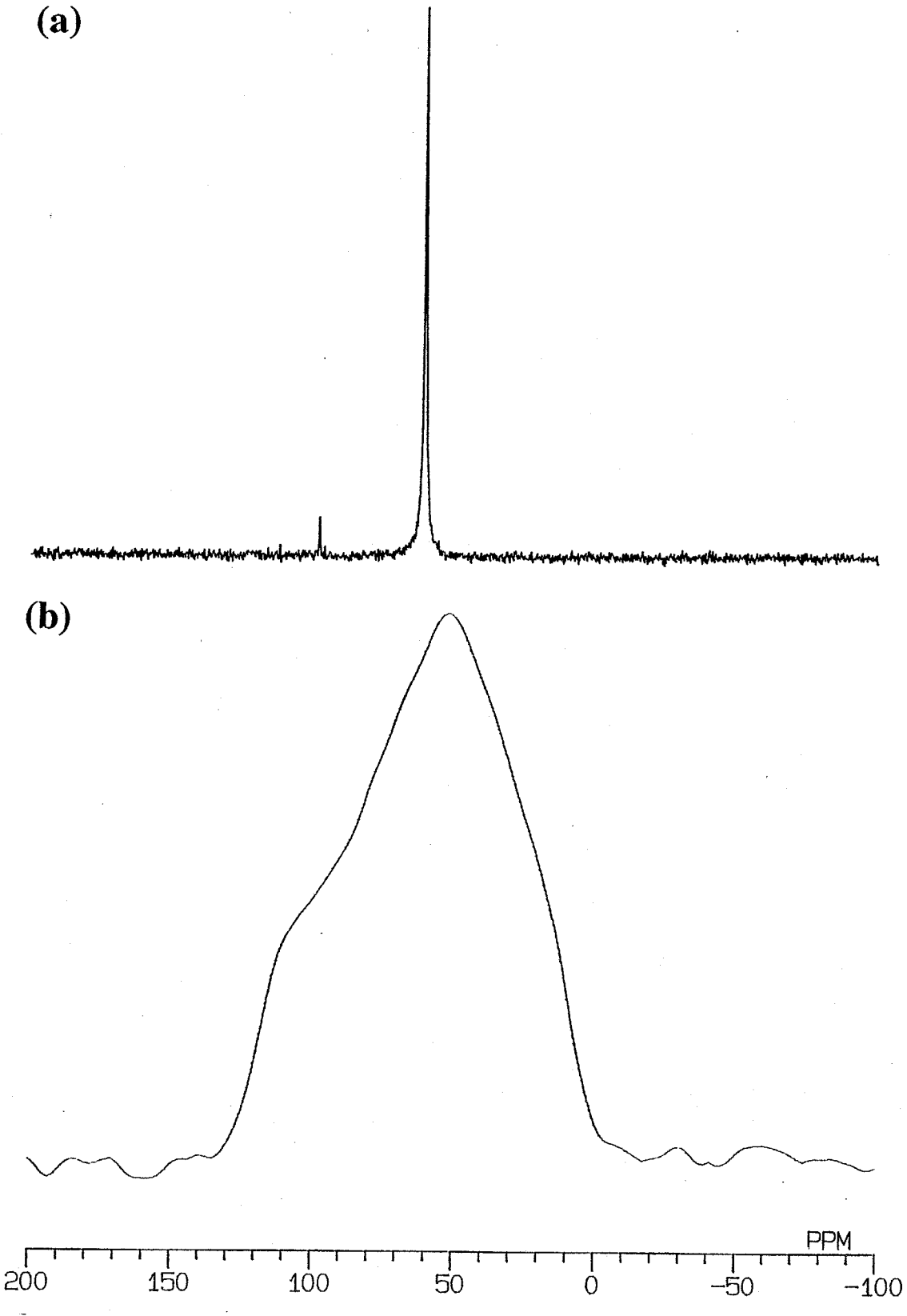

Fig.3.2 27.3MHz ^{15}N CP/MAS NMR spectrum (a) and 27.3 MHz ^{15}N CP static NMR spectrum (b) of BocGlyAla in the solid state.

Table 3.1 Observed ^{15}N isotropic chemical shifts and chemical shift tensor components of glycine amide nitrogen of BocGly* peptides (ppm from $^{15}NH_4NO_3$ aq.).

Sample	σ_{iso}	σ_{11}	σ_{22}	σ_{33}
BocGly	59.75	127.0	51.2	1.1
BocGlyAla	61.61	121.5	52.2	11.1
BocGlyPhe	54.04	112.7	56.1	-6.7
BocGlyAib	57.70	127.0	49.1	-3.0
BocGlyProOBzl	53.06	117.2	50.6	-8.6

Table 3.2 The geometrical parameters of glycine residue amide nitrogen of BocGly peptides.

Sample	Dihedral angle / deg.			Hydrogen bond length and angle				ref.
	ω	ϕ	ψ	N···O length(Å)	H···O length(Å)	N-H···O angle(deg.)	N···O=C angle(deg.)	
BocGly	174.0	-61.5	-15.1	3.01	—	—	113.1	13
BocGlyAla	178.8	-125.6	45.0	2.95	2.02	161.1	—	14
BocGlyPhe	-176.9	-88.0	-14.5	3.08	—	—	155.4	15
BocGlyAib	-159.4	89.5	165.1	3.08	—	—	116.4	16
BocGlyProOBzl	172.2	-109.5	164.4	3.10	2.24	163.4	136.7	17

^{15}N chemical shift calculation: In this work, relative ^{15}N NMR chemical shifts (magnetic shielding constants) of a dipeptide fragment, N-acetyl-glycine methylamide (forming hydrogen bonds with a formamide molecule) were calculated, employing the finite perturbation theory (FPT)-INDO method, as shown in detail in a previous paper[18]. The bond lengths and bond angles proposed by Momany et al.[19] were used. A HITAC M780H computer at the Computer Center of the Tokyo Institute of Technology and a HITAC S-820 computer at the Computer Center of the Institute for Molecular Science, Okazaki, were used for the calculation.

Results and Discussion

^{15}N NMR chemical shifts of the glycine residue of BocGly peptides in the solid state: A 27.3 MHz ^{15}N CP/MAS NMR spectrum and a 27.3MHz ^{15}N CP powder pattern spectrum of tert-butyloxy-carbonylglycylalanine (Boc-Gly-Ala) in the solid state were shown as a typical example in Fig.3.2. ^{15}N spectra of the other remaining samples were also obtained with similar resolutions. In the BocGly peptides, a nitrogen of the glycine residue forms urethane bond. Thus, its ^{15}N signal appears more upfield compared with that of the amide nitrogens. Signals were easily assigned with reference to solution-state ^{15}N NMR data reported previously[20] All the isotropic ^{15}N chemical shift values (σ_{iso}) and the principal values of the ^{15}N chemical shift tensors σ_{11}, σ_{22}, and σ_{33}; from the downfield to upfield) are tabulated in Table 3.1. The geometrical parameters obtained by X-ray diffraction studies[13-17] were tabulated in Table 3.2, where some of the geometrical parameters were estimated by using the unit cell parameters and fractional coordinates given in the literature. The hydrogen bond lengths ($R_{N\cdots O}$) of peptides

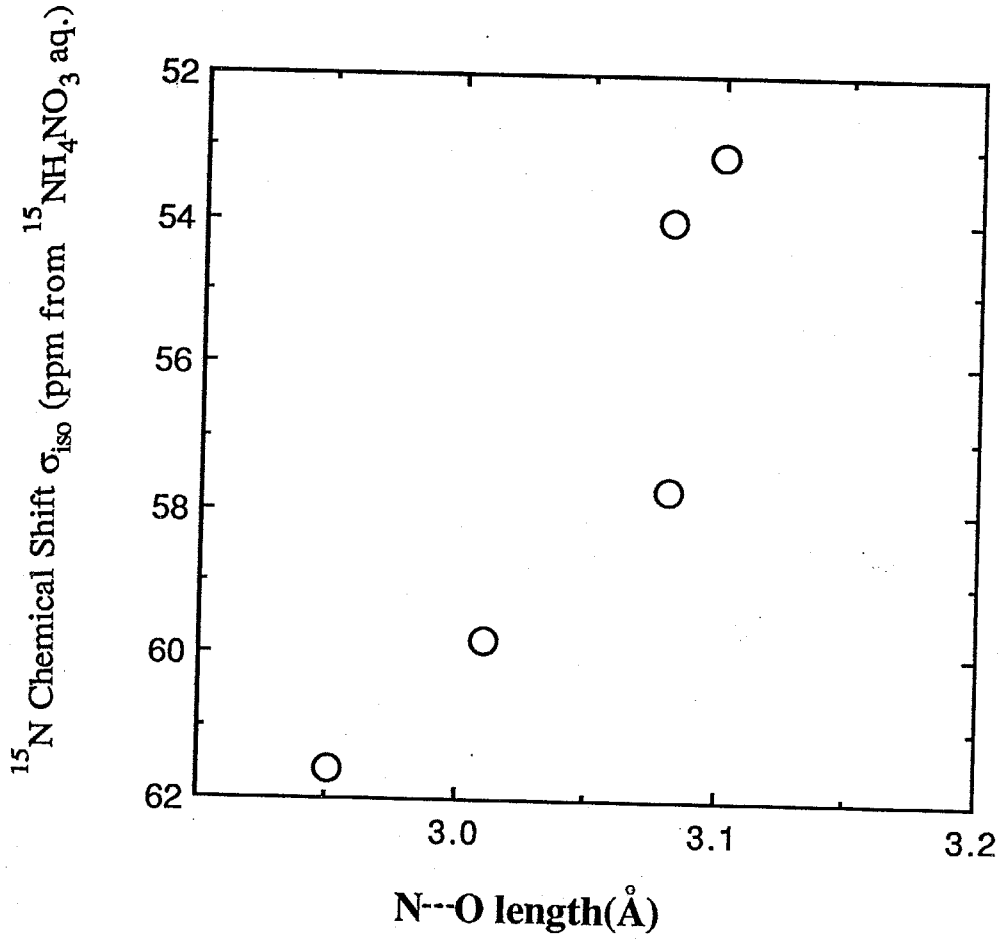

Fig.3.3 Plots of the observed isotropic ^{15}N chemical shifts(σ_{iso}) in the solid state against the N···O hydrogen bond length($R_{N\cdots O}$).

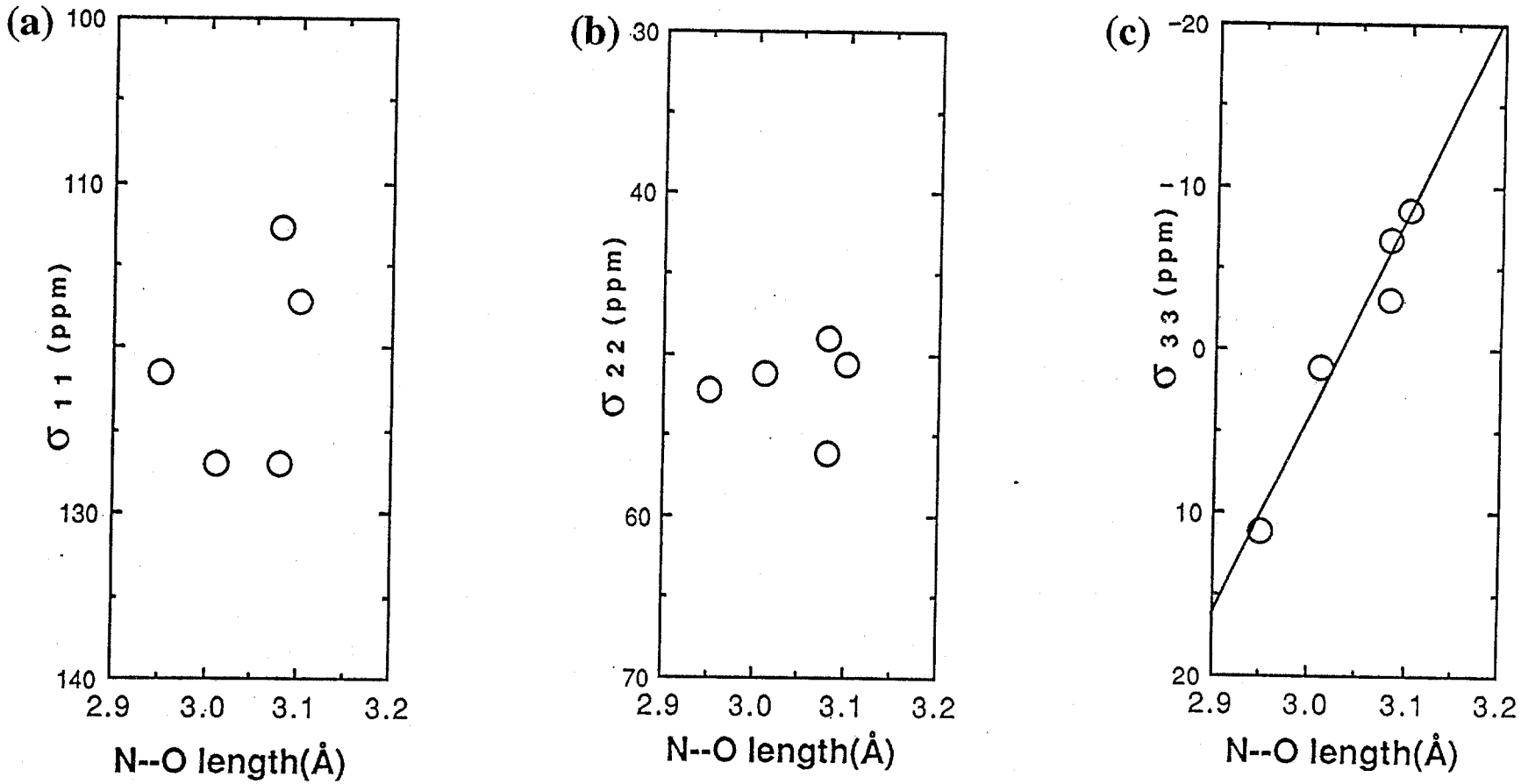

Fig.3.4 Plots of the observed principal values of ^{15}N chemical shift tensor σ_{11}(a) , σ_{22}(b) and σ_{33}(c), respectively in the solid state against the N···O hydrogen bond length($R_{N\cdots O}$).

used in this work are in the range from 2.95 to 3.08 Å. On the other hand, the hydrogen bond angles ∠C=O···N somewhat distribute and are in the range from 113 to 155° Fig. 3.3 shows the plot of the observed isotropic ^{15}N chemical shifts (σ_{iso}) of Gly NH against the hydrogen bond length $R_{N\cdots O}$. It is found that there is a clear relationship between σ_{iso} and $R_{N\cdots O}$, and a decrease of $R_{N\cdots O}$ leads to a decrease in shielding. This trend is similar to that in the relationship between carbonyl ^{13}C chemical shift and $R_{N\cdots O}$[20]. Figs.3.4 a)-c) show the plot of the observed principal values(σ_{11}, σ_{22}, and σ_{33}) of ^{15}N chemical shift tensor of Gly NH against $R_{N\cdots O}$, respectively. It is found that σ_{11} and σ_{33} are more sensitive than σ_{22} for change of $R_{N\cdots O}$. Change of 0.2 Å in $R_{N\cdots O}$ leads to the change of 20 ppm in σ_{11} and σ_{33}, although change of σ_{22} is 5 ppm. However, only σ_{33} is linearly downfield with a decreasing of $R_{N\cdots O}$, although in σ_{11} and σ_{22} there is no clear relationship with $R_{N\cdots O}$. These results show that such behavior is governed not only by the hydrogen bond length, but also by the hydrogen bond angle.

Theoretical calculation of ^{15}N shielding constant: In order to do a deep insight for the experimental finding that isotropic ^{15}N chemical shift and the principal value of σ_{33} depend upon the hydrogen bond length, theoretical calculation of ^{15}N chemical shifts were carried out by the FPT-INDO method. Figs.3.5 and 3.6 a)-c) show the calculated isotropic ^{15}N shielding (σ_{iso}) and their paramagnetic terms of shielding tensor components (σ_{11}, σ_{22} and σ_{33}) of Gly NH in the model compound, respectively. The calculated values are all expressed in ppm with an opposite sign to the experimental chemical shift values shown in Table 3.1. Note that the negative sign for the calculated shielding constant denotes deshielding, in contrast to the positive sign of the experimental

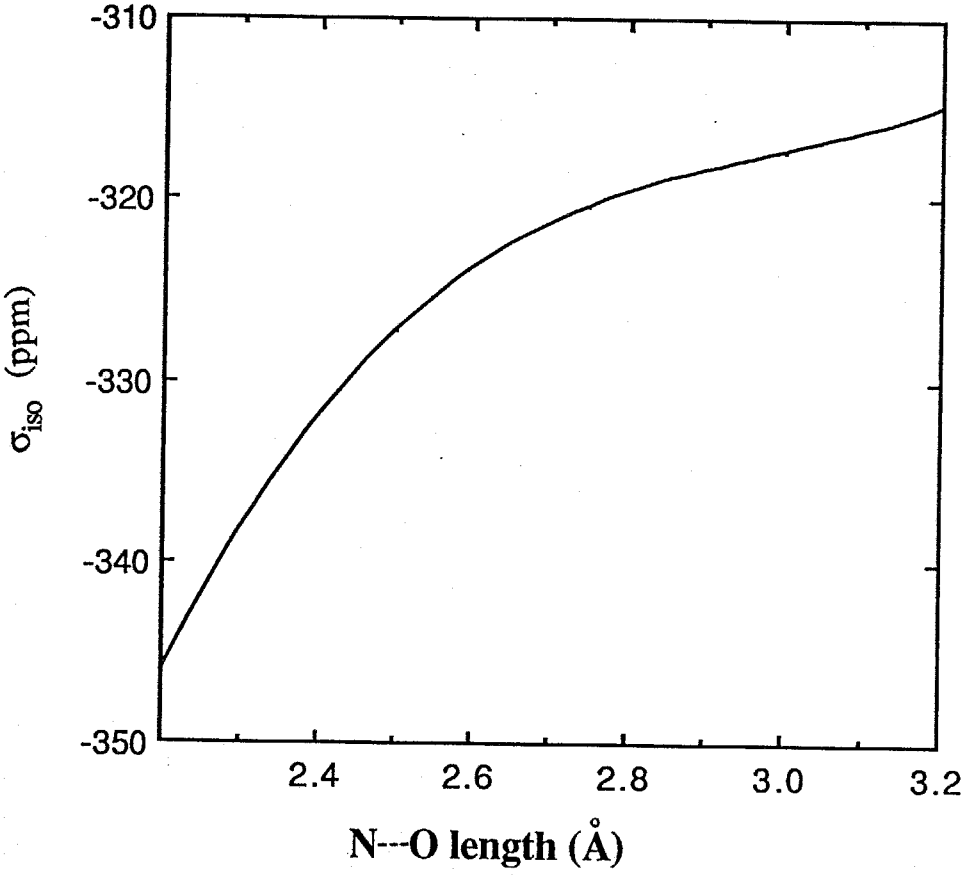

Fig.3.5 Variation of the calculated isotropic ^{15}N shielding (σ_{iso}) with the N···O hydrogen bond length($R_{N\cdots O}$).

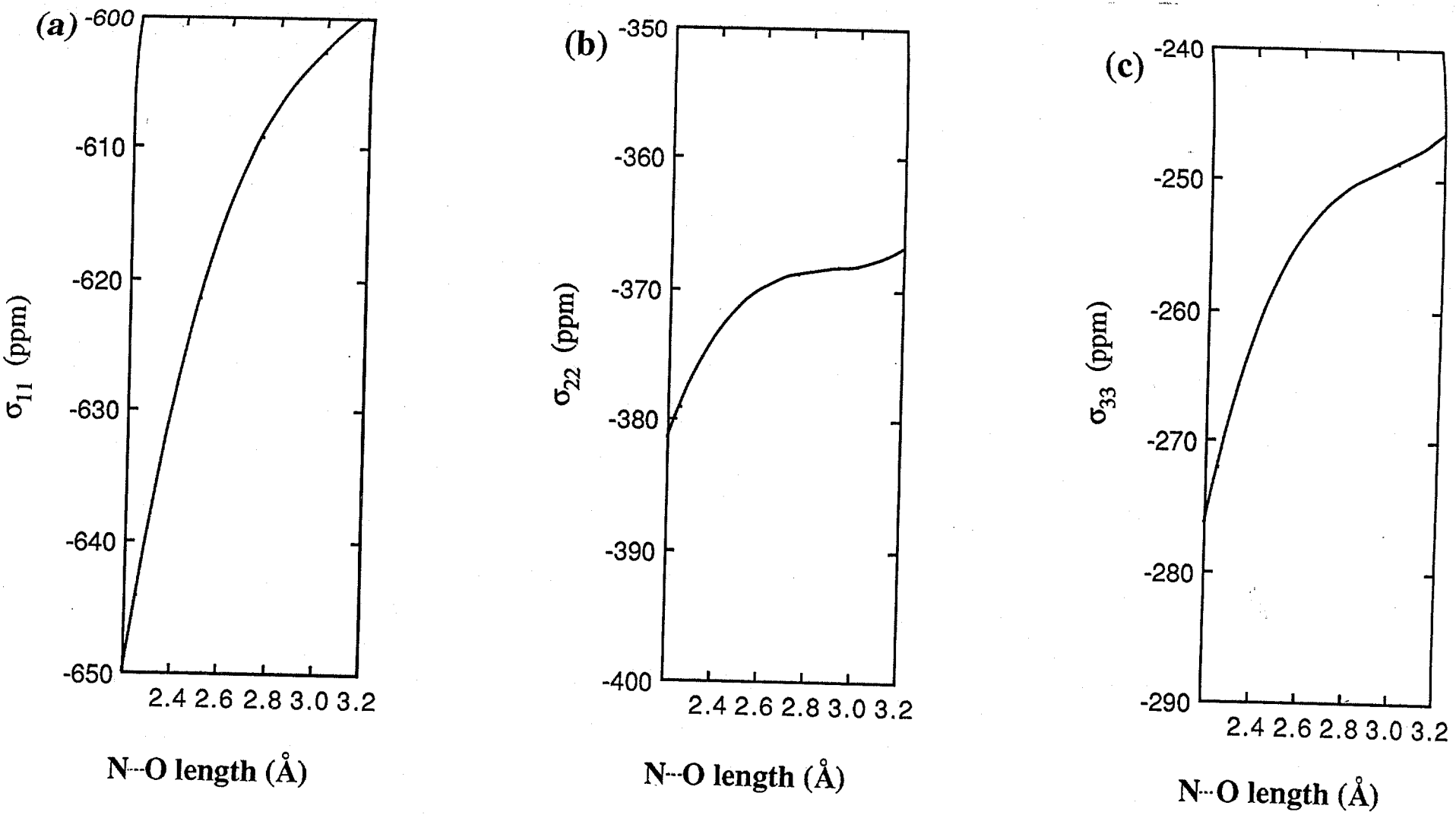

Fig.3.6 Variation of the calculated ^{15}N shielding tensor components with the N···O hydrogen bond length($R_{N\cdots O}$); σ_{11}(a) , σ_{22}(b) and σ_{33}(c), respectively.

chemical shift values. A shielding constant or tensor component is usually represented as a sum of the diamagnetic and the paramagnetic terms. However, the behavior of the shielding tensor can be predominantly explained by the paramagnetic term, since the diamagnetic term is isotropic. As shown in Fig.3.5, a decrease of $R_{N\cdots O}$ leads to a decrease of σ_{iso}. This agrees with the observed results. Therefore, such a relationship suggests that isotropic ^{15}N chemical shift value can be used in estimation of $R_{N\cdots O}$ as well as the case of carbonyl ^{13}C chemical shift reported previously[21]. Figs.3.6 b)-d) show the $R_{N\cdots O}$ dependence of the calculated principle values of ^{15}N chemical shift tensor (σ_{11}, σ_{22} and σ_{33}). It is shown that a decrease of $R_{N\cdots O}$ leads to decrease in shielding of σ_{11}, σ_{22} and σ_{33}. The magnitudes for changes of the shielding are in the order $\sigma_{11} > \sigma_{33} > \sigma_{22}$. Such an order for changes of the shielding agrees with the observed one. Further, a linear decrease of σ_{33} with a decrease of $R_{N\cdots O}$ agrees with the observed one. However, in the experimental results there is no relationship between $R_{N\cdots O}$ and σ_{11} or σ_{22}, but in the calculation there is a relationship between $R_{N\cdots O}$ and σ_{11} or σ_{22}. Why is this discrepancy? In the above calculation, the hydrogen bond length was only taken into account. To understand deeply the hydrogen-bonding, another important factor such as the hydrogen bond angle (that is the distortion from the linearity of hydrogen bond) should be taken into account. For this reason, the ^{15}N chemical shift was calculated as a function of the hydrogen bond angle ($\angle$N-H$\cdots$O) using the model compound (Fig.3.7). The H$\cdots$O length was fixed as 1.75 Å and then the hydrogen bond angle θ($\angle$N-H$\cdots$O) was varied. Figs 3.8 and 3.9 a)-c) show the plot of σ_{iso}, and σ_{11}, σ_{22} and σ_{33} against the angle θ, respectively. Fig.3.8 shows the $\angle$N-H$\cdots$O dependence of the calculated isotropic ^{15}N shielding (σ_{iso}). Change of the angle θ from 140° to 220° leads to change of 5 ppm in σ_{iso} compared with the value of

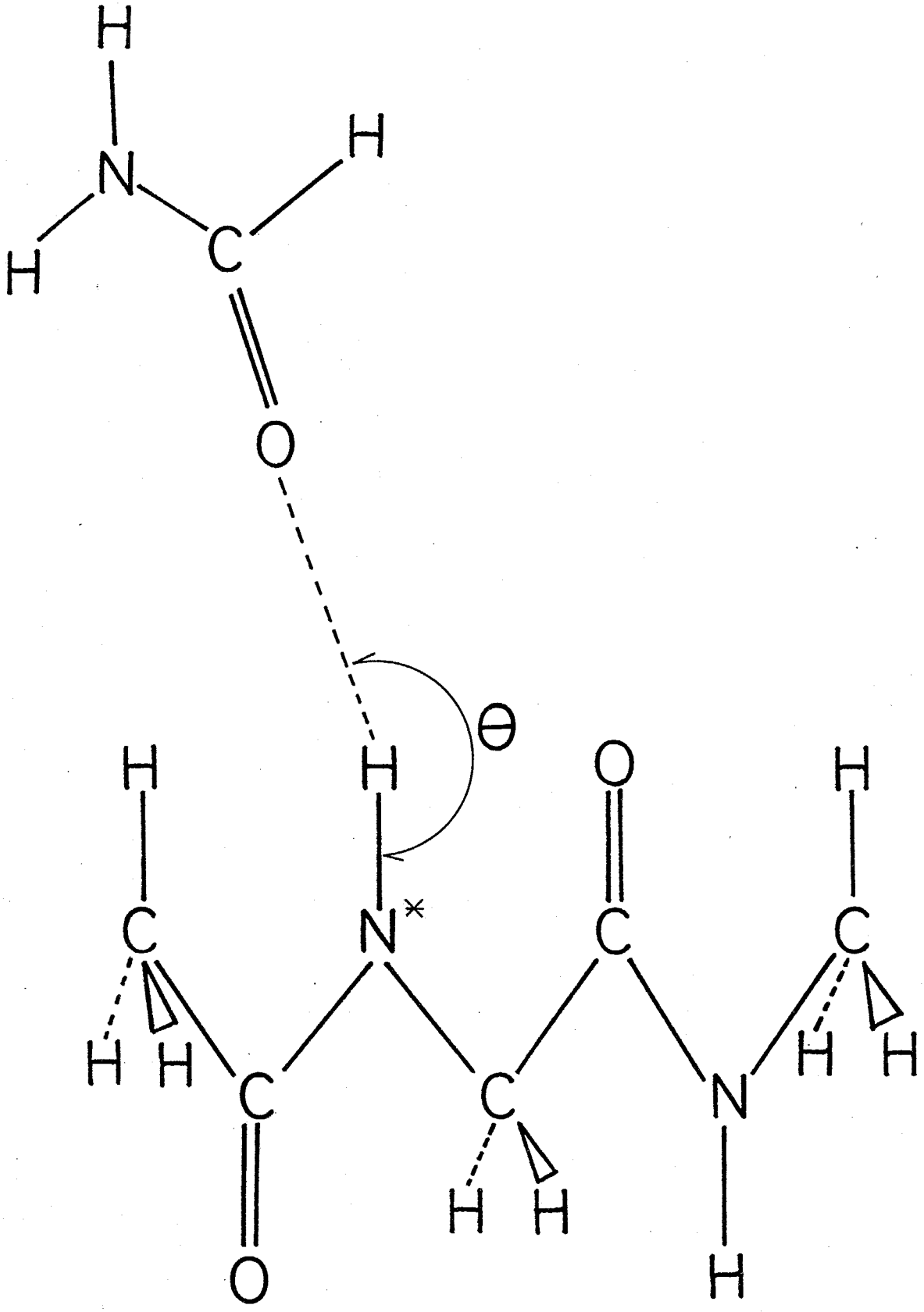

Fig.3.7 Molecular structure of N-acetyl-N'-methyl-glycine amide hydrogen-bonded with a formamide molecule.

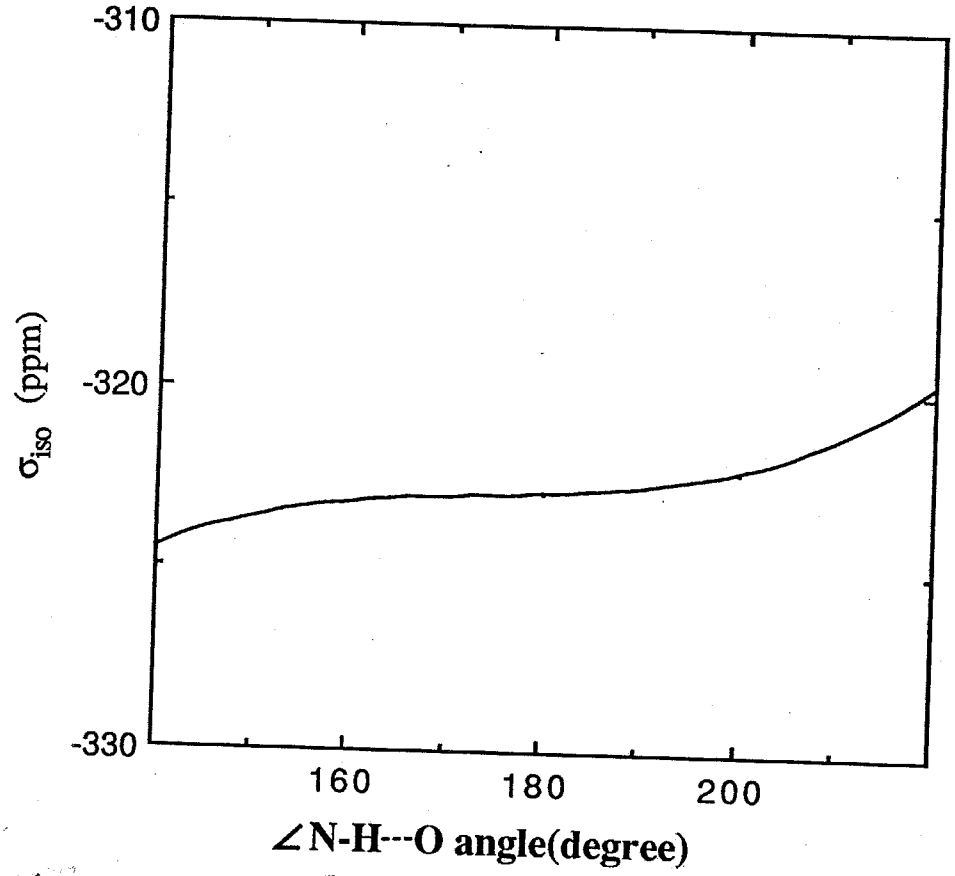

Fig.3.8 Variation of the calculated isotropic ^{15}N shielding (σ_{iso}) with the hydrogen bond angle ∠N-H···O (θ).

about 20 ppm induced by change of $R_{N\cdots O}$ from 2.4 to 3.2 Å. This change is not so large. Figs.3.9 a)-c) show the ∠N-H···O dependence of the calculated principal values of shielding tensors (σ_{11}, σ_{22} and σ_{33}). The magnitudes of changes in σ_{11} and σ_{22} are about 10 and 4 ppm, respectively, in going from θ=140° to 220°. In this range of θ, the magnitudes of changes in σ_{11} and σ_{22} are about 30 and 4 ppm, respectively, in going from 2.4 to 3.2 Å. On the other hand, the magnitude of change in σ_{33} is about 1 ppm in going from θ=140° to 220° and in this range of θ the magnitude of change in σ_{33} is about 15 ppm in going from $R_{N\cdots O}$ = 2.4 to 3.2 Å. Therefore, it can be said that σ_{11} and σ_{22} are relatively sensitive with change of θ, but σ_{33} is relatively insensitive with change of θ compared with the $R_{N\cdots O}$ dependence of σ_{11}, σ_{22}. For these results, the above experimental finding be understood that there is the relationship between hydrogen bond length and σ_{33} or σ_{iso} in spite of the distribution in the hydrogen bond angles, but there is no clear relationship between $R_{N\cdots O}$ and σ_{11} or σ_{22}.

The direction of the principal axes of the Gly NH shielding tensor: The direction of the principal axes of the Gly NH ^{15}N shielding tensor components has been determined by an NMR study of a BocGlyGlyGlyOBzl single crystal[11]. It has been reported that the σ_{11} component lies approximately along the N-H bond, the σ_{33} component lies approximately along the N-C' bond, and the σ_{22} component is aligned in the direction perpendicular to the peptide plane. The results of the FPT-INDO calculations are shown in Fig.3.10. The σ_{11} component lies approximately along the N-H bond. This agrees with the experimental results. However, the σ_{22} component lies approximately along the N-C' bond, the σ_{33} component is aligned in the direction perpendicular to the peptide plane. This is different from the

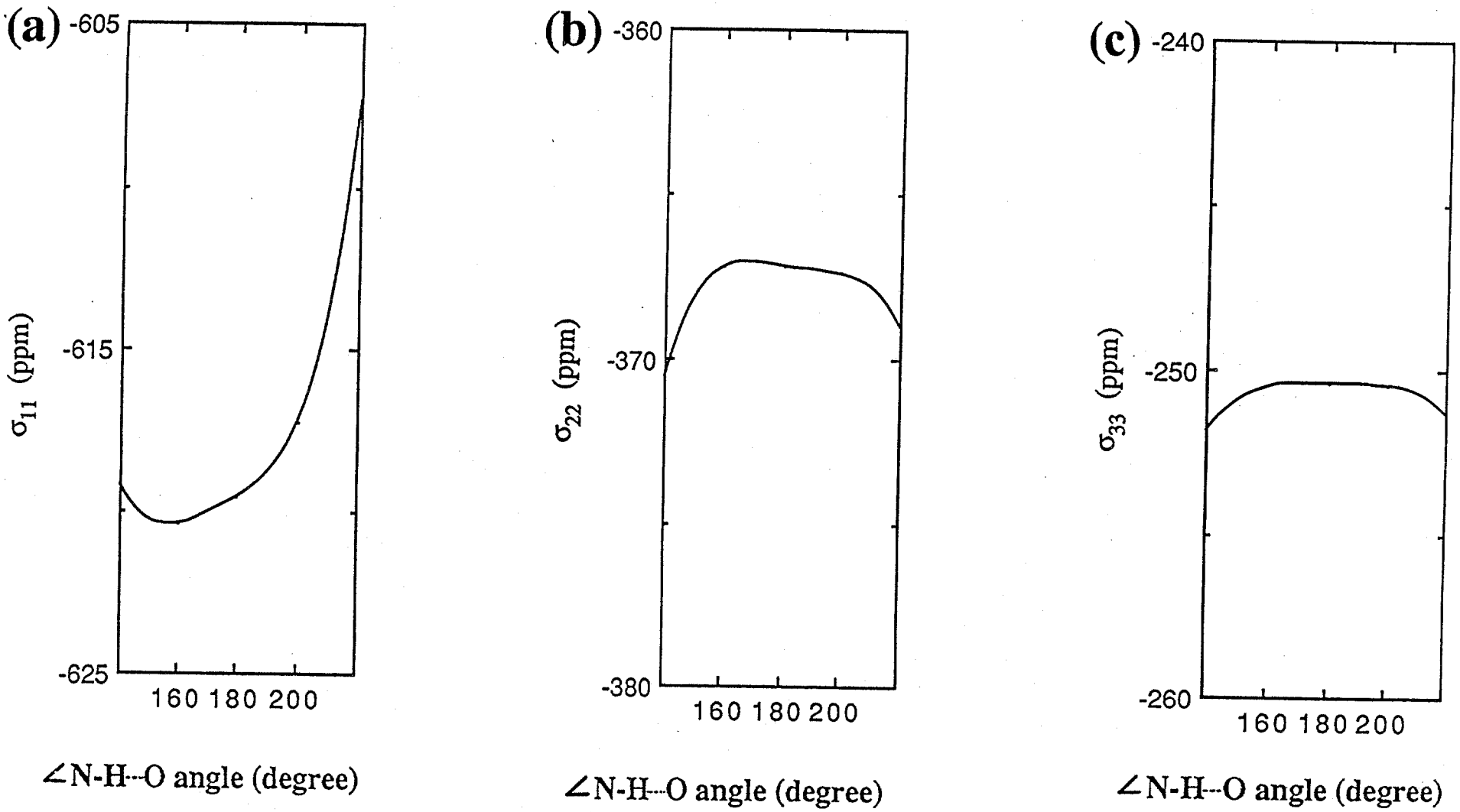

Fig3.9 Variation of the calculated ^{15}N shielding tensor components with the hydrogen bond angle ∠N-H···O (θ); σ_{11}(a), σ_{22}(b) and σ_{33}(c), respectively.

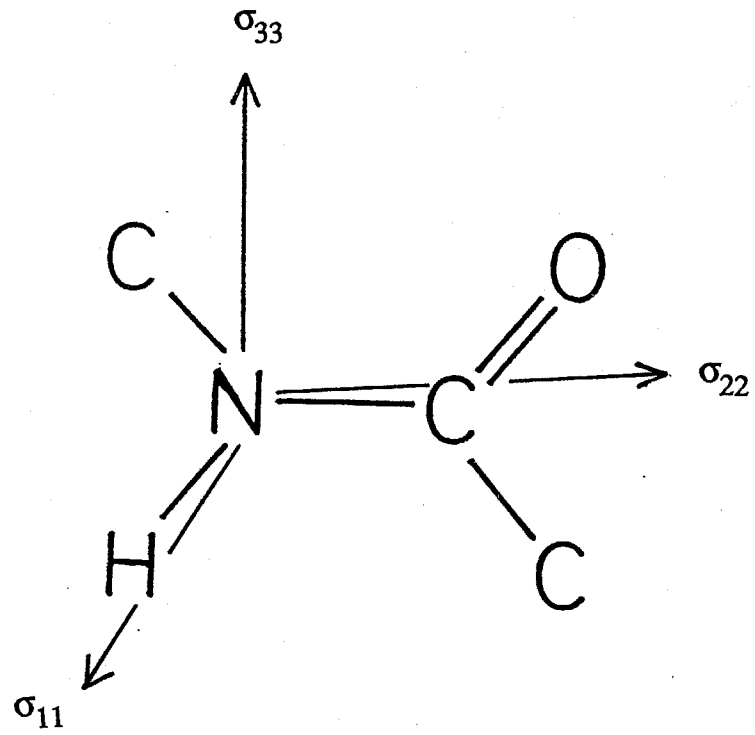

Fig.3.10 Orientation of the principal axes of the calculated ^{15}N shielding of glycine residue amide nitrogen using FPT-INDO method.

experimental results. In the experiment that it is not easy to determine the direction of the σ_{22} and σ_{33}, because the magnitudes of the σ_{22} and σ_{33} are very close to each other. In the process for determination of the directions of the σ_{22} and σ_{33} , even if the reverse assignment for the σ_{22} and σ_{33} was done, it seems that its assignment may be acceptable. It is difficult to differentiate them. The direction of σ_{11} can be easily determined, because the magnitude of σ_{11} is very different from other ones. The reason why in the theoretical calculation the most shield component σ_{33} is aligned in the direction perpendicular to the peptide plane is due to the fact that the orbital of nitrogen atom's lone-pair electrons are in its direction. The experimental results that the σ_{33} moves linearly downfield with a decrease of the hydrogen bond length, and the σ_{33} is not related with hydrogen bond angle, and that the σ_{11} and the σ_{22} are related with hydrogen bond length and hydrogen bond angle were reasonably explained by the theoretical calculation.

Finally, it can be concluded as follows. The observed isotropic ^{15}N chemical shift moves downfield with decrease of $R_{N\cdots O}$ and the principal value of the σ_{33} component moves linearly downfield with a decrease of $R_{N\cdots O}$. This was justified by quantum chemical calculation. Further, quantum calculations show that the σ_{11} and σ_{22} components are related with not only the hydrogen bond length, but also the hydrogen bond angle. These explains the experimental finding that there is no relationship between the hydrogen bond length and σ_{11} or σ_{22}. From these, it can be said that the ^{15}N chemical shift of amide nitrogen provides useful information about the hydrogen bond length and the hydrogen bond angle.

References

1) G. C. Levy and R. L. Lichter, *Nitrogen-15 Nuclear Magnetic Resonance Spectroscopy*; Wiley: New York, Chap. 6 (1979)
2) K. Wüthrich, *Nuclear Magnetic Resonance in Biological Research: Peptides and Proteins*; North-Holland: Amsterdam, Chap. 7 (1976)
3) G. A. Webb and M. Witanowski, *Proc. Indian Acad. Sci. (Chem. Sci.)*, **94** (1985) 241.
4) G. E. Hawkes, E. W. Randall and C. H. Bradley, *Nature (London)*, **257** (1975) 767.
5) W. W. Bachovchin and J. D. Roberts,*J. Am. Chem. Soc.*, **100** (1978) 8041.
6) K. L. Williamson, L. G. Pease and J. D. Roberts, *J. Am. Chem. Soc.*, **101** (1979) 714.
7) S. Kuroki, S. Ando, I. Ando, A. Shoji, T. Ozaki and G. A. Webb, *J. Mol. Struct.*, **240** (1990) 19.
8) A. Shoji, T. Ozaki, T.Fujito, K. Deguchi and I. Ando, *Macromolecules*, **20** (1987) 2441.
9) A. Shoji,T. Ozaki, T. Fujito, K. Deguchi, S. Ando and I. Ando, *Macromolecules*, **22** (1989) 2860.
10) A. Shoji, T. Ozaki, T. Fujito, K. Deguchi, S. Ando and I. Ando, *J. Am. Chem. Soc.*,**112** (1990) 4693.
11) a) Y. Hiyama, C. H. Niu, J. V. Silverton, A. Bavoso and D. A. Torchia, *J. Am. Chem. Soc.*, **110** (1988) 2378.
b) C. J. Hartzell, T. K. Pratum and G.Drobny, *J. Chem. Phys.* **87-8** (1987) 4324.
12) a) D. Zervas, D. Borovas and E. J. Gazis, *J. Am. Chem. Soc.*, **85** (1963) 3660.
b) E.Wunsch, *Synthese von Peptiden*, Thieme Verlag, Stuttgart, (1974) Teil 1 and 2.
c) N. Izumiya, T. Kato, M. Ohno and H. Aoyagi, *Peptide Synthesis*, Maruzen, Tokyo, (1975)
13) G. Valle, G. M. Bonora and C. Toniolo, *Gazzeta Chemica Italiana*, **114** (1984) 341.
14) P. M.Gadret, J. M. Leger and A. Carpy, *Acta Cryst.* **B33** (1977) 1067.
15) R.Murali, E. Subramanian and R. Parthasarathy, *Int. J. Peptide Protein Res.*, **27** (1986) 478.

16) G. D. Smith, V. Z. Pletnev, W. L. Duax,T. M. Baiasubramanian, H. E. Bosshard, E. W. Czerwinski, N. E. Kendrick, F. S. Mathews and G. R. Marshall, *J. Am. Chem. Soc.*, **103** (1981) 1493.
17) R. E. Marsh and M. R. N. Murthy, *J. Am. Chem. Soc.*, **99** (1977) 1251.
18) I. Ando, H. Saito, R. Tabeta, A. Shoji and T. Ozaki, *Macromolecules*, **17** (1984) 457.
19) F. A. Momany, R. F. McGuire, J. F. Yan and H. A. Scheraga, *J. Phys. Chem.*, **750** (1971) 2286.
20) G. A. Webb, *Annual Report on NMR Spectroscopy* ; Academic Press: London, (1986) Vol. 18
21) S. Ando, I. Ando, A. Shoji and T. Ozaki, *J. Am. Chem. Soc.*, **110** (1988) 3380.

Chapter 4

Hydrogen-Bonding Structure of Peptides and Polypeptides Containing Gly Residue in the Solid State as Studied by ^{17}O NMR Spectroscopy

4.1 Introduction

It has been reported that ^{13}C and ^{15}N NMR chemical shifts of solid peptides and polypeptides containing glycine residues and/or other amino acid residues have information about the conformation and hydrogen-bonding structure[1-7]. The carbonyl carbon ^{13}C chemical shift[1,2] and amide nitrogen ^{15}N chemical shift[3-5] of the peptides and polypeptides in the solid state are linearly displaced at downfield as the hydrogen bond length decreases. From these experimental findings, it has been demonstrated that ^{13}C and ^{15}N chemical shifts provide fruitful information about the hydrogen-bonding structure in peptides and polypeptides.

The oxygen atom is one of important atoms constituting hydrogen-bonding structure in peptides and polypeptides. Nevertheless, solid-state ^{17}O NMR study for peptides and polypeptides has never been carried out. This is due to very weak sensitivity for solid-state ^{17}O NMR measurement which comes from two following reasons. One is that ^{17}O nucleus is very low natural abundance to be 0.037 %. Another is that ^{17}O nuclear spin quantum number(I) is 5/2, which is quadrupolar nucleus, and so ^{17}O signal is broaden by nuclear quadrupolar effects in solid. On the other hand, solution-state ^{17}O NMR spectroscopy has been successfully employed to elucidate a number of structural problems in organic chemistry[8-11], because ^{17}O signal becomes very sharp due to the vanishment of quadrupolar

interaction by isotropic fast reorientation in solution. For example, as the oxygen atom is directly associated with the formation of hydrogen bond, hydrogen bonding for the carbonyl group in various compounds often results in large upfield shifts of the carbonyl ^{17}O NMR signal[12,13]. From these results, solution-state ^{17}O NMR has been established as a means for investigating structural characterizations.

From such situations, it can be expected that solid-state ^{17}O NMR provides deep insight for understanding hydrogen-bonding structure in solid peptides and polypeptides as described previously[14]. The present aim is to observe high-resolution ^{17}O NMR spectra of PG I, PG II, glycylglycine(GlyGly) and glycylglycine nitrate (GlyGly•HNO_3) in the solid state, which cover a wide range of hydrogen bond length, to obtain three kinds of NMR parameters such as chemical shift, quadrupolar coupling constant(e^2qQ/h) and asymmetric parameter(η_Q), and to understand the relationship between the hydrogen-bonding structure and these NMR parameters.

4.2 Experimental Section

Materials: 6% ^{17}O-labeled glycine(Gly) was prepared by glycine methyl ester in Na^{17}OH/methanol solution, where Na^{17}OH was prepared by reaction of 11 % ^{17}O-labeled water (purchased from Cambridge Isotope Lab.) with Na metal. Further, ^{17}O-labeled Gly N-carboxy-anhydride(NCA) was prepared using 6% ^{17}O-labeled Gly. 6% ^{17}O-labeled $(Gly)_n$ was prepared by heterogeneous polymerization of 6%-labeled ^{17}O-glycine-NCA in acetonitrile by using n-butylamine as the initiator. The mole ratio of NCA to initiator (A/I) was chosen as 100/5. The polymer of A/I = 100/1 was identified to take PG I (

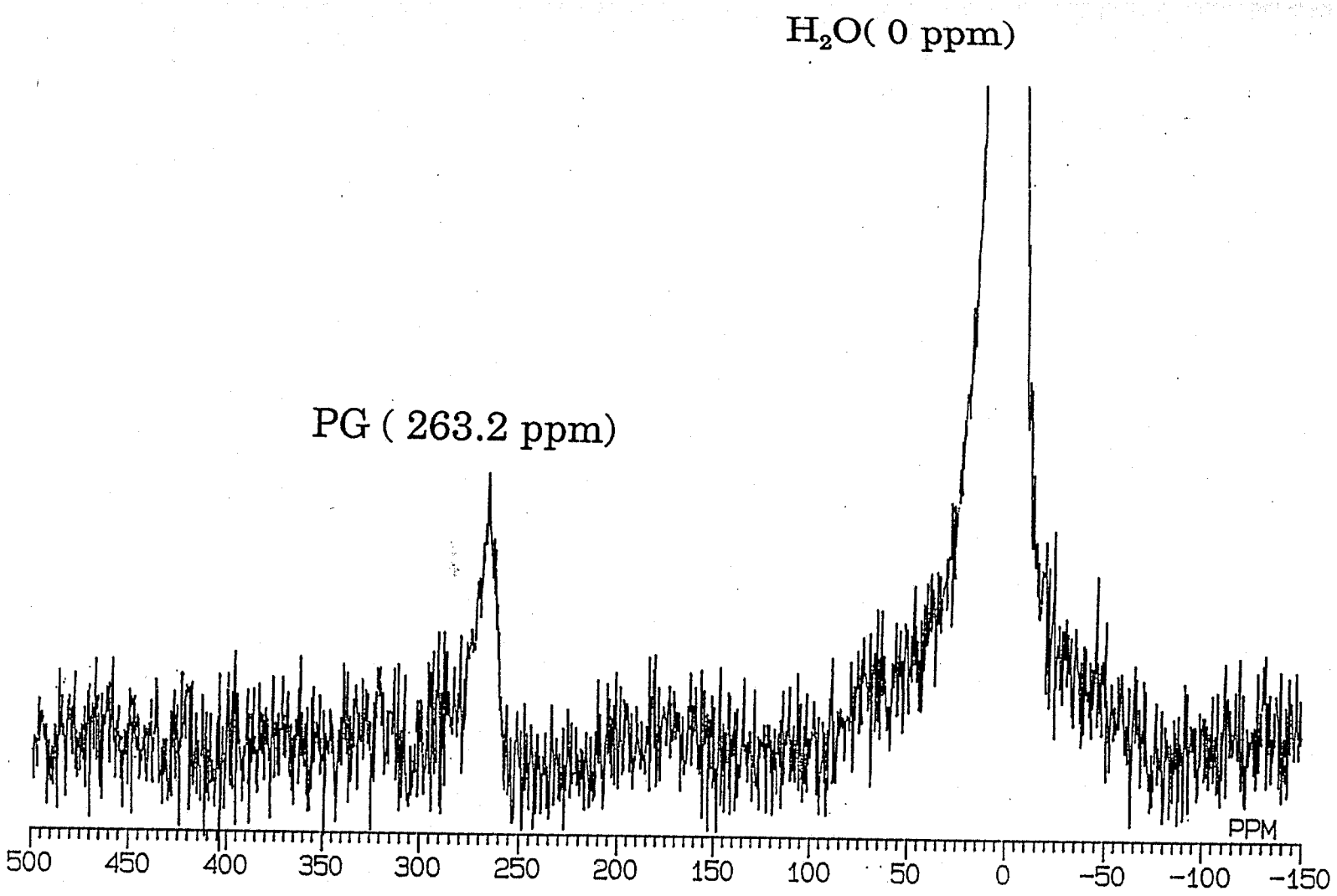

Fig.4.1 67.8MHz ^{17}O NMR spectra of PG in aqueous lithium bromide solution.

antiparallel β-sheet form)[15,16]. Conformation of this sample was converted to PG II (3_1-helix form) by the procedure of precipitation from aqueous lithium bromide solution[17]. The conformational characterization was made on the basis of ^{13}C CP/MAS(cross polarization/magic angle spinning) NMR. GlyGly was synthesized by stepwise elongation of N-hydroxysuccinimide active esters and amino acids. GlyGly•HNO_3 was obtained by slow evaporation from an equimolar mixture of GlyGly and nitric acid in water.

^{17}O-labeled samples were identified by measuring solution state ^{17}O NMR spectrum whether ^{17}O-labeling is completed or not. For examples, 67.8MHz ^{17}O NMR spectra of ^{17}O-labeled PG in aqueous lithium bromide solution was shown in Fig.4.1. The ^{17}O PG signal appears at 266.8 ppm relative to H_2O.

^{17}O NMR Measurements: ^{17}O CP static NMR spectra were recorded with a JEOL GSX-500 spectrometer operating at 67.8 MHz, with JEOL EX-400 spectrometer operating at 54.2 MHz, and with a JEOL GSX-270 spectrometer operating at 36.6 MHz, with a CP/MAS accessory at room temperature. 67.8 MHz ^{17}O solution-state NMR spectra were recorded with JEOL GSX-500 spectrometer at room temperature. The sample was contained in a cylindrical rotor made of silicon nitride. In the CP static methods, $Mg(^{17}OH)_2$ was used for ^1H-^{17}O CP matching ($\gamma_H B_H = 3\gamma_O B_O$)[18]. ^1H $\pi/2$ pulse length was 5 μs and ^{17}O $\pi/2$ pulse length was 5 μs for solid sample (which correspond to 15 μs for liquid sample such as water). ^1H decoupling field strength is 50 kHz. Repetition time was 5 s. The contact time was determined by using ^{17}O-GlyGly. In order to determine the optimum contact time for the ^{17}O CP static NMR measurement of solid peptide, the ^{17}O CP

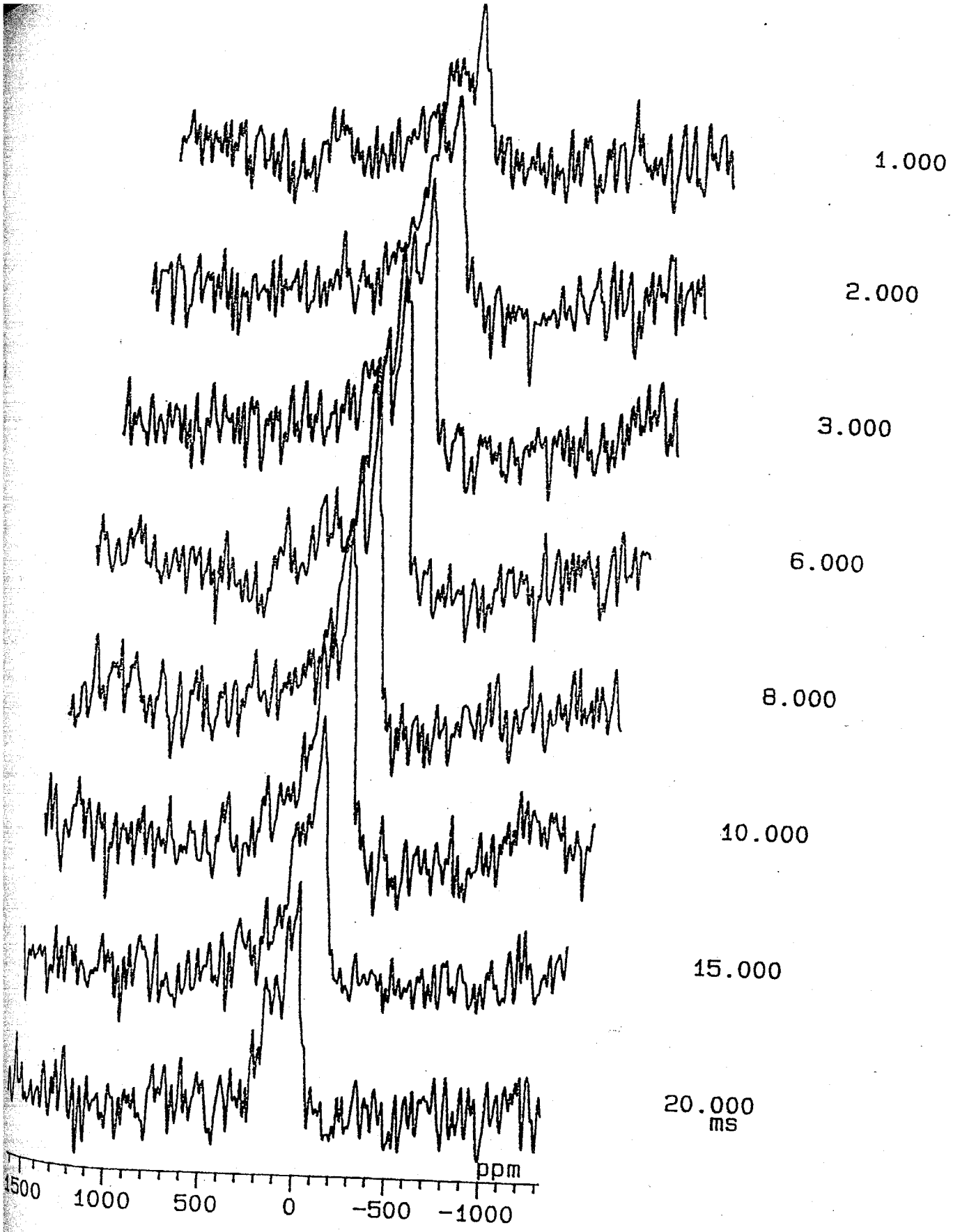

Fig.4.2 The ^{17}O NMR spectra for GlyGly as a function of the contact time.

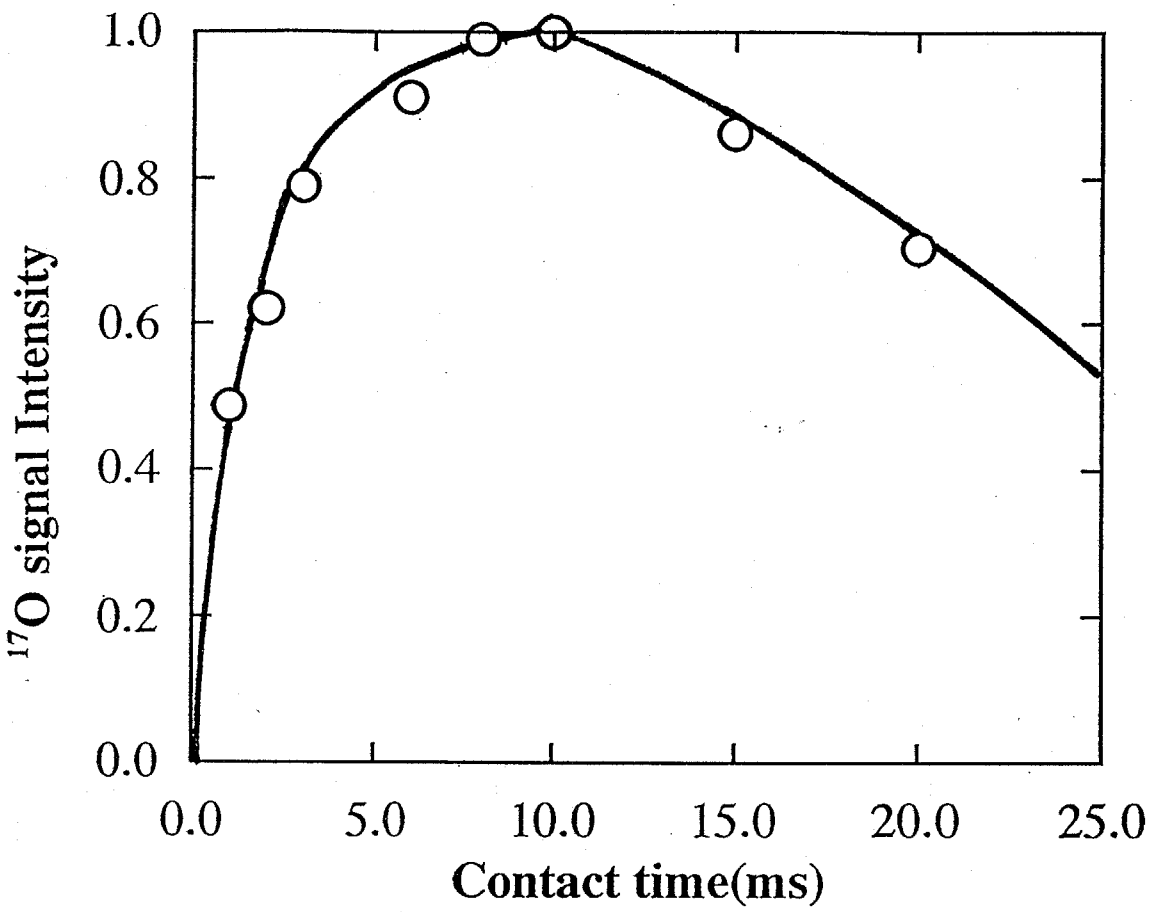

Fig.4.3 Plots of peak intensity versus cross-polarization contact time for the GlyGly.

spectra was observed as a function of contact time as shown Fig.4.2. For convenience, Fig.4.3 shows the plots of the ^{17}O NMR signal intensity for GlyGly against the contact time. Since the carbonyl oxygen atom links no hydrogen atom, long contact time is needed. The appropriate contact time was 9 ms. From the above plots, the T_{OH} and ^{1}H $T_{1\rho}$ values were determined to be 2.5 ms and 30.0 ms, respectively. The T_{OH} value of GlyGly is much longer compared with inorganic solid such as AlO(^{17}OH) whose T_{OH} value is 0.018 ms[18]. The ^{17}O chemical shifts were calibrated through external liquid water (δ= 0 ppm).

4.3 Theoretical Calculation

^{17}O Spectral Analysis: ^{17}O nucleus has 5/2 spin and has quadrupolar moment. Solid-state ^{17}O spectrum contains quadrupolar interactions, and for this, the central transition signal(-1/2, 1/2) becomes broad by the second-order perturbation. Therefore, ^{17}O static NMR signal contains eight kinds of NMR parameters such as nuclear quadrupolar coupling constant(e^2qQ/h)(which comes from the electrostatic interaction between the nuclear quadrupolar electric moment(eQ) and the electric field gradient tensor(eq)) , asymmetry parameter (η_Q), and principal values of chemical shielding tensor (σ_{11}, σ_{22} and σ_{33}), and the orientation of the principal values of chemical shift tensor in the quadrupolar frame of reference is defined by the three Euler angles(α, β, γ) as shown in Fig.4.4. In order to determine these parameters, computer simulation was carried out by superimposing the theoretical line shape[19-22] to the observed spectrum.

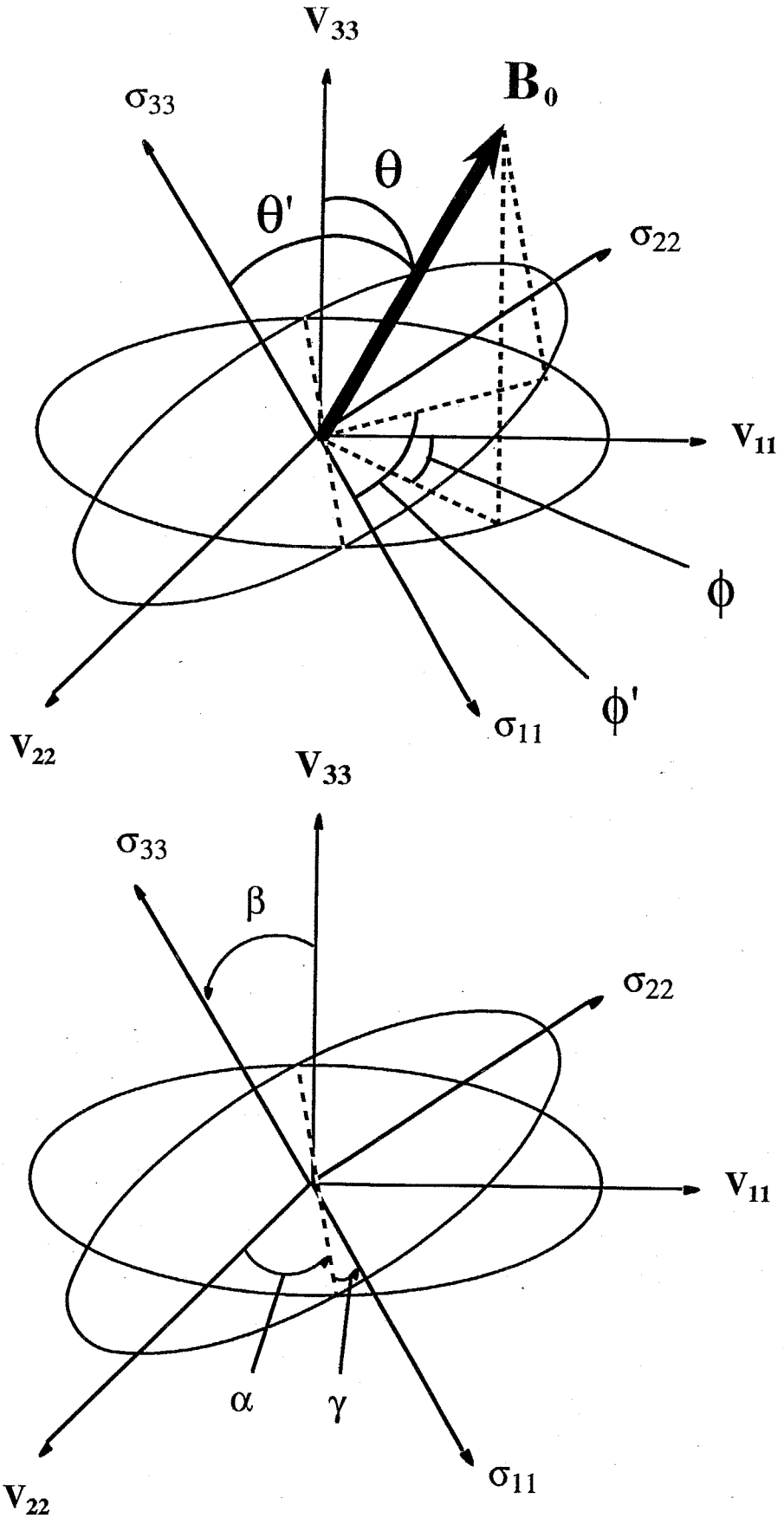

Fig.4.4 The magnetic field vector B_0 is oriented in the quadrupolar tensor by the angle (θ, ϕ) and in the chemical shielding tensor by (θ', ϕ'). The angles α, β and γ orient the chemical shielding tensor in the reference frame of the quadrupolar tensor.

In the presence of a quadrupolar interaction the quadrupolar Hamiltonian can be expressed by

$$H_{Q\pm 1/2} = -\frac{R}{6\omega_0}\left[A(\phi)\cos^4\theta + B(\phi)\cos^2\theta + C(\phi)\right] \qquad (4.1)$$

where

$$R = \omega_Q^2\left[I(I+1) - \frac{3}{4}\right]$$

$$\omega_Q = \frac{3e^2qQ}{2I(2I-1)h}$$

$$A(\phi) = -\frac{27}{8} - \frac{9}{4}\eta_Q\cos 2\phi - \frac{3}{8}\eta_Q^2\cos^2 2\phi$$

$$B(\phi) = \frac{30}{8} - \frac{\eta_Q^2}{2} + 2\eta_Q\cos 2\phi - \frac{3}{4}\eta_Q^2\cos^2 2\phi$$

$$C(\phi) = -\frac{3}{8} + \frac{\eta_Q^2}{2} + \frac{1}{4}\eta_Q\cos 2\phi - \frac{3}{8}\eta_Q^2\cos^2 2\phi$$

$$\eta_Q = \frac{V_{11} - V_{22}}{V_{33}}$$

$$|V_{33}| \geq |V_{22}| \geq |V_{11}|$$

$$V_{33} = eq$$

V_{11}, V_{22} and V_{33} are the values of the three principal elements of the electric field gradient tensor, Q is the quadrupolar moment, θ,ϕ are Euler angles relating the magnetic field $\mathbf{B_0}$ to the PAS of the electric gradient tensor of the nucleus.

In the presence of an anisotropic chemical shielding interaction Hamiltonian can be expressed as follows:

$$H_{CS} = \omega_0\left[\sigma_{11}\sin^2\theta\sin^2\phi + \sigma_{22}\sin^2\theta\cos^2\phi + \sigma_{33}\cos^2\theta\right]I_Z \quad .(4.2)$$

where σ_{11}, σ_{22} and σ_{33} are the three principal values of the chemical shielding tensor, ω_0 is the resonance frequency of nucleus, and θ and ϕ are Euler angles relating the magnetic field $\mathbf{B_0}$ to the PAS of the chemical shift tensor of the nucleus. It can be also expressed by the following form.

$$H_{CS} = \omega_0 \left[\sigma_0 + \frac{\delta}{2} \left\{ (3\cos^2\theta - 1) - \eta \sin^2\theta \cos 2\phi \right\} \right] I_Z \qquad (4.3)$$

where

$$\sigma_0 = \frac{1}{3}(\sigma_{11} + \sigma_{22} + \sigma_{33})$$

$$\delta = \sigma_{33} - \sigma_0$$

$$\eta = \frac{\sigma_{22} - \sigma_{11}}{\delta}$$

$\sigma_{33} \geq \sigma_{22} \geq \sigma_{11}$.

The total Hamiltonian expressed by Bauggher et al. is simply the sum of eqs. 4.1 and 4.3.

For more general case, one has to consider the second rank tensor properties of both the quadrupolar and shielding tensors. One cannot simply add two tensor quantities without considering the relative orientation of one tensor with respect to the other. In this case, there is no reason to believe that the PAS for the anisotropic shielding tensor will be coincident with that of the quadrupolar tensor. Hence, the first step in the analysis is to place the tensors in a common reference frame. As the quadrupolar interaction is more dominant, it is convenient to express the shielding tensor in the frame of the quadrupolar tensor. Thus, the quadrupolar resonance frequency is considered the same as that in eq.4.3. To obtain the Hamiltonian of the anisotropic chemical shielding tensor in this frame, I will utilize the standard method of employing Wigner rotation matrices. In the rotating frame, the secular chemical shielding Hamiltonian can be expressed as

$$H_{CS} = \omega_0 \sigma_0 I_Z + \gamma T_{20} R_{20}. \qquad (4.4)$$

$$T_{20} = \left(\frac{2}{3}\right)^{\frac{1}{2}} I_Z B_Z$$

To calculate the chemical shielding powder line shape in the presence of the second-order quadrupolar via angles $\Omega = (0,\theta,\phi)$. Then, from

the PAS frame of the quadrupolar it must be expressed the shielding tensor in terms of its PAS values. To do this, it will be carried out a further transformation in terms of the fixed angles (α,β,γ), which relate the quadrupolar PAS frame to the shielding PAS frame, i.e.

$$R_{20} = \sum_n D^{(2)}_{0,n}(0,\theta,\phi)^* r_{2n}$$

$$= \sum_n D^{(2)}_{n,0}(-\phi,\theta,0) r_{2n}$$

$$H_{CS} - \omega_0\sigma_0 I_Z = \gamma T_{20}[D_{00}(-\phi,\theta,0)r_{20} + D_{-10}(-\phi,\theta,0)r_{2-1} + D_{10}(-\phi,\theta,0)r_{21} + D_{-20}(-\phi,\theta,0)r_{2-2} + D_{20}(-\phi,\theta,0)r_{20}] \quad (4.5)$$

Where $D_{n,m}$ are the Wigner rotation matrix elements. When these elements are incorporated into this equation, eq.4.5 has the following form:

$$H_{CS} - \omega_0\sigma_0 I_Z = \gamma T_{20}[((3\cos^2\theta - 1)/2)r_{20} - \left(\frac{3}{8}\right)^{\frac{1}{2}} \sin 2\theta e^{-i\phi} r_{2-1} + \left(\frac{3}{8}\right)^{\frac{1}{2}} \sin 2\theta e^{-i\phi} r_{21} + \left(\frac{3}{8}\right)^{\frac{1}{2}} \sin^2\theta e^{-i\phi} + \left(\frac{3}{8}\right)^{\frac{1}{2}} \sin^2\theta e^{i2\phi} r_{22}] \quad (4.6)$$

$$T_{20} = \left(\frac{2}{3}\right)^{\frac{1}{2}} I_Z B_0$$

At this point the shielding tensor is transformed from the quadrupolar PAS to its own PAS frame and ρ_{2m} can be expressed as

$$r_{2m} = \sum_n D^{(2)}_{mn}(\alpha,\beta,\gamma)^* \rho_{2n}$$

$$= \sum_n D^{(2)}_{mn}(-\gamma,-\beta,-\alpha)\rho_{2n} \,. \quad (4.7)$$

Further

$$\rho_{2n} = \left(\frac{3}{2}\right)^{\frac{1}{2}} \delta$$

$$\rho_{2\pm2} = -\left(\frac{1}{2}\right)\eta\delta$$

$$\delta = \frac{2}{3}\left[\sigma_{33} - \left(\frac{\sigma_{11} + \sigma_{22}}{2}\right)\right]$$

$$\eta = \frac{\sigma_{11} - \sigma_{22}}{\sigma_{33} - \sigma_0}$$

and all other ρ_{2n} are vanished. Substitution of all the ρ_{2m}, D_{nm} and T_{20} in eq.4.7 into eq.4.6 yields eq.4.8; this gives us the shielding Hamiltonian of the chemical shift, which has been transformed to the quadrupolar PAS frame, expressed in terms of its value in the shielding frame:

$$\begin{aligned} H_{CS} - \omega_0\sigma_0 I_Z = \left(\frac{\omega_0 I_Z \delta}{2}\right)[&(3\cos^2\theta - 1)\left(\frac{3\cos^2\beta - 1}{2} - \frac{\eta}{2}\sin^2\beta\cos 2\gamma\right) \\ &+ \sin 2\theta\cos(\phi+\alpha)\left\{-\frac{3}{2}\sin 2\beta - \eta\sin\beta\cos\beta\cos 2\gamma\right\} \\ &+ \sin 2\theta\sin(\phi+\alpha)\{\eta\sin\beta\sin 2\gamma\} \\ &+ \frac{1}{2}\sin^2\theta\cos 2(\phi+\alpha)\left\{3\sin^2\beta - \eta\cos 2\gamma(1+\cos^2\beta)\right\} \\ &+ \frac{1}{2}\sin^2\theta\sin 2(\phi+\alpha)\{2\eta\cos\beta\sin 2\gamma\}] \end{aligned} \qquad (4.8)$$

Note that when $(\alpha,\beta,\gamma)=(0,0,0)$ eq.4.8 reduces to eq.4.3. In our line shape simulations the Hamiltonian of the system is the sum of eqs.4.1 and 4.8 as well as the Zeeman term.

From these Hamiltonians, the central transition (-1/2, 1/2) will be at the frequencies given by

$$\omega = \omega_{CS} + \omega_{Q\pm\frac{1}{2}} \,. \qquad (4.9)$$

where,

$$\begin{aligned} \omega_{CS} = \sigma_0 + \left(\frac{\delta}{2}\right)[&(3\cos^2\theta - 1)\left(\frac{3\cos^2\beta - 1}{2} - \frac{\eta}{2}\sin^2\beta\cos 2\gamma\right) \\ &+ \sin 2\theta\cos(\phi+\alpha)\left\{-\frac{3}{2}\sin 2\beta - \eta\sin\beta\cos\beta\cos 2\gamma\right\} \\ &+ \sin 2\theta\sin(\phi+\alpha)\{\eta\sin\beta\sin 2\gamma\} \\ &+ \frac{1}{2}\sin^2\theta\cos 2(\phi+\alpha)\left\{3\sin^2\beta - \eta\cos 2\gamma(1+\cos^2\beta)\right\} \end{aligned}$$

$$+\frac{1}{2}\sin^2\theta\sin 2(\phi+\alpha)\{2\eta\cos\beta\sin 2\gamma\}] \qquad (4.10)$$

$$\omega_{Q\pm\frac{1}{2}} = -\frac{R}{6\omega_0{}^2}\left[A(\phi)\cos^4\theta + B(\phi)\cos^2\theta + C(\phi)\right]\times 10^6 \qquad (4.11)$$

These formulas are described by ppm unit. It can be obtained quadrupolar spectrum from the integral over whole spherical angle.

$$\cos\theta = \frac{p}{M} \qquad (4.12)$$

$$\phi = \frac{2\pi}{M}p \quad (p=0,1,\ ...,\ M). \qquad (4.13)$$

when M=200, and p is changed from 0 to M, cos θ and ϕ are obtained from eqs.4.12 and 4.13, and ω is obtained by substituting these values in eq.4.9.

The static powder spectrum by integration over possible orientations was calculated. Sun 4 SPARC Station was used for the calculations. It takes for about 1 minute to obtain a simulated spectrum.

The direction of the principal axes of the electric field gradient and chemical shielding calculations: In this work, I calculated relative direction of the principal axes of the electric field gradient and chemical shielding of a dipeptide fragment, N-acetyl-N'-methyl glycineamide(forming hydrogen bonds with a formamide molecule), employing the finite perturbation theory(FPT)-MNDO-PM3 method. In the following chapter, I will describe this methods in detail. The bond lengths and bond angles proposed by Momany et al.[23] were used. Sun 4 SPARC Station was used for the calculations.

4.4 Results and Discussion

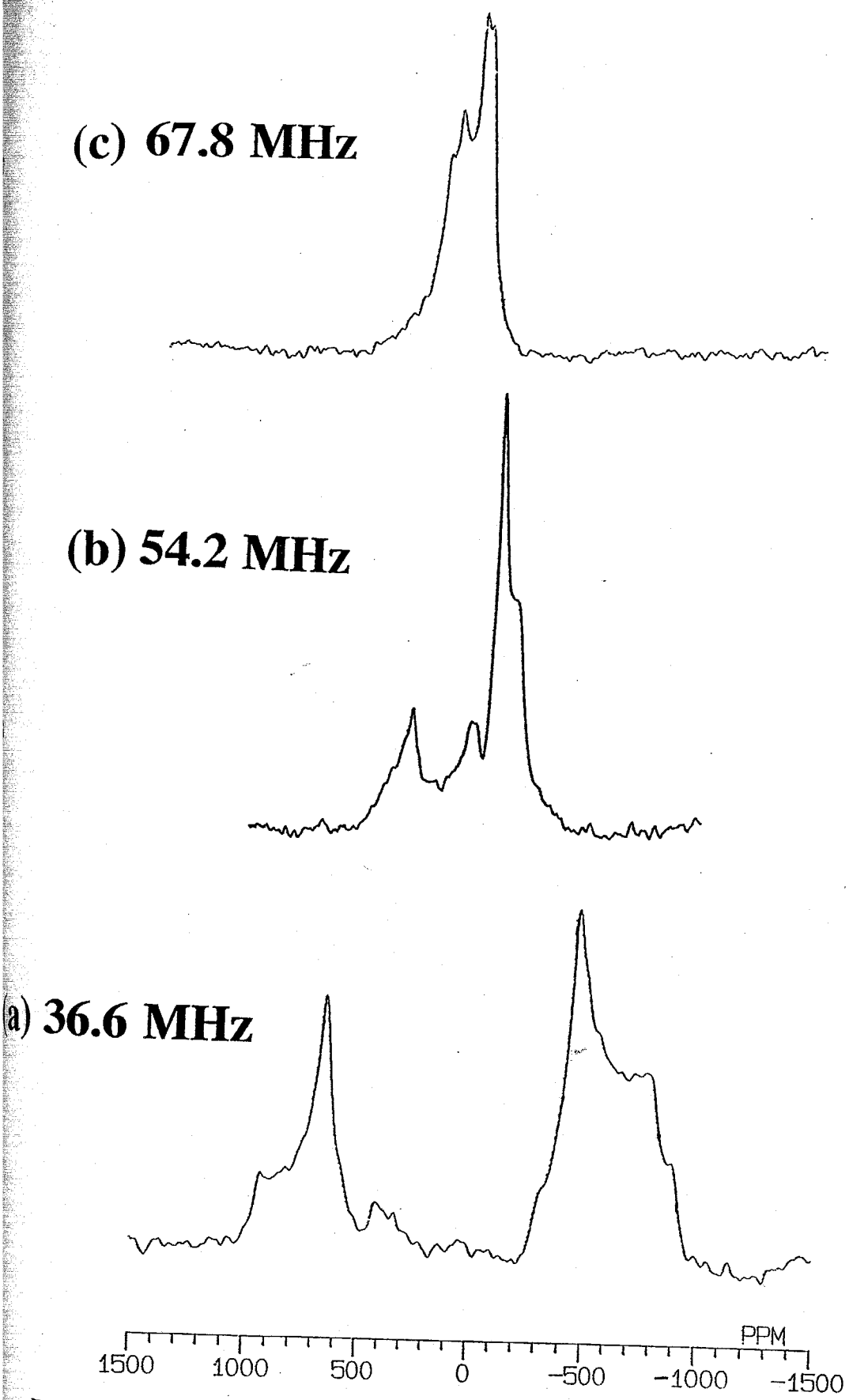

Fig.4.5 36.6 (a), 54.2 (b) and 67.8 (c) MHz CP static spectra of GlyGly in the solid state, respectively

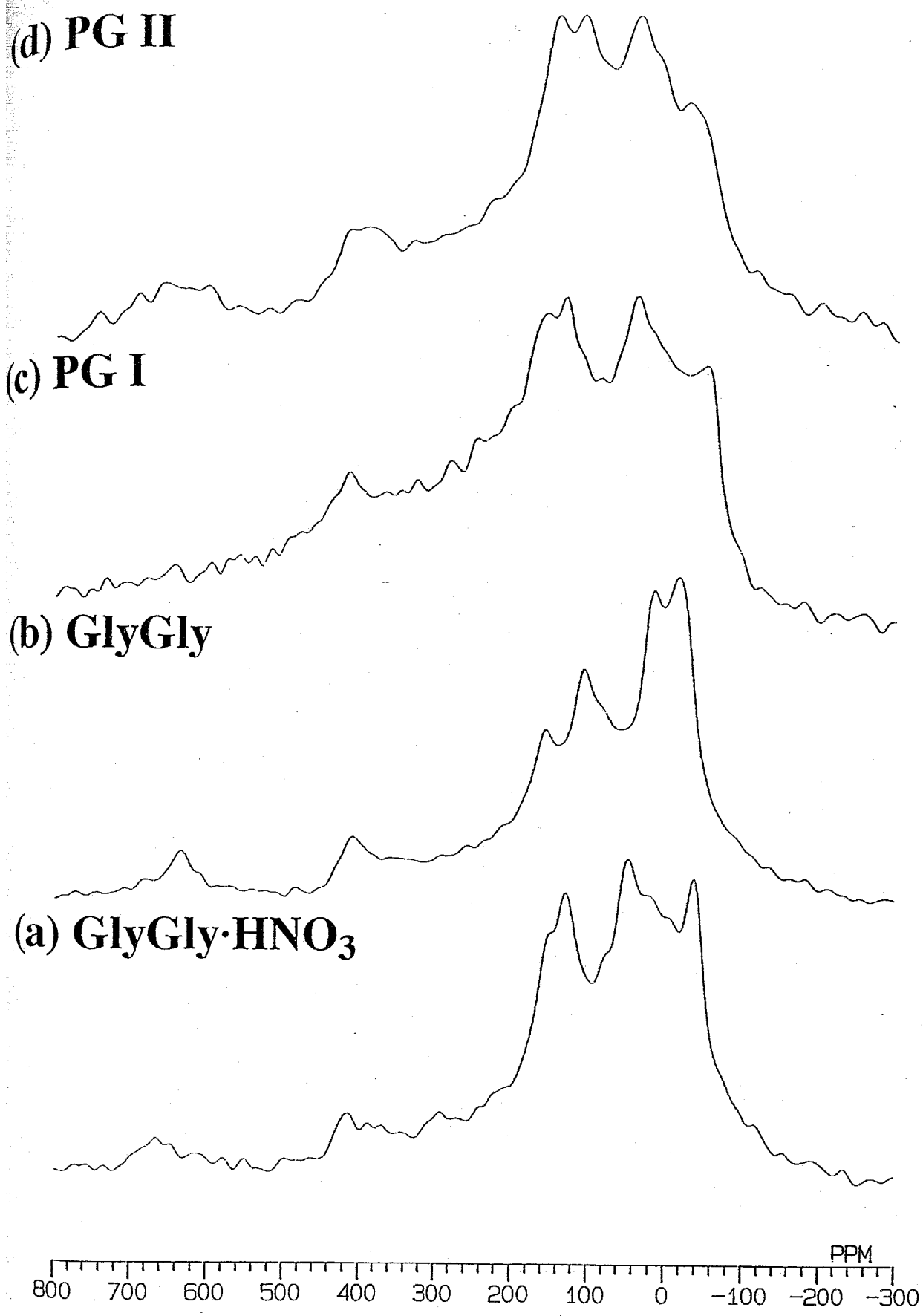

Fig.4.6 67.8 MHz ^{17}O CP static NMR spectra of GlyGly·HNO_3 (a), GlyGly (b), PGI (c), and PGII (d), respectively.

Static ^{17}O CP spectra of ^{17}O-labeled peptides and polypeptides: Static ^{17}O CP NMR spectra of GlyGly were observed at 36.6, 54,2 and 67.8 MHz as shown in Fig.4.5. Each of the spectra at 36.6 and 54.2 MHz consists of two major splitting signals, but the spectrum at 67.8 MHz has only one major signal. Such splitting comes from the quadrupolar interaction. By the computer simulation, the quadrupolar coupling constant e^2qQ/h was determined to be 8.55 MHz. This value is much larger than that for amide ^{14}N nitrogen nuclei(1.11MHz). It is seen that the NMR spectra strongly depend on the measurement frequency because quadrupolar effect depends on the measurement frequency and the broadening of ^{17}O NMR signal is further increased by quadrupolar effect as the measurement frequency is decreased. Therefore, it can be said that high-frequency measurement is needed for quadrupolar nucleus such as ^{17}O.

Fig.4.6 shows 67.8 MHz static ^{17}O CP NMR spectra of PG I, PG II, GlyGly and GlyGly•HNO_3. The computer simulations were performed for superimposing theoretically-calculated spectra to the experimental spectra on computer display. To determine the ^{17}O NMR parameters unequivocally, the computer simulations for different frequencies such as 36.6, 54,2 and 67.8 MHz were carried out. At first, for examples, Fig.4.7 shows 67.8, 54,2 and 36.6 MHz static ^{17}O CP NMR spectra of GlyGly together with theoretically-calculated spectra. Next, Fig.4.8 shows 67.8 static ^{17}O CP NMR spectra of PG I, PG II, GlyGly and GlyGly•HNO_3 together with theoretically-calculated spectra, respectively. The ^{17}O NMR parameters of PG I, PG II, GlyGly and GlyGly•HNO_3 obtained by computer simulations are shown in Table 4.1. From these results, the δ_{11}, δ_{22} and δ_{33} values of the samples change from 546 to 574 ppm, 382 to 425 ppm, and -132 to -101 ppm,

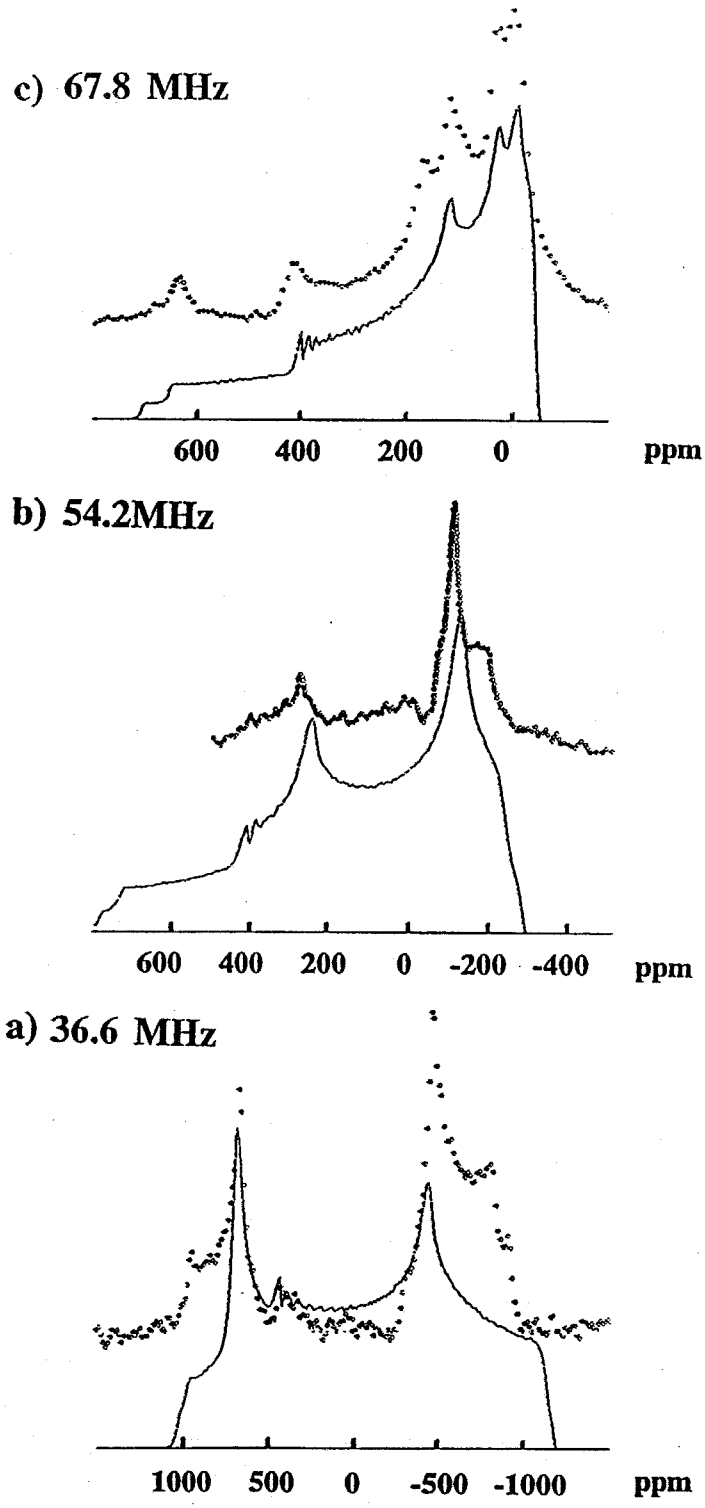

Fig.4.7 36.6 MHz (a), 54.2 MHz (b) and 67.8 MHz (c) ^{17}O CP static spectra of GlyGly together with theoretically-simulated spectra, respectively.

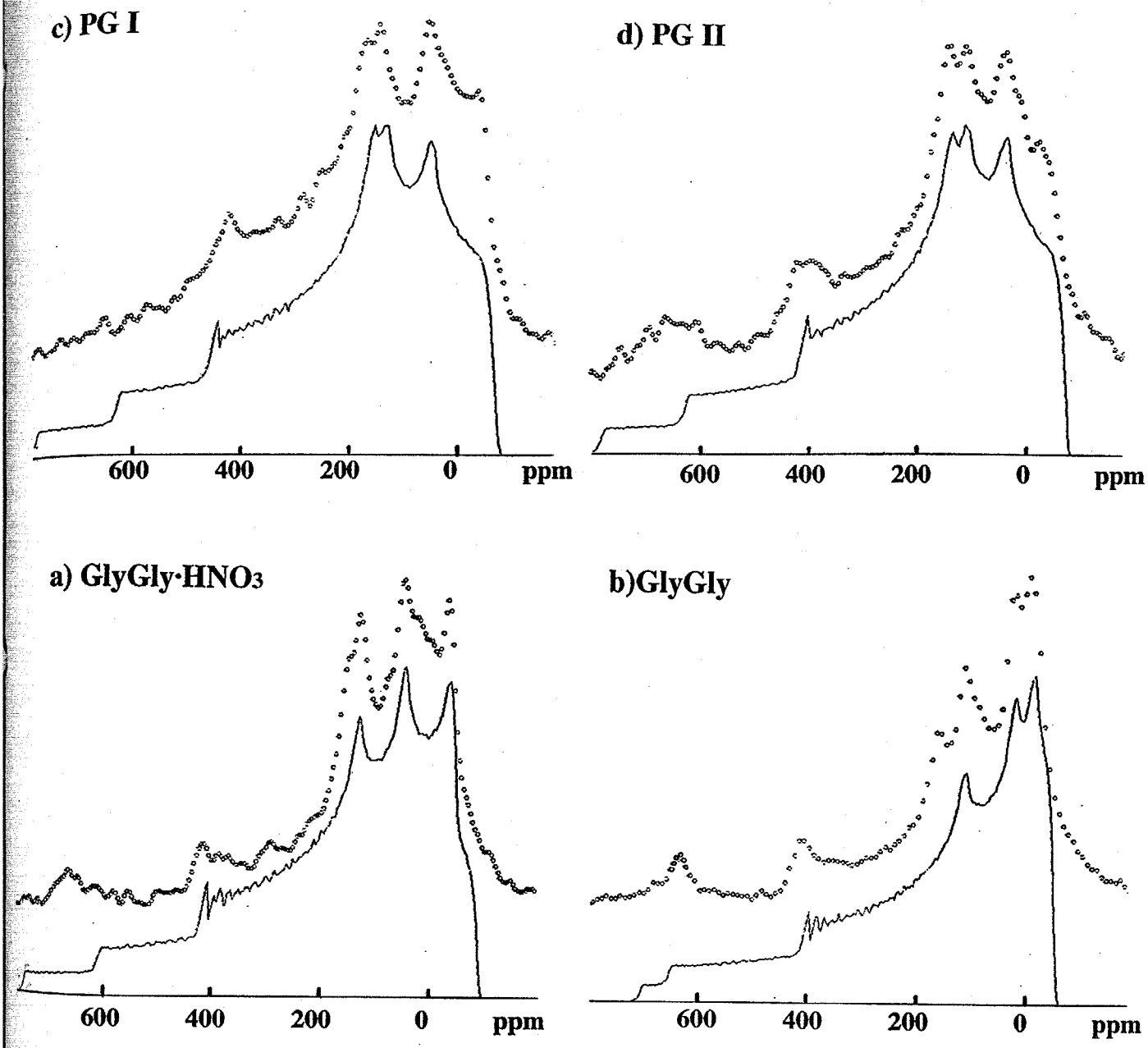

Fig.4.8 67.8 MHz ^{17}O CP static NMR spectra of GlyGly·HNO_3 (a), GlyGly (b), PGI (c), and PGII (d) together with theoretically-simulated spectra, respectively.

Table 4.1 Determined ^{17}O NMR parameters of solid peptides containing Gly residue.

Sample	e^2qQ/h (MHz)	η_Q	Chemical shift tensor (ppm) δ_{11}	δ_{22}	δ_{33}	δ_{iso}	$\Delta\delta^b$	η^c	Angle Δ^a(deg.) α	β	γ
polypeptides											
PG II	8.30	0.29	562	410	-108	288	396	0.38	92	89	-81
PG I	8.55	0.26	574	425	-101	299	400	0.37	100	91	-79
oligopeptides											
GlyGly	8.55	0.45	546	382	-132	265	397	0.41	94	90	-87
GlyGly•HNO_3	8.75	0.47	559	408	-127	280	407	0.37	94	89	-81

a) Angle Δ indicates the Euler angles between the principal axes of the quadrupolar tensor and the chemical shift tensor.
b) $\Delta\delta = \delta_{iso} - \delta_{33}$.
c) $\eta = (\delta_{11} - \delta_{22}) / \Delta\delta$.

respectively. The magnitude of change in chemical shift is much larger than that of the carbonyl ^{13}C and amide ^{15}N chemical shift. Every $\Delta\delta$ defined by $\Delta\delta=\delta_{33}-\delta_{iso}$, is about 400 ppm, which is much larger than of the carbonyl ^{13}C and amide ^{15}N chemical shift, which are about 170, 100 ppm, respectively. Every η value defined by $\eta=(\delta_{22}-\delta_{11})/\Delta\delta$ is about 0.4. These values are common to the carbonyl oxygen in peptides. Though the chemical shift tensor is axially-symmetry ($\delta_{11}=\delta_{22}$) for the case of carbonyl oxygen of L-alanine amino acid as reported by Fiat et al.[24,25], the chemical shift tensor of carbonyl oxygen in peptide is not axially-symmetry from these results. The e^2qQ/h values change from 8.30 MHz to 8.75 MHz. This values are larger than the e^2qQ/h value of L-leucine which is 8.0 MHz at 190 K[25]. The η_Q values of polypeptides such as PG I and II are 0.26 and 0.29, and the η_Q values of oligopeptides such as GlyGly and GlyGly•HNO_3 are 0.45, 0.47, respectively. This difference may come from large difference in molecular packing between them. Further, it is found that the principal axis of the quadrupolar tensor and the principal axis of the ^{17}O chemical shielding tensor for carbonyl oxygen of peptides and polypeptides are not coincident with each other. The relationship these two principal axes is shown in Fig.4.9 for the situation of PG II. Each of the above NMR parameters is strongly influenced by the electronic structure of molecules. This seems to be slight difference in their affects by the characteristic electronic distribution of the carbonyl oxygen of peptides and polypeptides.

The direction of the principal axes of the electric field gradient tensor and the chemical shielding of carbonyl oxygen: No studies have ever tried to determine the direction of the

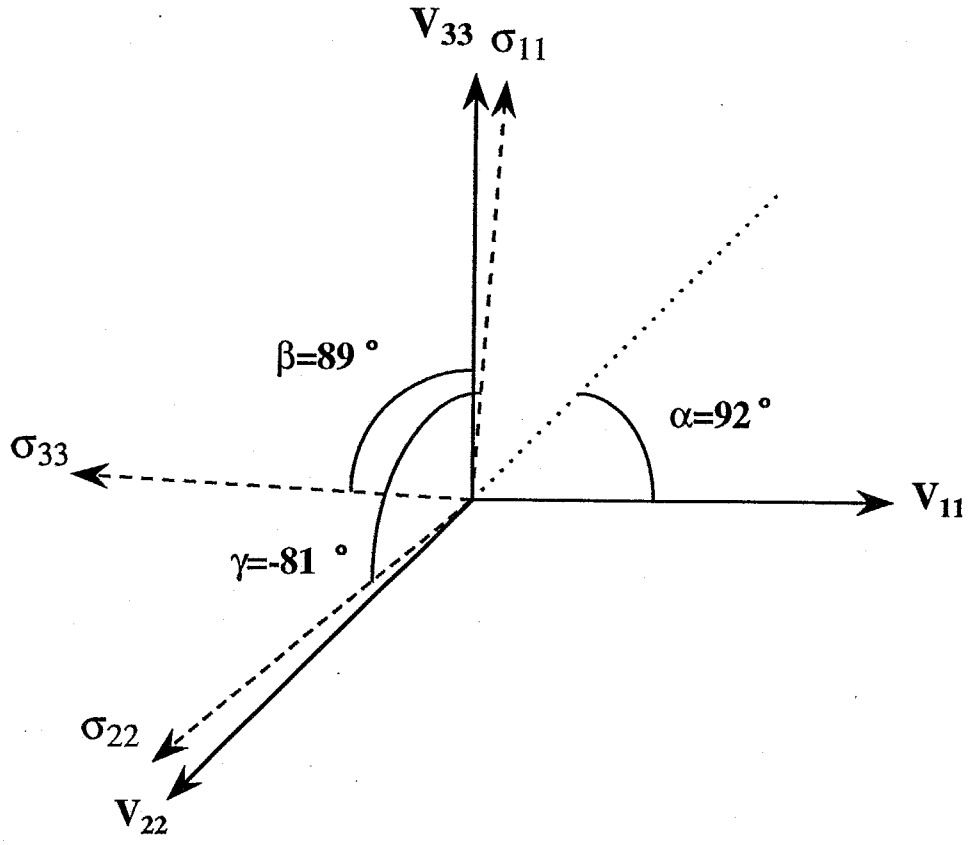

Fig4.9 The relationship between the principal axes of quadrupolar tensor and chemical shift tensor on carbonyl oxygen for the situation of PG II.

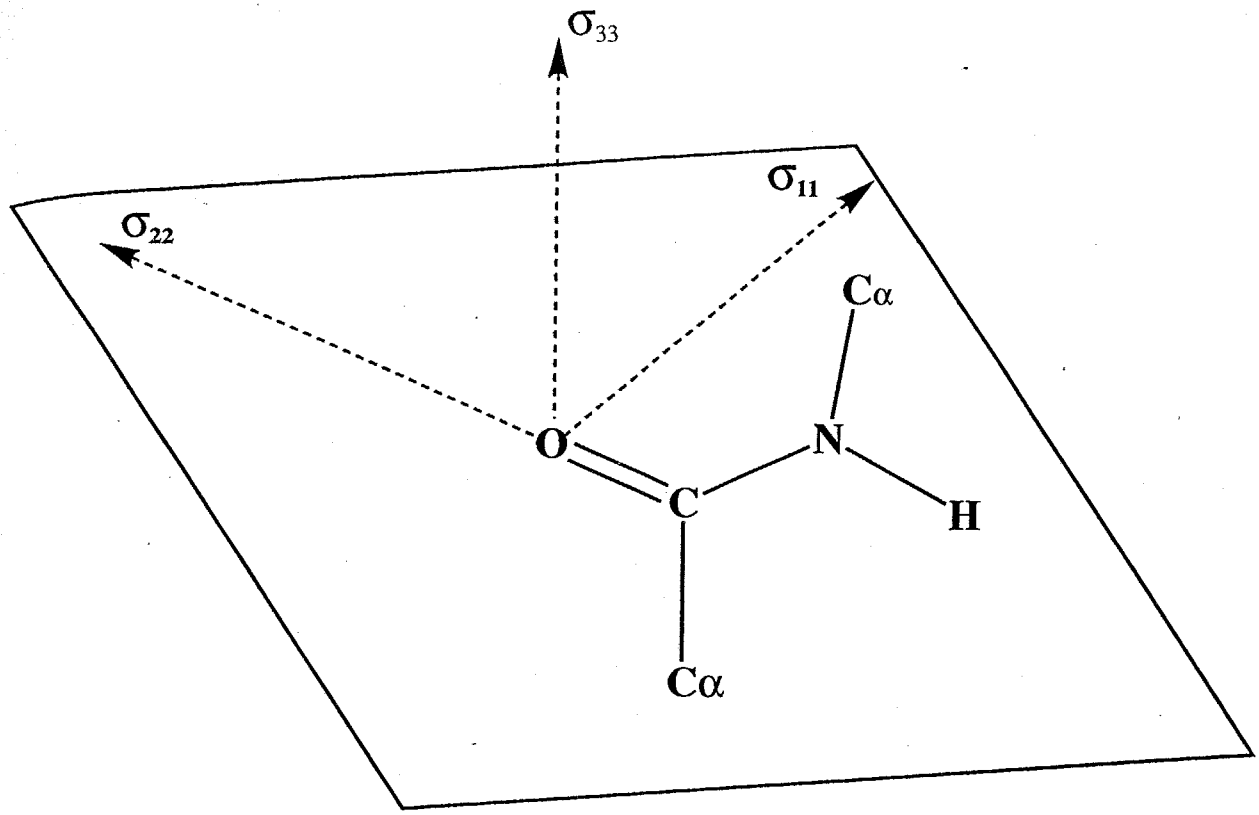

Fig.4.10 The direction of the principal axes of the chemical shielding of carbonyl oxygen employing FPT-MNDO-PM3 method.

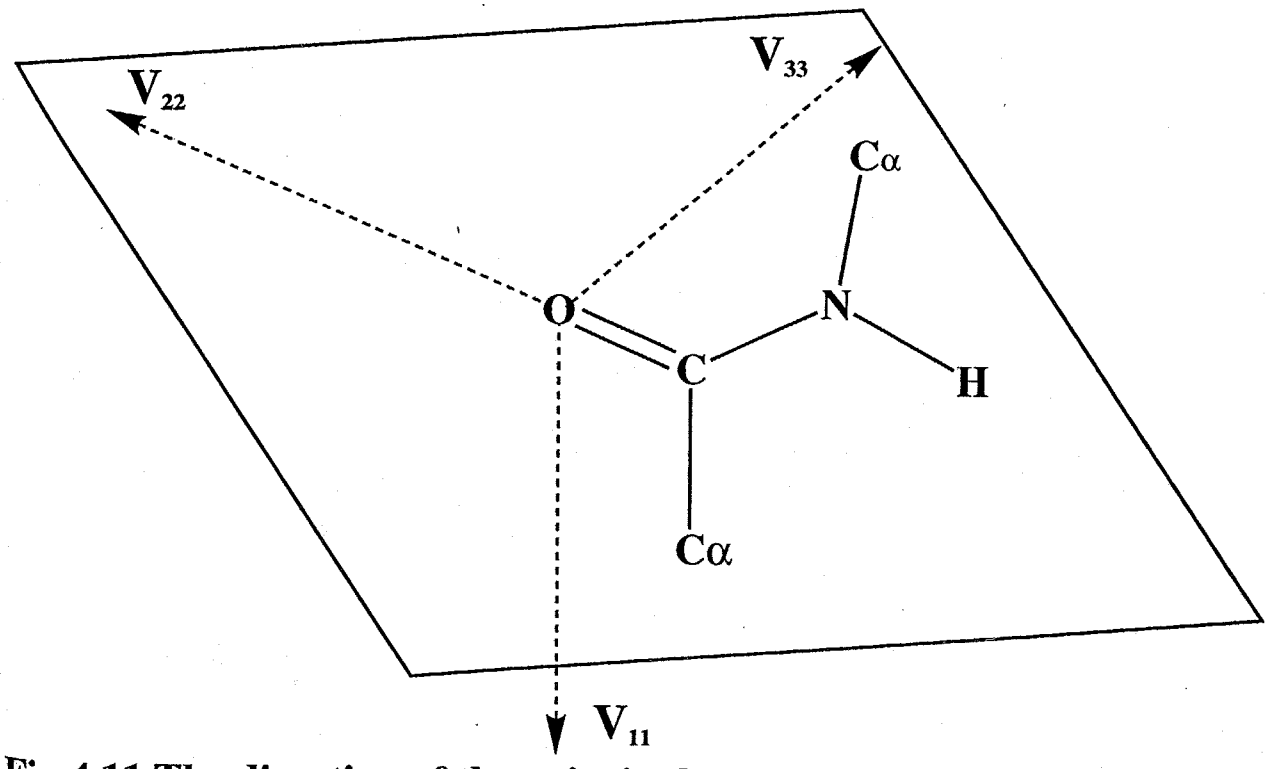

Fig.4.11 The direction of the principal axes of the electric field gradient tensor of carbonyl oxygen employing FPT-MNDO-PM3 method.

principal axes of the electric field gradient tensor and the chemical shielding of carbonyl oxygen from experiment. I tried to determine the direction of the principal axes of the chemical shielding of the carbonyl oxygen is shown in Fig.4.10 as determined by FPT-MNDO-PM3 method. The σ_{22} component lies approximately along the C=O bond, the σ_{11} component is aligned in the direction perpendicular to the C=O bond on the peptide plane, and the σ_{33} which is the most shielded component is aligned in the direction perpendicular to the peptide plane. It is a very interested result that the most shield component σ_{33} is not aligned along the direction of the C=O bond or the direction of lone pair electron which are aligned 120° or -120° from the C=O bond direction on the peptide plane. It can be said that sp^2 hybrid property of the carbonyl bond get out because of the double bonding property of the peptide bond.

On the other hand, the direction of the principal axes of the electric field gradient tensor of the carbonyl oxygen is shown in Fig. 4.11 as determined by FPT-MNDO-PM3 method. The V_{22} component lies approximately along the C=O bond, the V_{33} component is aligned in the direction perpendicular to the C=O bond on the peptide plane, and the V_{11} is aligned in the direction perpendicular to the peptide plane. It can be said that the largest component V_{33} of the electric field gradient lies along the molecular chain direction. The relationship between the electric field gradient tensor and the chemical shielding employing this calculation agree with the experimental results in Fig.4.9.

Nuclear quadrupolar coupling constant (e^2qQ/h) of carbonyl oxygen of peptides and polypepides: The geometrical parameters

Table 4.2 The geometrical parameters and hydrogen-bonding geometrical parameters of peptides containing Gly residue.

	Geometrical parameters		Hydrogen-bonding geometrical parameters						
	Dihedral angle(deg.)		H.B. length(Å)		H.B. angle (deg.)		H.B. dihedral angle(deg.)		ref.
Sample	ϕ	ψ	N···O	H···O	∠C=O···N	∠N-H···O	N-C=O···H	C=O···H-N	
PG II	-78.0	145.8	2.73	1.84	159	146	-47	157	17
PG I	-149.9	146.5	2.95	2.16	149	133	68	-173	16
GlyGly	157.1	151.0	2.94	1.97	157	157	-161	-145	26
GlyGly •HNO_3	165.6	148.9	3.12	2.38	162	165	3	-156	27

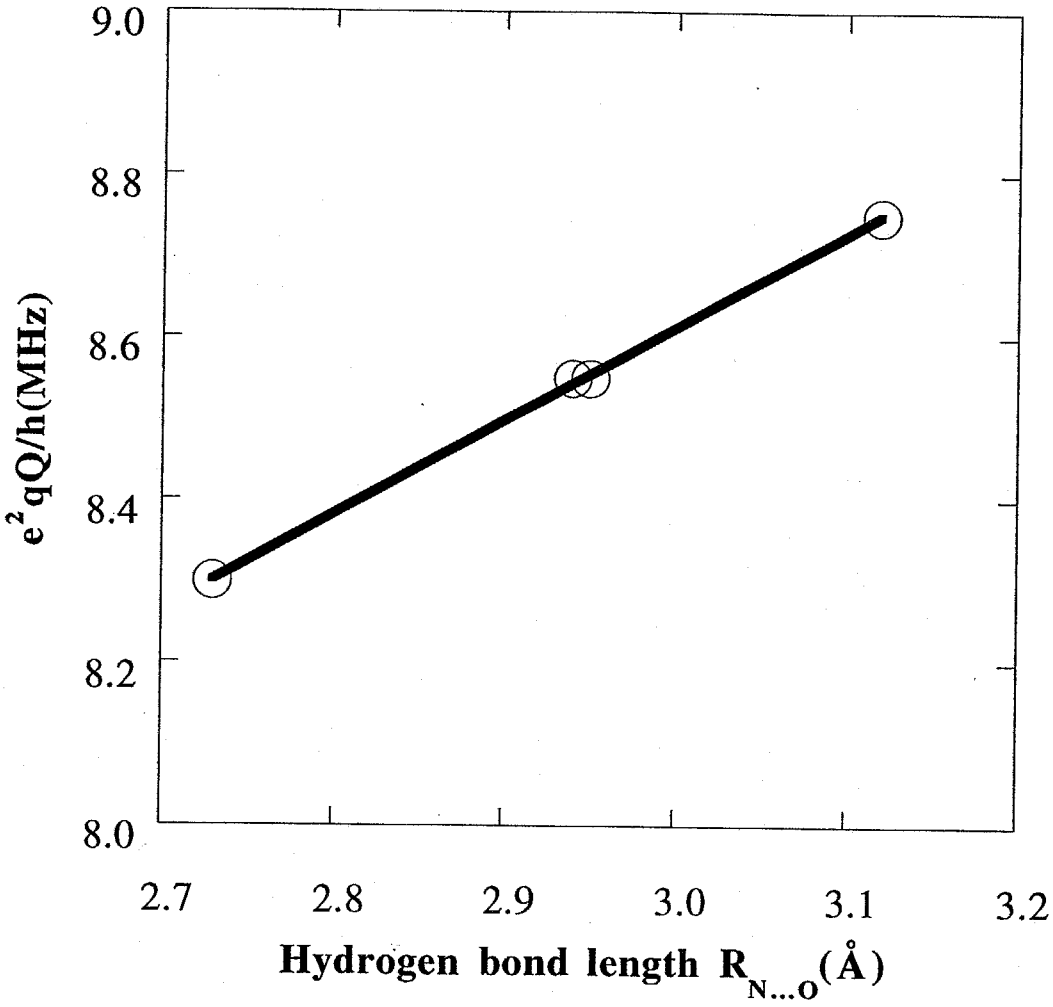

Fig.4.12 Plots of the e^2qQ/h against the hydrogen bond length.

and hydrogen-bonding geometrical parameters of these peptides and polypeptides are shown in Table 4.2. Some of the geometrical parameters were calculated by using the unit cell parameters and fractional coordinates as given in the literature[16,17,26,27]. Fig.4.12 shows the plot of the observed e^2qQ/h values against the hydrogen bond length. The e^2qQ/h values decrease linearly with a decrease of the hydrogen bond length ($R_{N\cdots O}$). This relationship is expressed by

$$e^2qQ/h(MHz)=5.15+1.16R_{N\cdots O}(Å) . \qquad (4.14)$$

This change comes from change of the q values which are the largest component of electric gradient tensor(V_{33}). This experimental result shows that the decrease in the hydrogen bond length leads to the decrease of electric gradient. The q value seem to be very sensitive in the hydrogen-bonding length change.

^{17}O NMR chemical shifts of carbonyl oxygen of peptides and polypeptides: From Table 4.1, there is large difference in the chemical shift value between peptides and polypeptides. Fig.4.13 shows the plot of the observed isotropic ^{17}O chemical shifts (δ_{iso}) against the hydrogen bond length ($R_{N\cdots O}$). The δ_{iso} values in both peptides and polypeptides move upfield with decrease in the hydrogen bond length($R_{N\cdots O}$). Figs.4.14a)-c) show the plot of the observed principal values of ^{17}O chemical shifts against the hydrogen bond length ($R_{N\cdots O}$). Every principal value in both peptides and polypeptides moves upfield with decrease in the hydrogen bond length($R_{N\cdots O}$).

What is the origin of the difference of chemical shift between peptides and polypeptides? There seem to be two origins. One is the

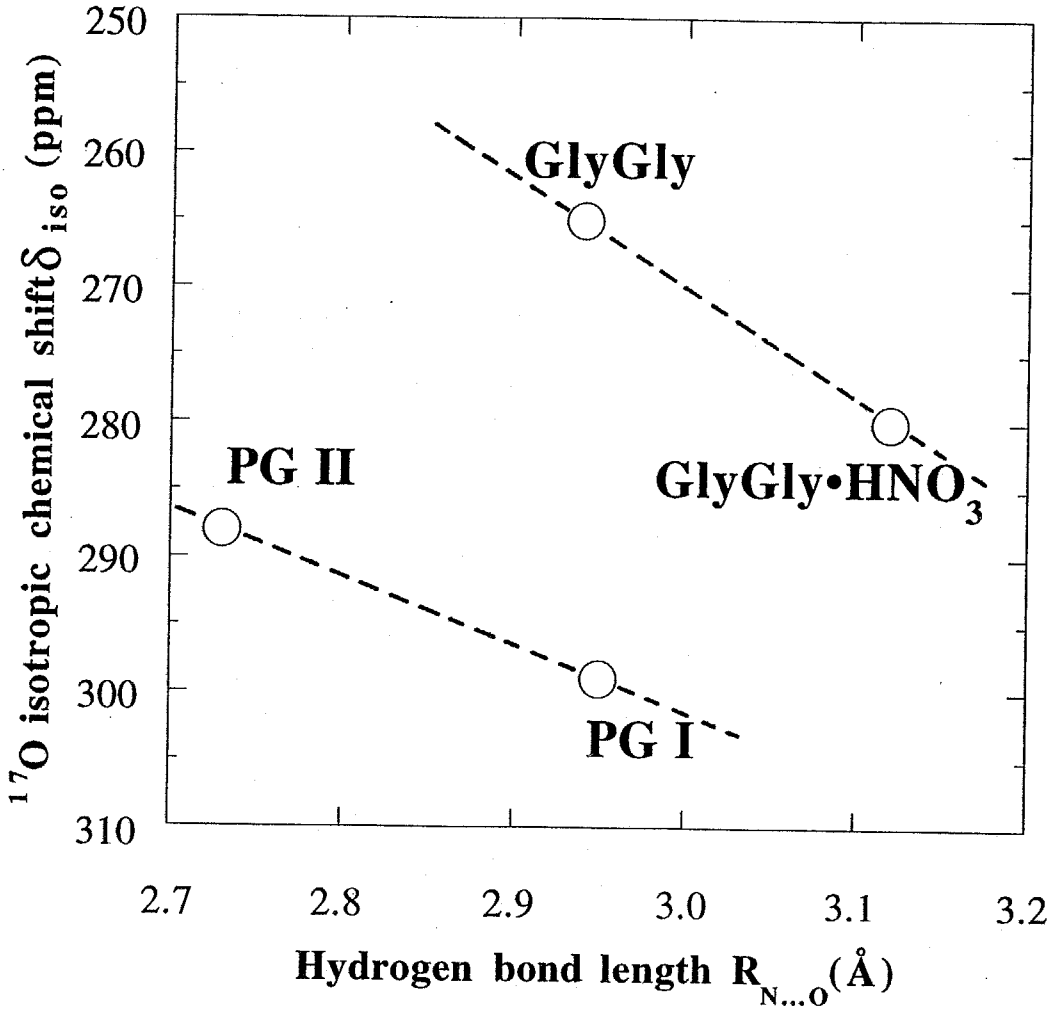

Fig.4.13 Plots of the observed isotropic ^{17}O chemical shift against the hydrogen bond length .

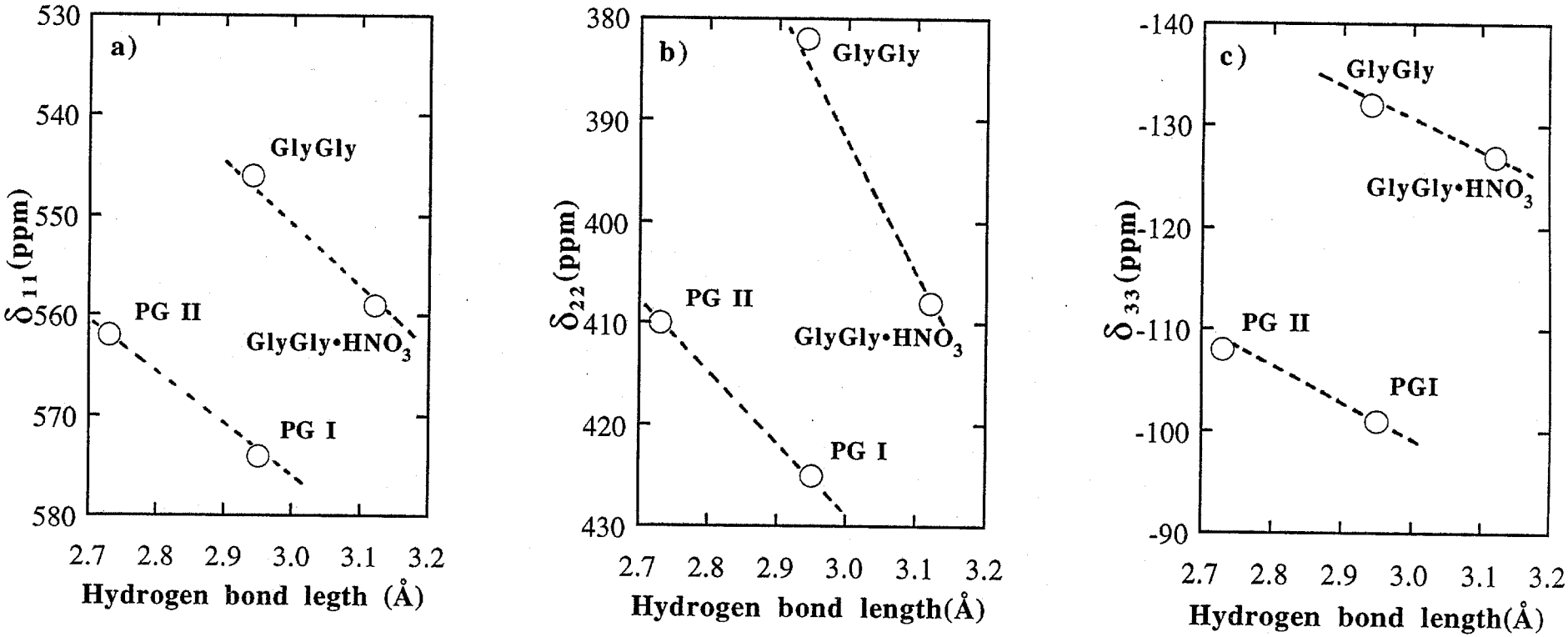

Fig. 4.14 Plots of the observed principal values of ^{17}O chemical shift tensor δ_{11}(a), δ_{22}(b) and δ_{33}(c), respectively against the N···O hydrogen bond length($R_{N\cdots O}$).

difference between peptides and polypeptides comes from the hydrogen bond angle and hydrogen bond dihedral angle are also related to the ^{17}O chemical shift. Another is the difference in molecular packing between them.

The spatial location of these samples is shown in Figs.4.15 using the Table 4.2 parameters. Figs.4.15 show us the following: The dihedral angle N-C=O···H (defined by ξ here) shows a measure of the location of the amide group on the peptide plane. In the case of GlyGly(ξ=-160°) and GlyGly•HNO_3(ξ=3°), the amide group related to hydrogen-bonding is nearly in the peptide plane and four atoms related to hydrogen-bonding such as C, O, H, and N are located on the peptide plane. On the other hand, in the case of PG I(ξ=68°) and II(ξ=-47°), the amide group related to hydrogen-bonding is away from the peptide plane. The location of the amide group seems to affect the δ value. In the following chapter, the relationship between the ^{17}O chemical shift and the hydrogen bond angle and hydrogen bond dihedral angle will be discussed by using quantum chemical calculation.

Finally, it can be concluded as follows. From the observed carbonyl oxygen ^{17}O NMR spectra of PG I, PG II, GlyGly, and GlyGly•HNO_3 in the solid state, it is found that the e^2qQ/h values decrease linearly with a decrease in the hydrogen bond length. This indicates that it is possible to determine the hydrogen bond length through the observation of e^2qQ/h values. It was found that there is difference in η_Q between the polypeptides and oligopeptides. This may come from large difference in molecular packing between them. The chemical shift values in both peptides and in polypeptides move upfield with a decrease in the hydrogen bond length. However, there is difference in

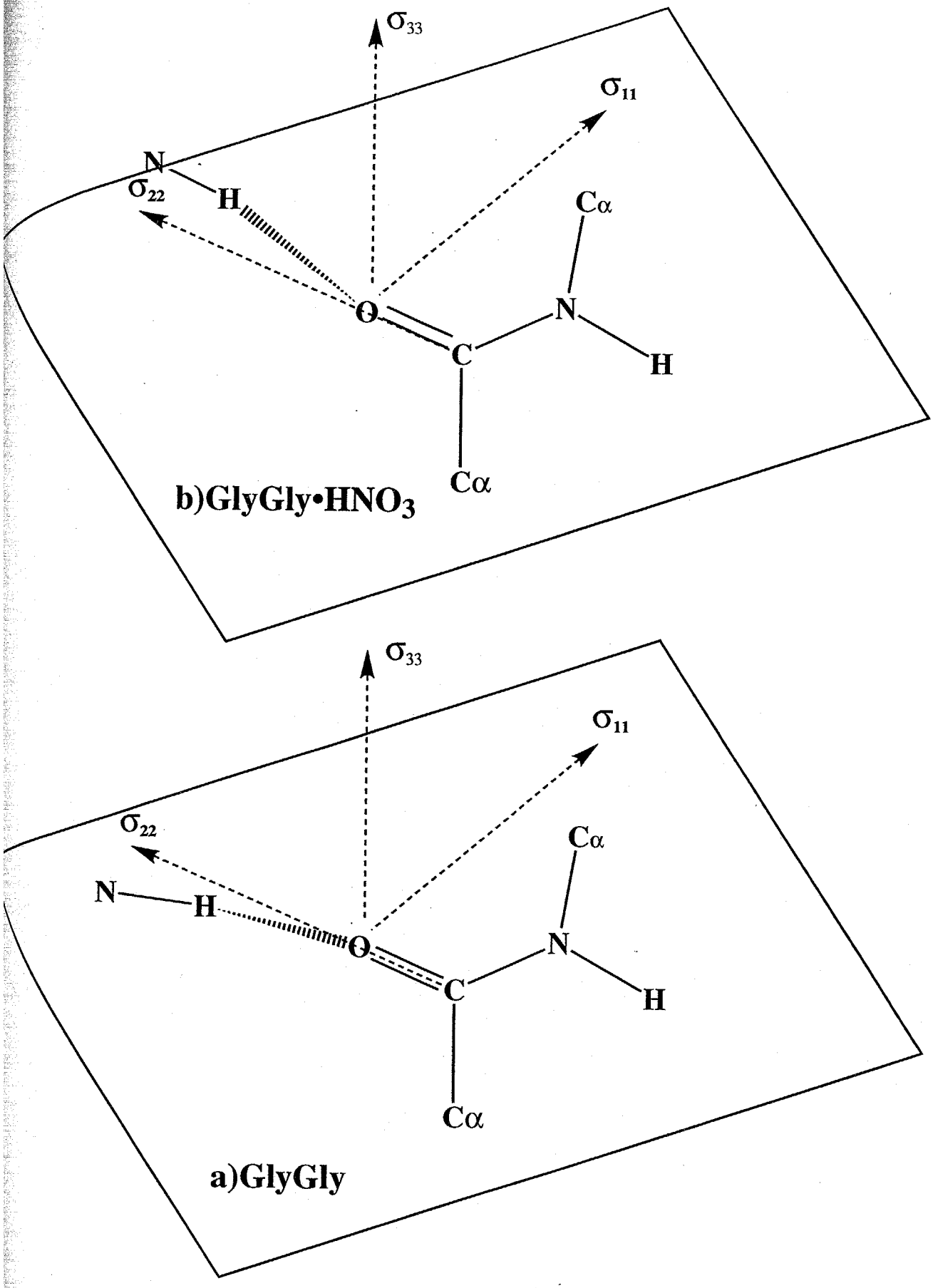

Fig.4.15 The hydrogen-bonding spatial location of peptides.

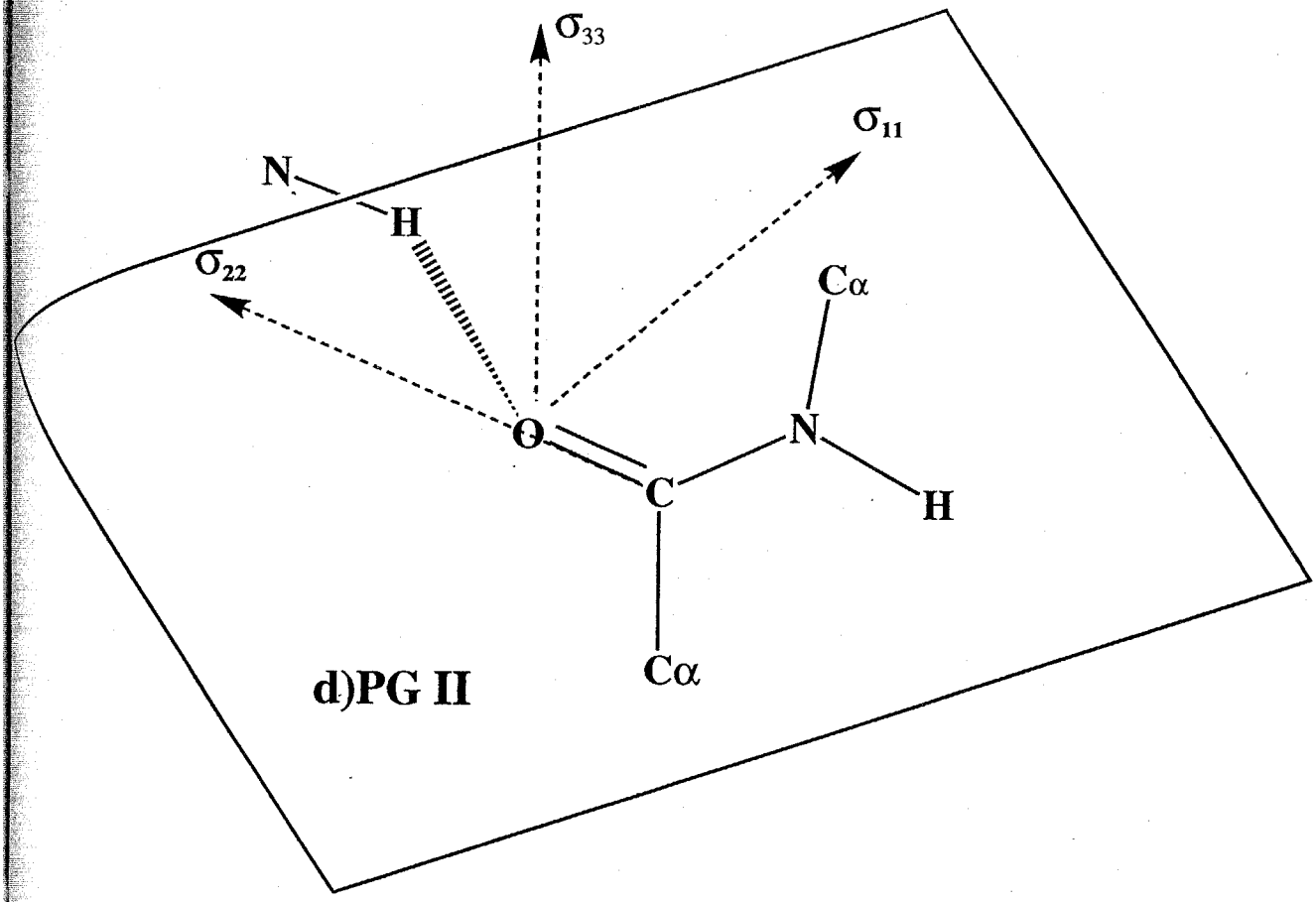

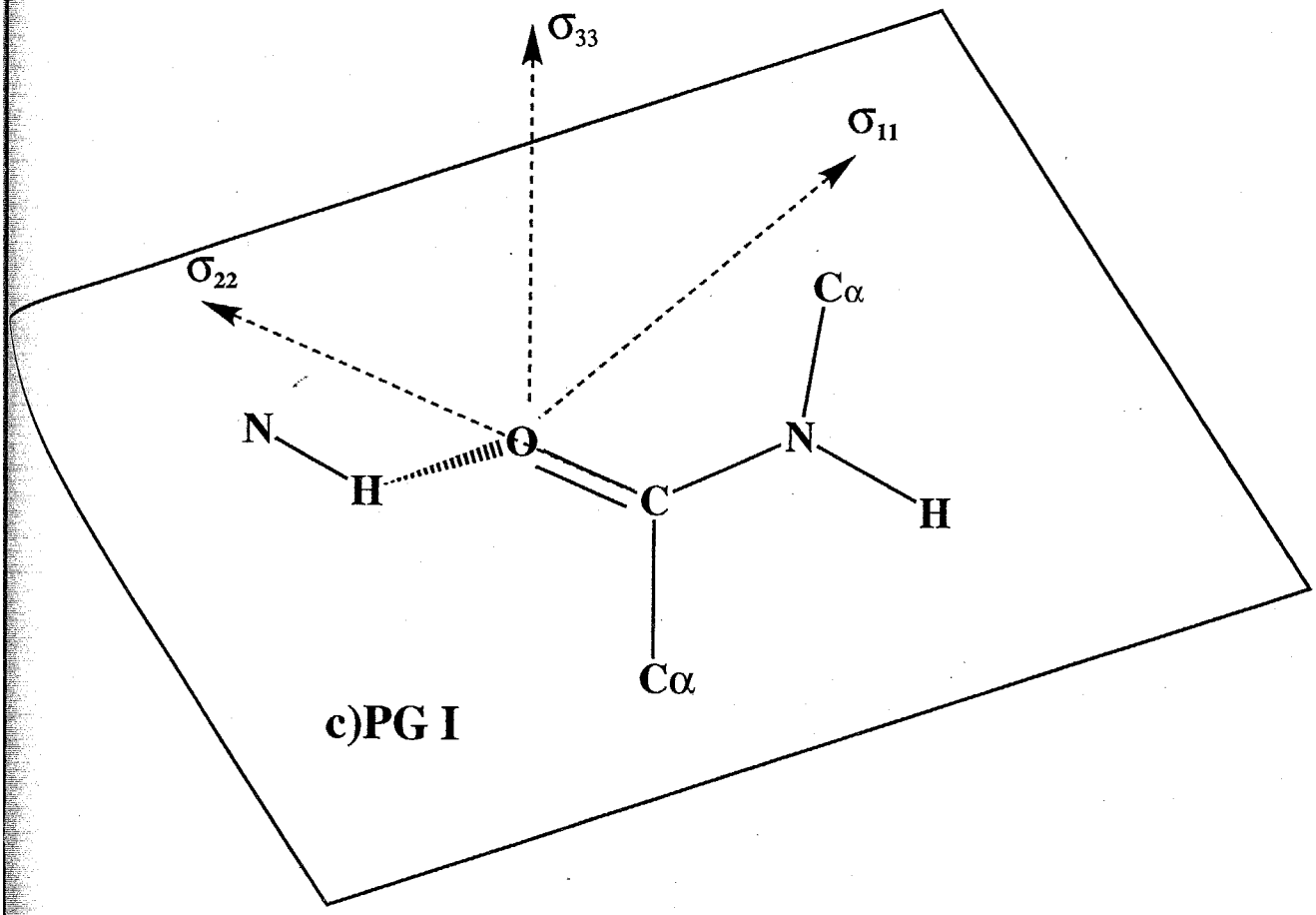

Fig.4.15 (continued)

the chemical shift value between peptides and polypeptides. This may come from difference in molecular packing between them. From these experimental findings, it was demonstrated that ^{17}O NMR spectroscopy becomes a useful mean for elucidating the hydrogen-bonding structure in solid peptides and polypeptides.

References

1) S.Ando, I.Ando, A.Shoji and T.Ozaki, *J. Am. Chem. Soc.*, **110** (1988) 3380.

2) N.Asakawa, S.Kuroki, H.Kurosu, I.Ando, A.Shoji and T.Ozaki, *J. Am. Chem. Soc.*, **114** (1992) 3261.

3) S.Kuroki, S.Ando, I.Ando, A.Shoji, T.Ozaki and G.A.Webb, *J. Mol. Struct.*, **240** (1990) 19.

4) S.Kuroki, N.Asakawa, S.Ando, I.Ando, A.Shoji and T.Ozaki *J. Mol. Struct.*, **245** (1991) 69.

5) A.Shoji, S.Ando, S.Kuroki and I.Ando, *Ann. Rept. NMR Spectrosc.*, **26** (1993) 55.

6) S.Ando, T.Yamanobe, I.Ando, A.Shoji, T.Ozaki, R.Tabeta and H.Saito, *J.Am.Chem.Soc.*, **107** (1985) 7648.

7) A.Shoji, T.Ozaki, S.Ando, I.Ando, T.Fujito and K.Deguchi, *Preprints of the Society of Fiber Science and Technology Japan*, Tokyo, (1989) S-125.

8) D.W.Boykinm ed., *^{17}O NMR Spectroscopy in Organic Chemistry,* CRC Press, Boca Raton, FL, 1991

9) A.L.Baumstark and D.W.Boykin, *^{17}O NMR Spectroscopy: Applications to Structural Problems in Organic Chemistry, in Advances in Oxygenated Processes*, **Vol.III**, A.L.Baumstark ed., JAI Press, 1991, p.141.

10) W.G.Klemperer, in *"The Multinuclear Approach to NMR Spectroscopy"*, J.B.Lambert and F.G.Riddell, Dordrecht, Holland,1983, p.245.

11) J.P.Kintzinger, in *"Newly Accessible Nuclei"*, P.Laszlo, ed., Academic Press, New York, **Vol.2**, 1983, p.79.

12) D.W.Boykin and A.L.Baumstark, *New Journal of Chemistry*, **16** (1992) 357.

13) D.W.Boykin and A.Kumar, *J. Heterocyclic Chem.*, **29** (1992) 1.

14) S.Kuroki, I,Ando, A.Shoji and T.Ozaki, *J. Chem. Soc., Chem.Commun.*, Issue **5** (1992) 433.

15) K.H.Meyer and Y.Go, *Helv. Chim. Acta*, **17** (1934)1488.

16) W.T.Astbury, C.H.Dalgleish, S.E.Darmon and G.B.B.M. Sutherland, *Nature*, **69** (1948), 596.

17) F.H.C.Crich and A.Rich, *Nature*, **176**(1955) 780.

18) T.H.Walter, G.L.Turner and E.Oldfield, *J.Magn.Reson.* **76** (1988) 106.

19) R.Goc and D.Fiat, *Physica . Status. Solidi. B*, 1987, **140** (1987) 243.
20) P.J.Chu and B.C.Gerstein, *J.Chem.Phys.*, **91** (1989) 2081.
21) J.T.Cheng, J.C.Edwards and P.D.Ellis, *J. Phys. Chem.*, **94** (1990) 553.
22) W.P.Power, R.E.Wasylishen, S.Mooibroek, B.A.Pettit and W.Danchura, *J. Phys. Chem.*, **94** (1990), 591.
23) F.A.Momany, R.F.McGuire, J.F.Yan and H.A.Scheraga, *J.Phys.Chem.*, **99** (1971),1251.
24) R.Goc, E.Ponnusomy, J.Tritt-Goc and D.Fiat, *Int. J. Pept. Protein Res.* **31** (1988) 130.
25) R.Goc, J.Tritt-Goc and D.Fiat, *Bull. Magn. Reson.*, **11** (1989) 238.
26) A. Kevick, A. R. Al-Karaghouli and T. F. Koetzle, *Acta.Cryst.*, **B33** (1977) 3796.
27) S. N. Rao, and R. Parthasarathy, *Acta Cryst.*, **B29** (1973) 2379.

Chapter 5

Theoretical Approaches of Nuclear Quadrupolar Coupling Constants and Chemical Shieldings

5.1 Introduction

In the preceding chapter, it has been stated that the ^{17}O NMR spectra of solid peptides and polypeptides containing Gly residue were successfully measured, and the NMR parameters were obtained, which are nuclear quadrupolar coupling constant (e^2qQ/h), asymmetric parameter of electric field gradient tensor(η_Q) and chemical shift(δ). From the observed carbonyl oxygen ^{17}O NMR spectra, the principal values of ^{17}O chemical shift tensor have many information about the geometry of hydrogen-bonding. On the other hand, the e^2qQ/h values decrease linearly with a decrease of the hydrogen bond length. It can be said that it is possible to determine the hydrogen bond structure through the observation of ^{17}O chemical shift values and e^2qQ/h values. From these experimental findings, it was clarified that ^{17}O NMR spectroscopy becomes a useful means for elucidating the hydrogen-bonding structure in solid peptides and polypeptides.

The nuclear quadrupolar coupling arises from interaction of nuclear quadrupolar moment eQ with electric field gradient eq at the site of nucleus. This field gradient (which involve nuclear and electronic contributions) and the asymmetry parameters η_Q are sensitive measure of the electronic charge distributions in the vicinity of the nucleus. Thus, they represent a means of probing the accuracy of molecular wavefunctions[1,2]. Several semi-empirical and ab initio MO methods have been used for calculating the electric field gradient values and relation it to structural features and to electronic distributions[1-7].

On the other hand, the chemical shielding arises because of the simultaneous interaction of a nucleus with an electron and that of the electron with applied magnetic field $\mathbf{B_0}$. A general theory has been give by Ramsey[8,9]. Since the chemical shieldings are sensitive to the electronic structure of molecules, we can obtain information about the electronic structure with high accuracy through the chemical shielding.

In the preceding chapters, the FPT-INDO method was used for calculating the chemical shieldings. The FPT-INDO theory has as advantage of permitting the calculation of the paramagnetic term without the explicit wave functions of excited states and the one-electron excitation energies, which are rarely obtained in high accuracy by the usual semi-empirical MO approximations. This approach reproduces reasonably well the experimental ^{13}C and ^{15}N chemical shifts of peptides and polypeptides[10-13]. In the INDO method, two-electron repulsion integrals of arbitrary atomic orbitals, ϕ_μ and ϕ_ν, regardless of s, p_σ and p_π electrons on atoms A and B respectively, are assumed to be $<\mu\mu|\nu\nu>=\gamma_{AB}$, where is constant comes from experimental results. Semi-empirical approximation of these 2-center integrals by multiple-multiple interaction has led to the MNDO(modified neglect of diatomic overlap) method developed by Dewar et al.[14] based on the NDDO (neglect of diatomic differential overlap) approximation. The MNDO method give good geometrical parameters and also their merits and deficiencies have been pointed out. The obvious way to deal with this was to modify the core repulsion function (CRF) in the MNDO method. The AM1(austin model 1) method[15] introduced a second set of parameters as shown in e.q.5.2, Gaussian core-core interaction to correct for excessive long-renege repulsion in the original MNDO core-core repulsion term. Further, in the MNDO-PM3 (parametric method 3) method[16], core-core repulsion term is

same type formula as AM1 method, but more optimized parameter set is used. The hydrogen-bonding can be evaluated better by the MNDO-PM3 method than the MNDO or the MNDO-AM1 method.

In this chapter, the theoretical approach of calculating the quadropular coupling constants and the chemical shieldings on the basis of quantum chemistry will provide systematic information on the hydrogen-bonding structure and its electronic state.

5.2 Theory

MNDO-PM3 method[14-16]: MNDO, AM1 and PM3 methods are based on the NDDO (neglect of diatomic differential overlap) approximation, except for core-core repulsion term, these methods use same formulas. Each of core-core repulsion terms is,

MNDO method:

$$E_{AB}^{core} = Z_A Z_B \left(s^A s^A \middle| s^B s^B\right)\left\{1 + f_{AB} e^{-a_A R_{AB}} + e^{-a_B R_{AB}}\right\} \qquad (5.1)$$

AM1 method:

$$\begin{aligned} E_{AB}^{core} &= Z_A Z_B \left(s^A s^A \middle| s^B s^B\right)\left\{1 + f_{AB} e^{-a_A R_{AB}} + e^{-a_B R_{AB}}\right\} \\ &+ \frac{Z_A Z_B}{R_{AB}}\left\{\sum_{i=1}^{4} K_{Ai} \exp\left[-L_{Ai}(R_{AB} - M_{Ai})^2\right]\right. \\ &\left. + \sum_{k=1}^{4} K_{Bj} \exp\left[-L_{Bj}(R_{AB} - M_{Bj})^2\right]\right\} \end{aligned} \qquad (5.2)$$

PM3 method:

$$\begin{aligned} E_{AB}^{core} &= Z_A Z_B \left(s^A s^A \middle| s^B s^B\right)\left\{1 + f_{AB} e^{-a_A R_{AB}} + e^{-a_B R_{AB}}\right\} \\ &+ \frac{Z_A Z_B}{R_{AB}}\left\{\sum_{i=1}^{2} a_{kA} \exp\left[-b_{kA}(R_{AB} - c_{kA})^2\right]\right. \\ &\left. + \sum_{k=1}^{2} a_{kB} \exp\left[-b_{kB}(R_{AB} - c_{kB})^2\right]\right\} \end{aligned} \qquad (5.3)$$

where, Z_A is effective charge of core A, and S_A is the s orbital of atom A. When atom A is nitrogen or oxygen and atom B is hydrogen, f_{AB}:=R_{AB} , and in the other case, f_{AB}: =1. R_{AB} is the distance between core A and core B. α_A, K_{Ai}, M_{Ai}, a_{kA}, b_{kA} and c_{kA} are parameters optimized for each atom as reproduced the experimental data on the heat of formation, dipole moment and ionization potential.

The method of electric field calculation: The field gradient tensor eq_I is given by

$$eq_I = e\left[\sum_{K\neq I}\frac{Z_K\left(3R_{IK}R_{IK}-R_{IK}^2 1\right)}{R_{IK}^5} -2\sum_{i=1}^{n}\sum_{k,l=1}^{M} c_{ki}c_{li}\left\langle \varphi_k\left|\frac{3r_I r_I - r_I^2 1}{r_I^5}\right|\varphi_l\right\rangle\right]. \qquad (5.4)$$

where eq_I: is the field gradient tensor at the quadrupolar nucleus I, Z_K is charge of nucleus to K, R_{IK} is the vector from nucleus I to K, 1 is the unit dyadic, r_I is the vector from nucleus I to electron vector and n is the number of doubly occupied MO's Φ_r.

The first term in eq 5.4 is the nuclear contribution and the second term is the electronic contribution. Though the nuclear term of the electric field gradient can be easily calculated using point charge in the nucleus, the electronic contribution term which means the second differential of the overlap of the electron orbitals in the nucleus cannot be easily evaluated.

Electronic contribution term of the electric field gradient tensor was evaluated. The diagonal term of the electric field gradient integral is

$$R_{xx} = \left\langle \varphi_A\left|\frac{3x_c^2 - r_c^3}{r_c^5}\right|\varphi_B\right\rangle . \qquad (5.5)$$

The off-diagonal term is

$$R_{xy} = \left\langle \varphi_A \left| \frac{3x_c y_c}{r_c^5} \right| \varphi_B \right\rangle . \tag{5.6}$$

In order to evaluate these integral, the representation of Larry et al.[17] is used as follows.

$$\frac{3x_c^2 - r_c^3}{r_c^5} = \frac{1}{3}\left(\frac{2\partial^2}{\partial C_x^2} - \frac{\partial^2}{\partial C_y^2} - \frac{\partial^2}{\partial C_z^2} \right)\left(\frac{1}{r_c} \right) \tag{5.7}$$

$$\frac{3x_c y_c}{r_c^5} = \frac{\partial^2}{\partial C_x \partial C_y}\left(\frac{1}{r_c} \right) . \tag{5.8}$$

eq.5.7 is substituted in eqs.5.5,

$$R_{xx} = \frac{1}{3}\left[2\frac{\partial^2}{\partial x^2}\left\langle \varphi_A \left| \frac{1}{r_c} \right| \varphi_B \right\rangle - \frac{\partial^2}{\partial y^2}\left\langle \varphi_A \left| \frac{1}{r_c} \right| \varphi_B \right\rangle - \frac{\partial^2}{\partial z^2}\left\langle \varphi_A \left| \frac{1}{r_c} \right| \varphi_B \right\rangle \right] \tag{5.9}$$

$$\frac{\partial}{\partial x}\left\langle \varphi_A \left| \frac{1}{r_c} \right| \varphi_B \right\rangle = \left\langle \frac{\partial \varphi_A}{\partial x} \left| \frac{1}{r_c} \right| \varphi_B \right\rangle + \left\langle \varphi_A \left| \frac{1}{r_c} \right| \frac{\partial \varphi_B}{\partial x} \right\rangle \tag{5.10}$$

The term in eq.5.9 is described as eq.5.11.

$$\frac{\partial^2}{\partial x^2}\left\langle \varphi_A \left| \frac{1}{r_c} \right| \varphi_B \right\rangle = \left\langle \frac{\partial^2 \varphi_A}{\partial x^2} \left| \frac{1}{r_c} \right| \varphi_B \right\rangle$$

$$+2\left\langle \frac{\partial \varphi_A}{\partial x} \left| \frac{1}{r_c} \right| \frac{\partial \varphi_B}{\partial x} \right\rangle + \left\langle \varphi_A \left| \frac{1}{r_c} \right| \frac{\partial^2 \varphi_B}{\partial x^2} \right\rangle \tag{5.11}$$

$$\frac{\partial \varphi_A}{\partial x} = \frac{\partial}{\partial x}\left(x_A^{l_A} y_A^{m_A} z_A^{n_A} e^{-\alpha_A r_A^2} \right) = \left(l_A x_A^{l_A - 1} - 2\alpha_A x_A^{l_A + 1} \right) y_A^{m_A} z_A^{n_A} e^{-\alpha_A r_A^2} \tag{5.12}$$

$$\frac{\partial^2 \varphi_A}{\partial x^2} = l_A(l_A - 1)x_A^{l_A - 2} - 2\alpha_A(2l_A + 1)x_A^{l_A} + 4\alpha_A^2 x_A^{l_A + 2} \tag{5.13}$$

From eq.5.13, the first term of eq.5.11 is

$$\left\langle \frac{\partial^2 \varphi_A}{\partial x^2} \left| \frac{1}{r_c} \right| \varphi_B \right\rangle$$

$$= \left[l_A(l_A - 1)V_x^{-20} - 2\alpha_A(2l_A + 1)V_x^{00} + 4\alpha_A^2 V_x^{20} \right] V_y^{00} V_z^{00} . \tag{5.14}$$

The second term is

$$\left\langle \frac{\partial \varphi_A}{\partial x} \left| \frac{1}{r_c} \right| \frac{\partial \varphi_B}{\partial x} \right\rangle$$

$$= \left[l_A l_B V_x^{-1-1} - 2l_A \alpha_B V_x^{-1+1} - 2l_B \alpha_A V_x^{+1-1} + 4\alpha_A \alpha_B V_x^{11} \right] V_y^{00} V_z^{00} .$$

(5.15)

The third term is

$$\left\langle \varphi_A \left| \frac{1}{r_c} \right| \frac{\partial^2 \varphi_B}{\partial x^2} \right\rangle$$

$$= \left[l_B(l_B-1)V_x^{0-2} - 2\alpha_B(2l_B+1)V_x^{00} + 4\alpha_B^2 V_x^{02} \right] V_y^{00} V_z^{00}. \quad (5.16)$$

On the other hand, eq.5.8 is substituted in eq.5.6,

$$R_{xy} = \frac{\partial^2}{\partial x \partial y} \left\langle \varphi_A \left| \frac{1}{r_c} \right| \varphi_B \right\rangle \quad (5,17)$$

$$\frac{\partial^2}{\partial xy} \left\langle \varphi_A \left| \frac{1}{r_c} \right| \varphi_B \right\rangle = \left\langle \frac{\partial^2 \varphi_A}{\partial x \partial y} \left| \frac{1}{r_c} \right| \frac{\partial \varphi_B}{\partial y} \right\rangle + \left\langle \frac{\partial \varphi_A}{\partial x} \left| \frac{1}{r_c} \right| \frac{\partial \varphi_B}{\partial y} \right\rangle$$

$$+ \left\langle \frac{\partial \varphi_A}{\partial y} \left| \frac{1}{r_c} \right| \frac{\partial \varphi_B}{\partial x} \right\rangle + \left\langle \varphi_A \left| \frac{1}{r_c} \right| \frac{\partial^2 \varphi_B}{\partial x \partial y} \right\rangle \quad (5.18)$$

$$\frac{\partial^2 \varphi_A}{\partial x \partial y} = \left(l_A x_A^{l_{A-1}} - 2\alpha_A x_A^{l_{A+1}} \right) \left(m_A y_A^{m_{A-1}} - 2\alpha_A y_A^{m_{A+1}} \right) z_A^{n_A} e^{-\alpha_A r_A^2} \quad (5.19)$$

From eq.5.19, the first term of eq.5.18 is

$$\left\langle \frac{\partial^2 \varphi_A}{\partial x \partial y} \left| \frac{1}{r_c} \right| \frac{\partial \varphi_B}{\partial y} \right\rangle = \left(l_A V_x^{-10} - 2\alpha_A V_x^{10} \right) \left(m_A V_y^{-10} - 2\alpha_A V_y^{10} \right) V_z^{00}. \quad (5.20)$$

The second term is

$$\left\langle \frac{\partial \varphi_A}{\partial x} \left| \frac{1}{r_c} \right| \frac{\partial \varphi_B}{\partial y} \right\rangle = \left(l_A V_x^{-10} - 2\alpha_A V_x^{10} \right) \left(m_B V_y^{0-1} - 2\alpha_A V_y^{01} \right) V_z^{00}. \quad (5.21)$$

The third term is

$$\left\langle \frac{\partial \varphi_A}{\partial y} \left| \frac{1}{r_c} \right| \frac{\partial \varphi_B}{\partial x} \right\rangle = \left(m_A V_y^{-10} - 2\alpha_A V_y^{10} \right) \left(l_B V_x^{0-1} - 2\alpha_B V_x^{01} \right) V_z^{00}. \quad (5.22)$$

The forth term is

$$\left\langle \varphi_A \left| \frac{1}{r_c} \right| \frac{\partial^2 \varphi_B}{\partial x \partial y} \right\rangle = \left(l_B V_x^{0-1} - 2\alpha_B V_x^{01} \right) \left(m_B V_y^{0-1} - 2\alpha_B V_y^{01} \right) V_z^{00}. \quad (5.23)$$

From these eqs., every integral is evaluated, and we can obtain the electronic contribution term of the electric field gradient tensor.

The chemical shielding calculation using the FPT-MNDO-PM3 methods were evaluated by Ando[18] or Wu et al.[19]

The basis set using practical calculation was STO-6G basic set. Sun 4 SPARC Station was used for the calculations.

5.3 Results and Discussion

Electric field gradient calculation of some oxygen containing compounds: In order to confirm the reliability for electric field gradient calculation, the electric field gradient of some oxygen-containing compounds was calculated, of which quadrupolar coupling constants were already determined by NMR and NQR experiments[20-25]. The calculated results were shown in Table 5.1 with the experimental ones. The calculation results explain the experimental results qualitatively. From these results, it can be said that the calculation is reliable to discuss the relationship between electric field gradient and hydrogen-bonding structure.

Electric field gradient calculation on the carbonyl oxygen of hydrogen-bonded peptides model: In order to obtain a deep insight for the experimental finding that the e^2qQ/h values decrease linearly with a decrease in the hydrogen bond length, theoretical calculations of the electric field gradient were carried out by the MNDO-PM3 method using the model compounds as shown in Figs.5.1-3. Fig.5.4 a) shows the hydrogen bond length $R_{N\cdots O}$ dependence of the calculated e^2qQ/h values of Gly carbonyl oxygen in the model compound(Fig.5.1). The e^2qQ/h values decrease with a decrease in the hydrogen bond length $R_{N\cdots O}$. Figs.5.b) and c) show the hydrogen bond angle $\angle C{=}O\cdots H$(defined by θ) and hydrogen bond dihedral angle

Table 5.1 Calculated electric field gradient of some oxygen-containing compounds with their experimental quadrupolar coupling constant.

Compound	V_{11}	V_{22}	V_{33}	η_Q(cal.)	η_Q(exp.)	e^2qQ/h(cal.)	e^2qQ/h(exp.)	ref.
O_2(Gas)	-0.5154	-0.5156	1.0310	0.00	0.00	-6.28	-8.42	20
CO(Gas)	0.1164	0.1164	-0.2328	0.00	0.00	1.42	4.43	21
H_2O(Ice)	0.6532	1.5943	-2.2475	0.42	0.60	13.73	11.33	22
HCOOH(Solid)								
C=O	0.7727	0.9320	-1.7047	0.09	0.07	10.41	7.80	23
COH	0.3684	1.2441	-1.6125	0.54	0.08	9.85	6.90	24
H_2CO(Gas)	0.7005	1.2581	-1.9586	0.28	0.70	11.96	12.37	25
HOOH(Solid)	0.5271	2.1600	-2.6871	0.61	0.68	16.41	16.31	26

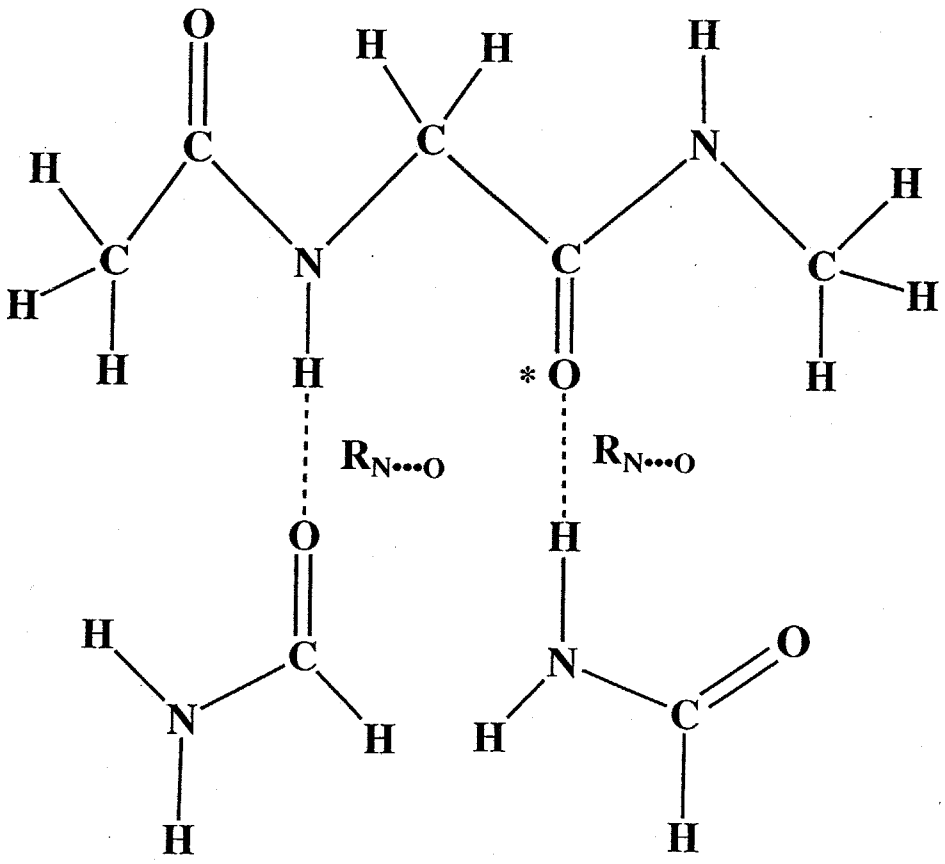

Fig.5.1 Structural model of N-acetyl-N'-methylglycine amide forming hydrogen bonds with two formamide molecules.

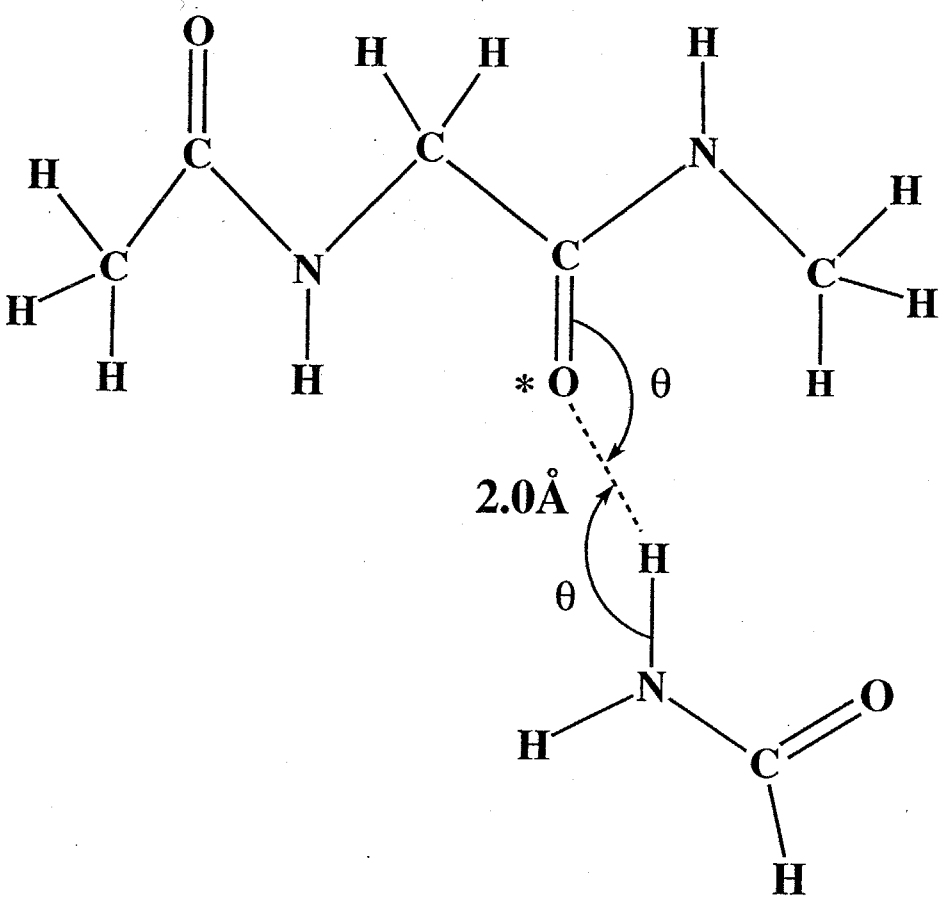

Fig.5.2 Structural model of N-acetyl-N'-methylglycine amide forming hydrogen bond with a formamide molecule.

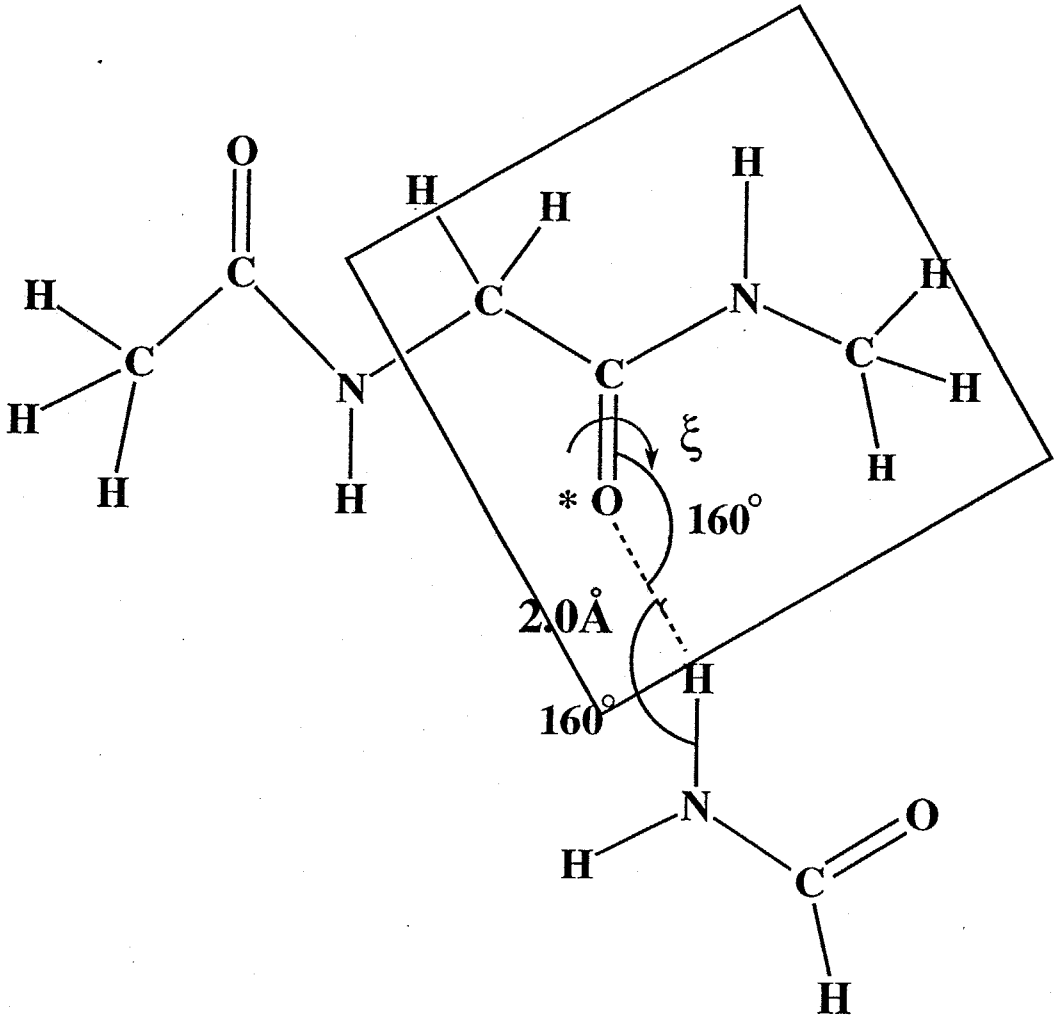

Fig.5.3 Structural model of N-acetyl-N'-methylglycine amide forming hydrogen bond with a formamide molecule.

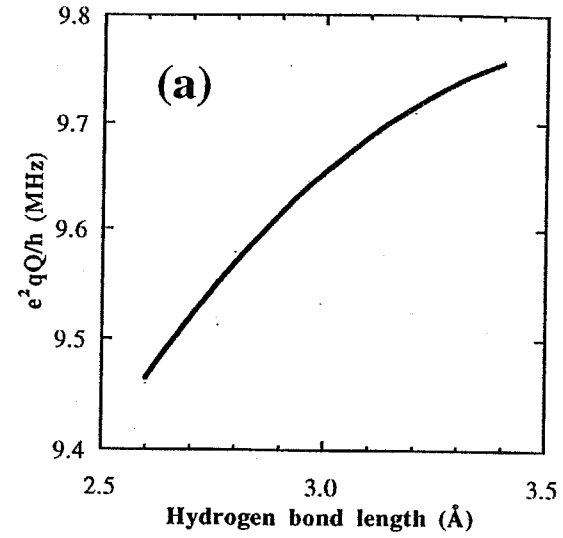

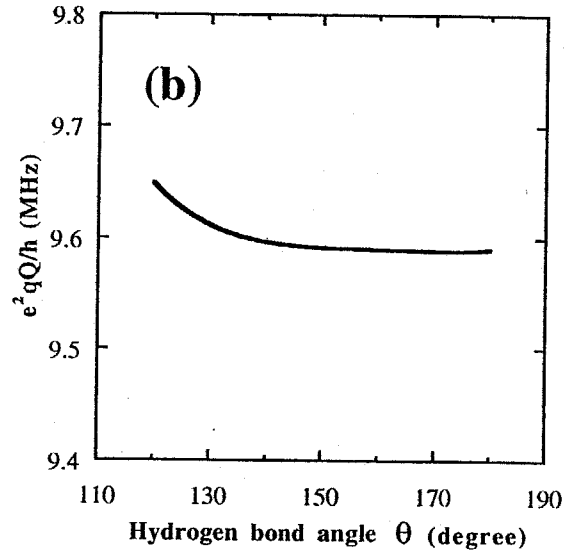

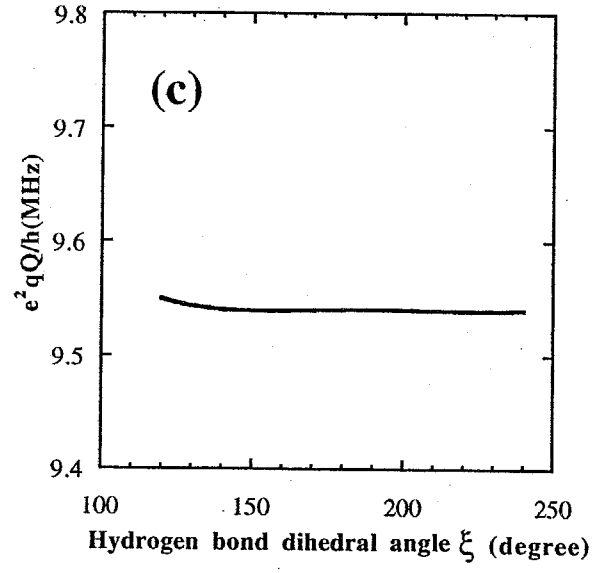

Fig.5.4 Plots of the calculated e^2qQ/h against hydrogen bond length (a), hydrogen bond angle θ (b) and hydrogen bond dihedral angle ξ (c), respectively.

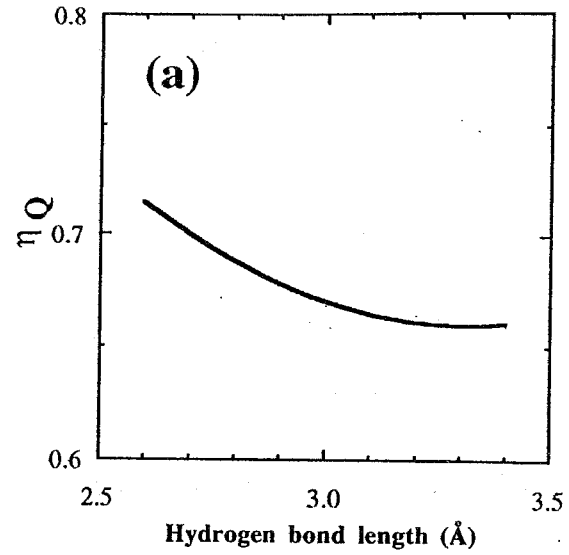

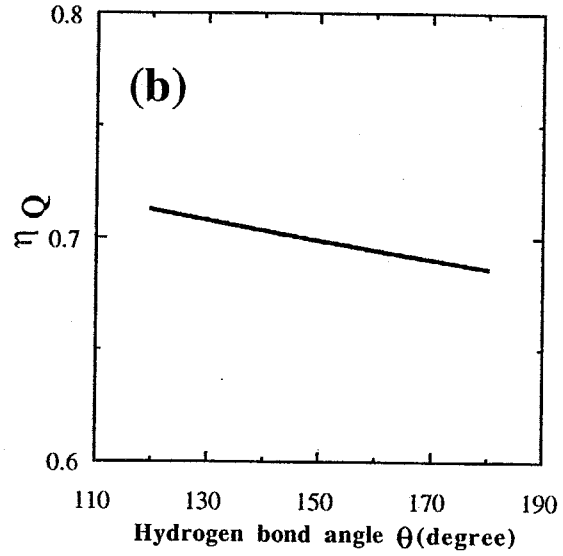

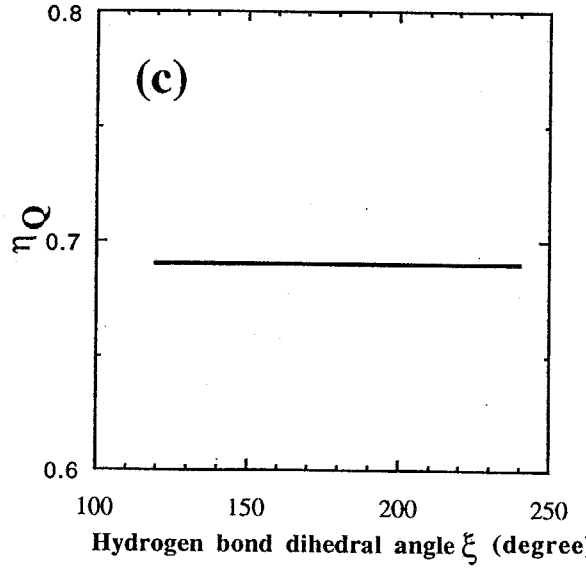

Fig.5.5 Plots of the calculated η_Q against hydrogen bond length (a), hydrogen bond angle θ (b) and hydrogen bond dihedral angle ξ (c), respectively.

N-C=O···H(defined by ξ) dependence of the calculated e^2qQ/h values of Gly carbonyl oxygen in the model compounds(Figs.5.2 and 3). It is found that the magnitude of the e^2qQ/h values change is small for a change of θ or ζ. It can be said that the e^2qQ/h values are dependent of the hydrogen bond length. The result that the e^2qQ/h values decrease with a decrease in the hydrogen bond length agrees with the experimental finding.

Figs.5.5a)-c) show the hydrogen bond length $R_{N\cdots O}$, hydrogen bond angle(θ) and hydrogen bond dihedral angle (ξ) dependence of the calculated η_Q values which are asymmetric parameter of the electric field gradient of Gly carbonyl oxygen. It is found that the magnitude of the η_Q values change is small for the change of $R_{N\cdots O}$, θ or ξ. It can be said that η_Q values does not depend on hydrogen-bonding structure. The difference in the η_Q values between peptides and polypeptides obtained in the preceding chapter, may come from large difference in molecular packing .

Chemical shielding calculation of the carbonyl oxygen of hydrogen-bonded peptides model: Fig.5.6 shows the hydrogen bond length dependence of the calculated isotropic chemical shielding (σ_{iso}) of Gly carbonyl oxygen in the model compound (Fig.5.1). Figs.5.7 shows the hydrogen bond length dependence of the calculated principal values (σ_{11}, σ_{22} and σ_{33}) of chemical shielding. Note that the opposite sign for the calculated shielding denotes deshielding, in contrast to the positive sign of the experimental chemical shift values. The σ_{iso} values largely increase with a decrease in the hydrogen bond length, and every principal value of oxygen chemical shielding increases with a decrease in the hydrogen bond length.

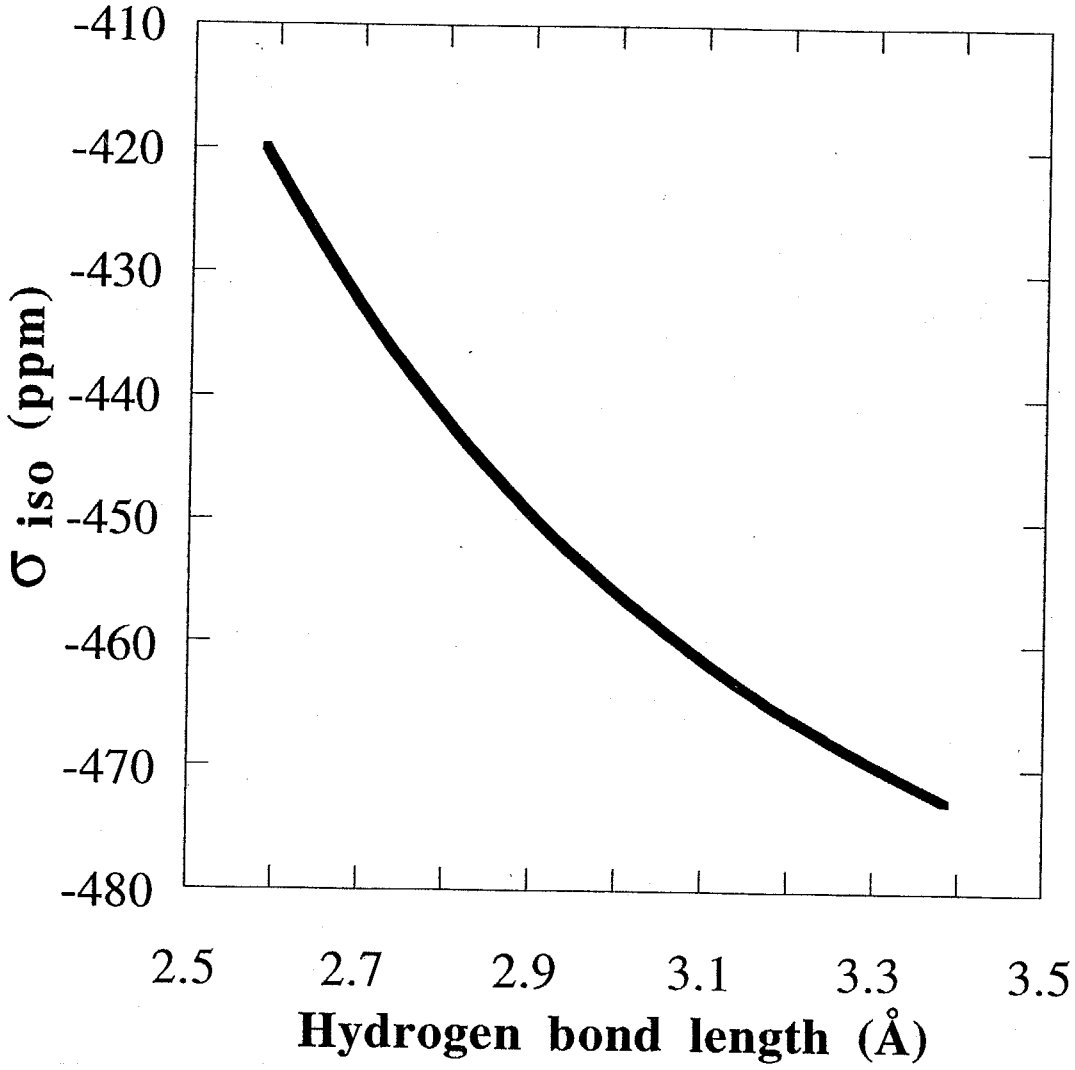

Fig.5.6 Plots of the calculated ^{17}O isotropic chemical shielding against the hydrogen bond length.

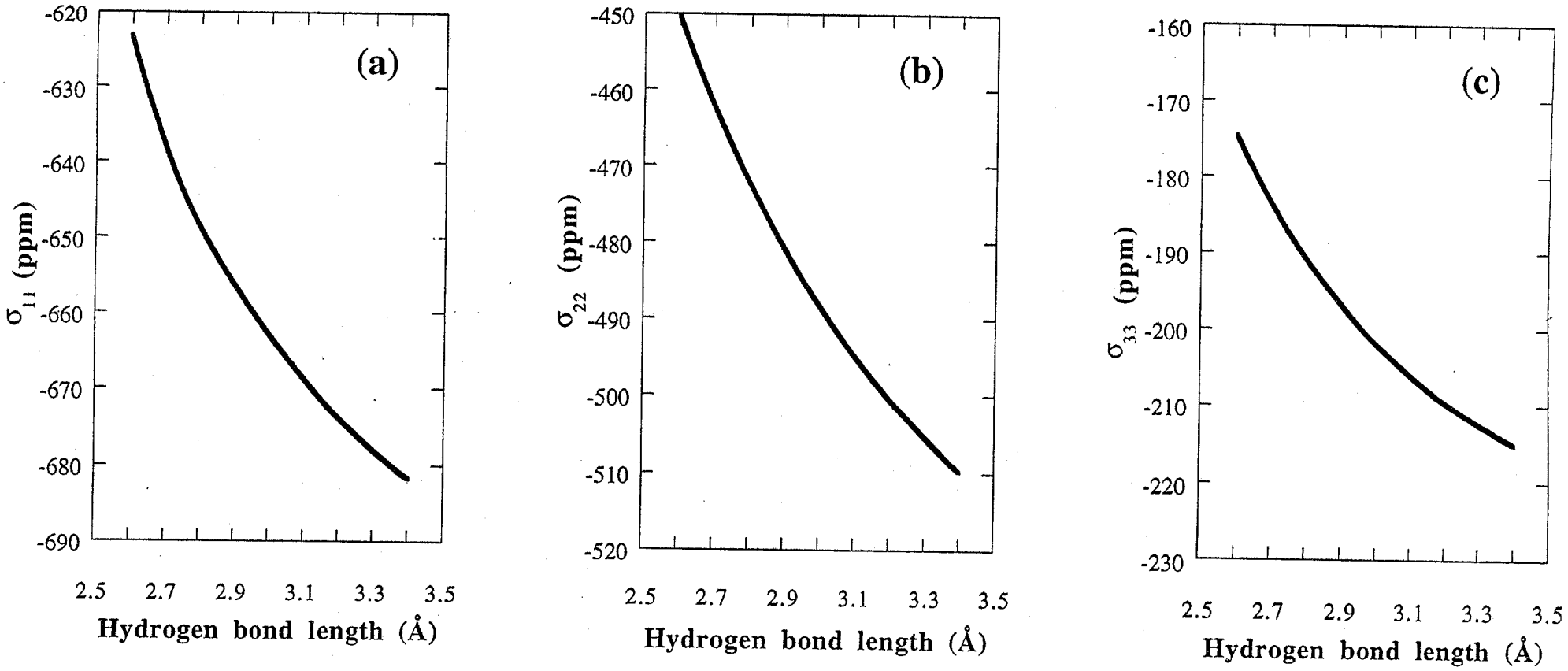

Fig.5.7 Plots of the calculated ^{17}O shielding tensor components σ_{11} (a), σ_{22}(b) and σ_{33}(c) against the hydrogen bond length, respectively .

Fig.5.8 shows the hydrogen bond angle θ dependence of the calculated isotropic chemical shielding (σ_{iso}) of Gly carbonyl oxygen in the model compound(Fig.5.2). It is found that the magnitude of change in σ_{iso} is small for a change of θ. Figs.5.9 shows the hydrogen bond angle θ dependence of the calculated principal values (σ_{11}, σ_{22} and σ_{33}) of chemical shielding. The σ_{22} values increase with a decrease in a θ and the σ_{11} and σ_{33} values decrease with a decrease in θ. Because the σ_{22} and the σ_{11} and σ_{33} values changes are compensated with each other, the change of σ_{iso} is small against θ

Figs.5.10 and 5.11 show the hydrogen bond dihedral angle ξ dependence of the calculated isotropic chemical shielding (σ_{iso}) of Gly carbonyl oxygen in the model compound (Fig.5.3), and the hydrogen bond dihedral angle ξ dependence of the calculated principal values (σ_{11}, σ_{22} and σ_{33}) of chemical shielding, respectively. It is found that the magnitude of the change in σ_{iso} is small against ξ, and that the magnitude of the change in σ_{11}, σ_{22} and σ_{33} is small against ξ.

From these calculated results, isotropic chemical shieldings (σ_{iso}) of Gly carbonyl oxygen depend on hydrogen bond length and do not depend on hydrogen bond angle and hydrogen bond dihedral angle. These calculations explain the experimental finding that the chemical shift values in peptides and in polypeptides move upfield with a decrease in the hydrogen bond length, obtained in the preceding chapter. So that the difference in the chemical shift value between peptides and polypeptides may come from difference in long-range molecular packing between them.

The direction of the principal axes of the electric field gradient tensor and the chemical shielding of carbonyl oxygen: The direction of the principal axes of the electric field

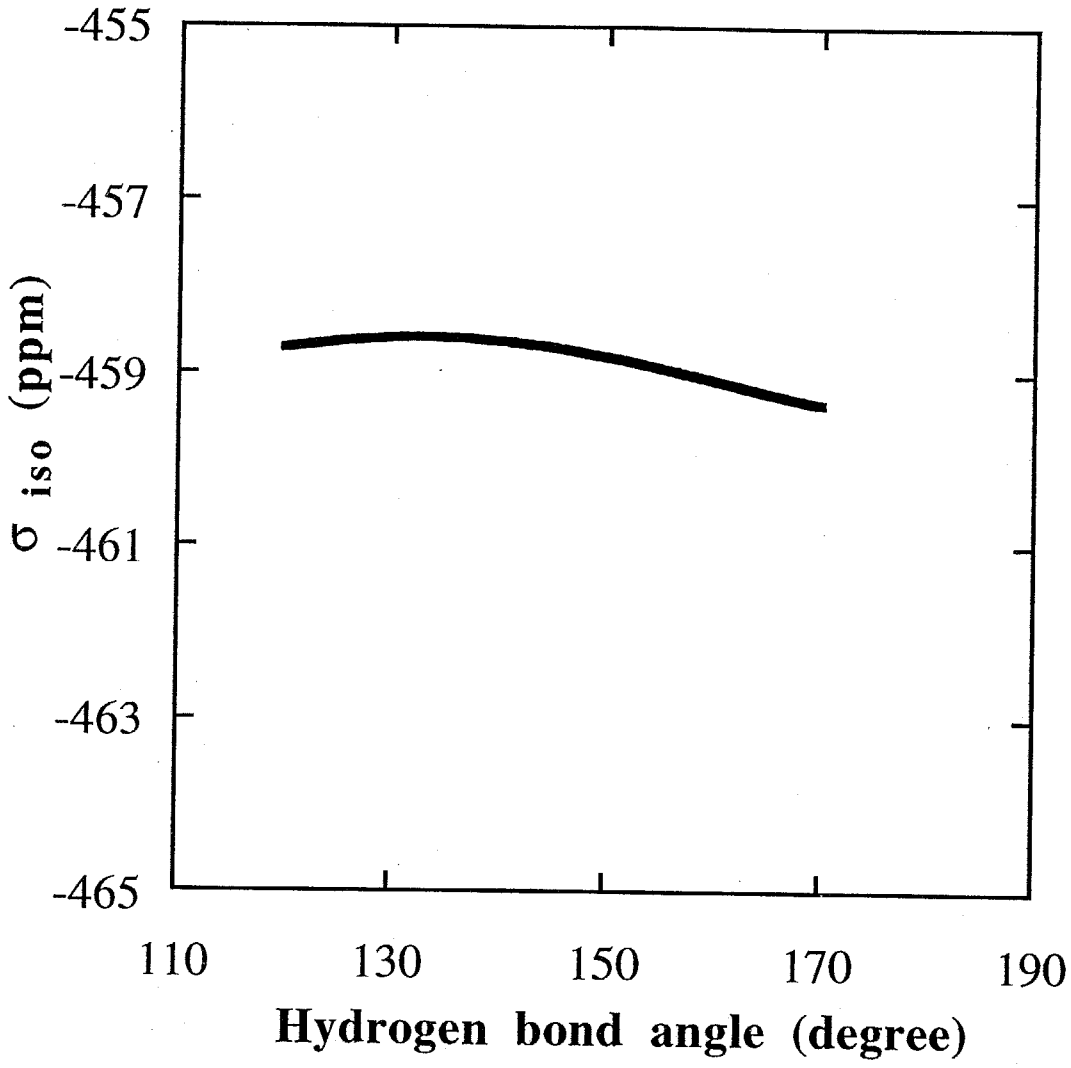

Fig.5.8 Plots of the calculated ^{17}O isotropic chemical shielding against the hydrogen bond angle.

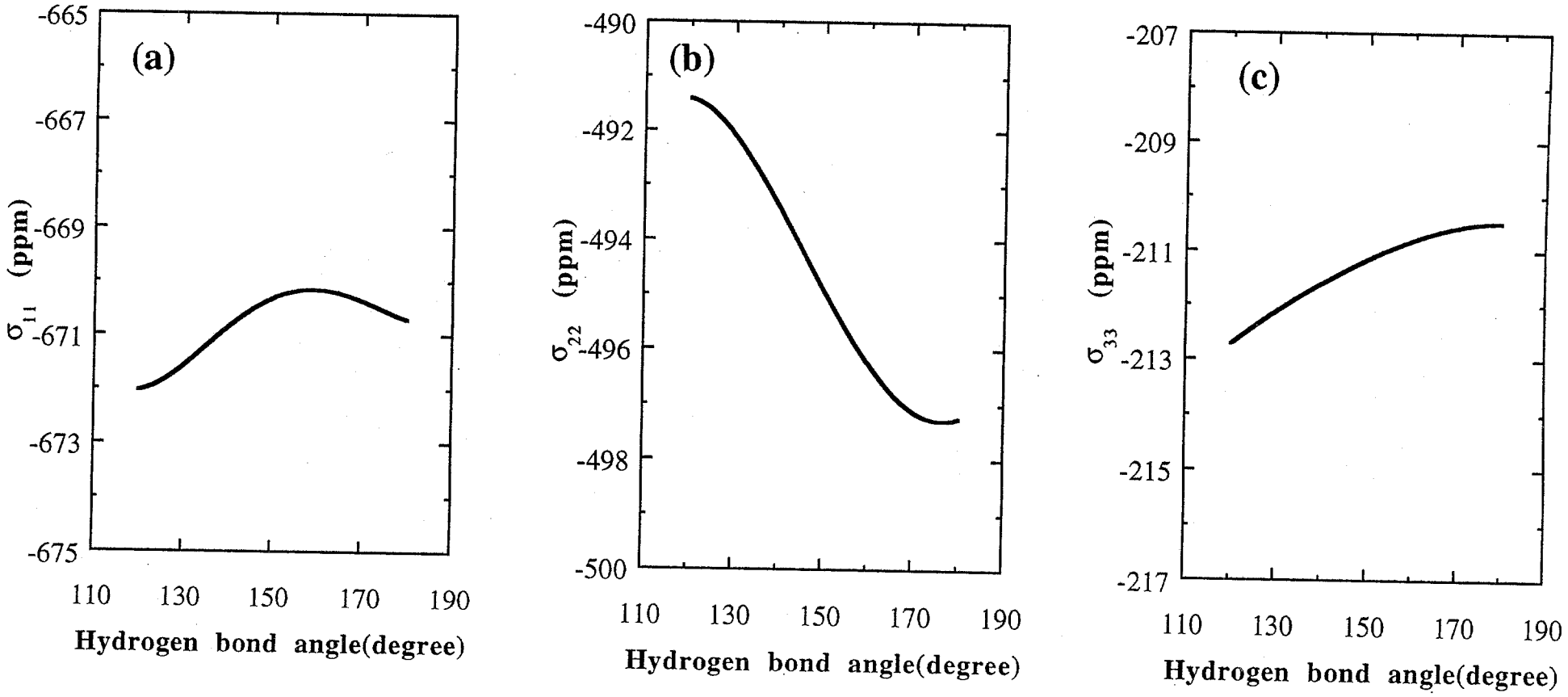

Fig.5.9 Plots of the calculated ^{17}O shielding tensor components σ_{11} (a), σ_{22} (b) and σ_{33} (c) against the hydrogen bond angle θ , respectively.

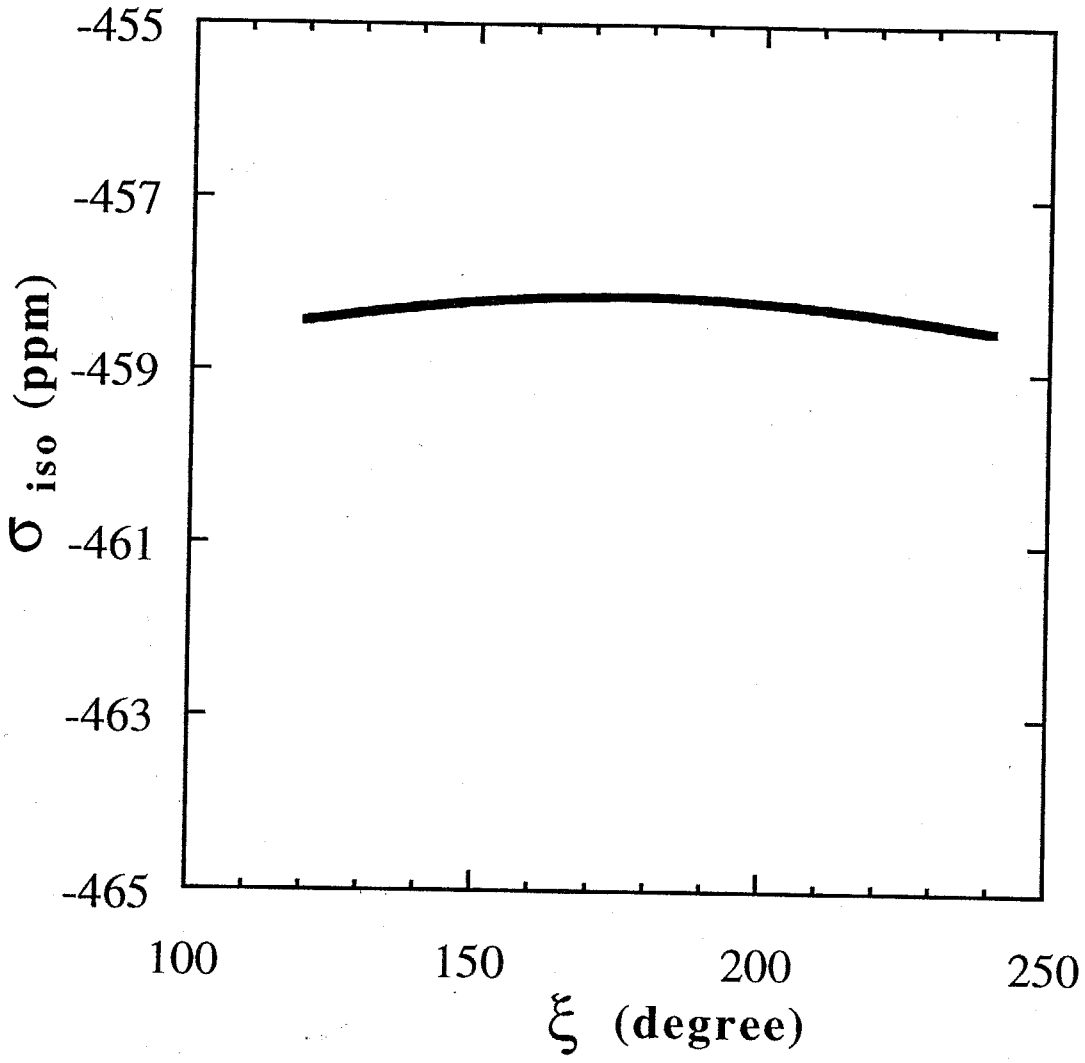

Fig.5.10 Plots of the calculated ^{17}O isotropic chemical shielding against the hydrogen bond dihedral angle.

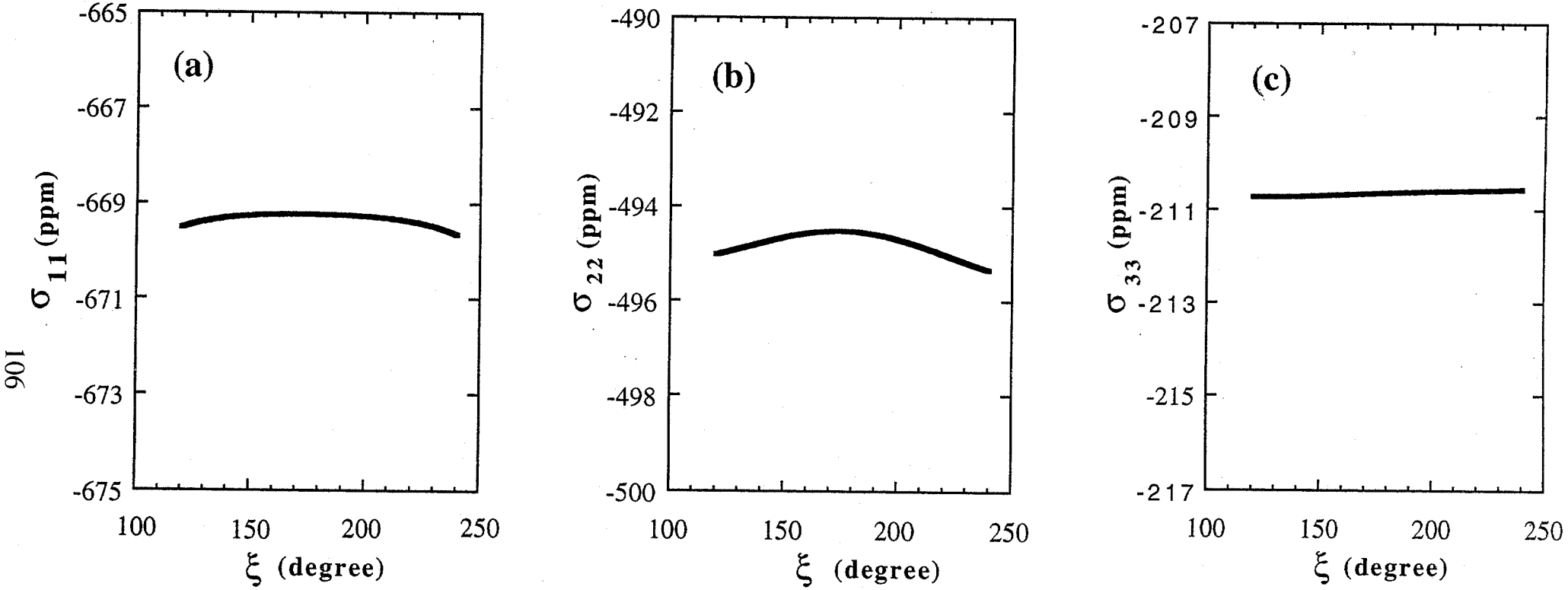

Fig.5.11 Plots of the calculated ^{17}O shielding tensor components σ_{11} (a), σ_{22}(b) and σ_{33} (c) against the hydrogen bond dihedral angle ξ , respectively.

gradient tensor and the chemical shielding of carbonyl oxygen was shown in the preceding chapter(Fig.4.9). The direction of the principal axes of the chemical shielding of the carbonyl oxygen is shown in Fig.5.12 as determined by the FPT-MNDO-PM3 method. The σ_{22} component lies approximately along the C=O bond, the σ_{11} component is aligned in the direction perpendicular to the C=O bond on the peptide plane, and the σ_{33} which is the most shielded component is aligned in the direction perpendicular to the peptide plane. On the other hand, the direction of the principal axes of the electric field gradient tensor of the carbonyl oxygen are shown in Fig.5.13 as determined by the FPT-MNDO-PM3 method. The V_{22} component lies approximately along the C=O bond, the V_{33} component is aligned in the direction perpendicular to the C=O bond on the peptide plane, and the V_{11} is aligned in the direction perpendicular to the peptide plane. It can be said that the largest component V_{33} of the electric field gradient lies along the molecular chain direction.

The relationship between chemical shielding axes and the electric field gradient axes is a good agreement with the experimental results in preceding chapter. It can be said that the reliability of the calculation is sufficient to do discussion on such problem.

Finally, it can be concluded as follows. The quantum-chemical approach of calculating the quadrupolar coupling constants and the chemical shieldings will provide systematic information on the conformation and electronic state. The theoretical calculations of the electric field gradients of hydrogen-bonded carbonyl oxygen were successfully carried out by the MNDO-PM3 method. From these calculated results, it was found that the calculated e^2qQ/h value decreases with a decrease in the hydrogen bond length, and the chemical

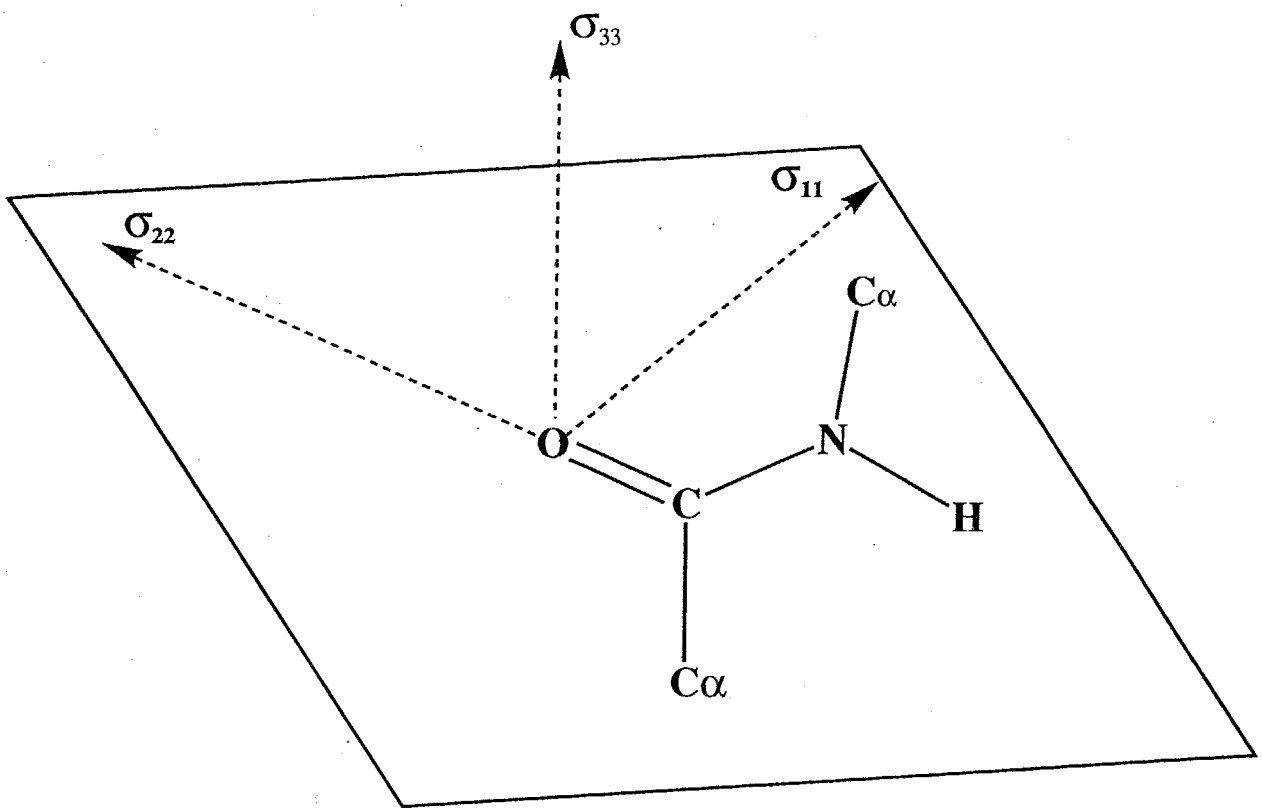

Fig.5.12 The direction of the principal axes of the chemical shielding of carbonyl oxygen employing FPT-MNDO-PM3 method.

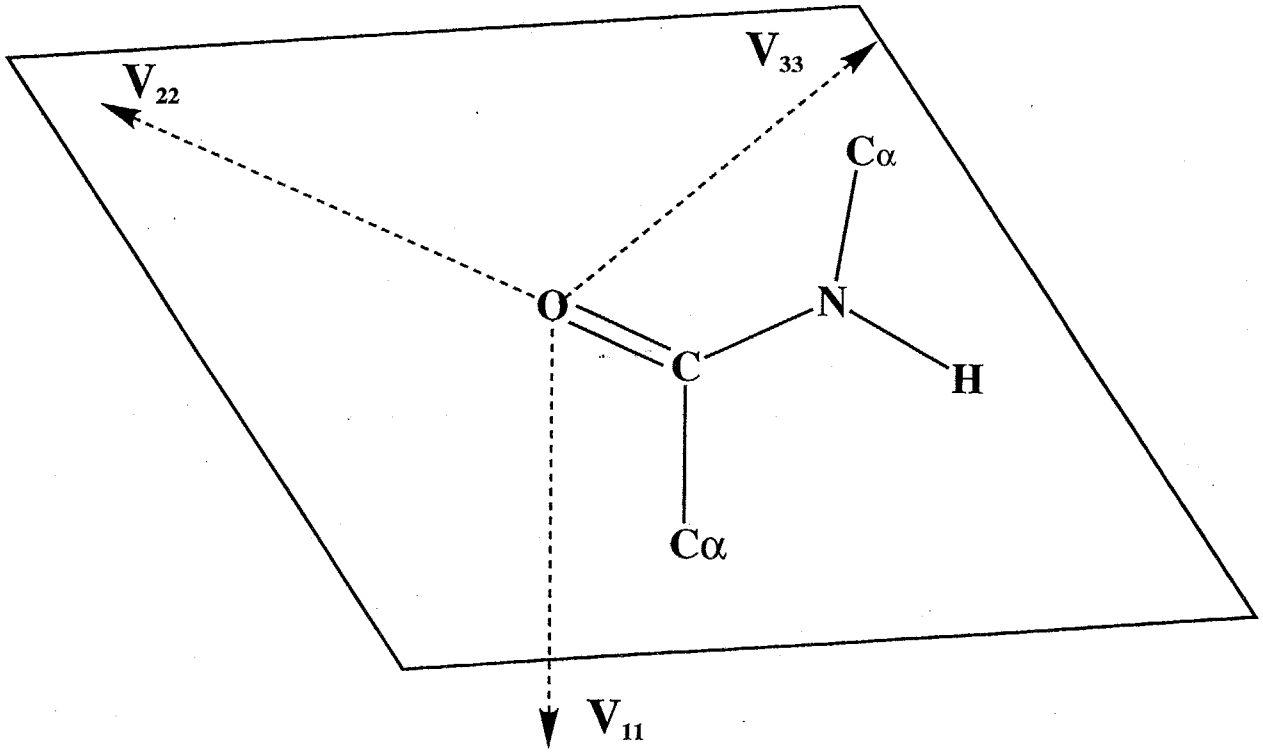

Fig.5.13 The direction of the principal axes of the electric field gradient tensor of carbonyl oxygen employing FPT-MNDO-PM3 method.

shielding values move upfield with a decrease in the hydrogen bond length. These calculations explain the experimental finding obtained in the preceding chapter. Further, the direction of the principal axes of the electric field gradient tensor and chemical shielding of the carbonyl oxygen were reasonably obtained by the FPT-MNDO-PM3 method.

References

1) E.A.C.Lucken, *Nuclear quadrupole coupling constants*. Academic press, London-New York, 1969.

2) E.Scrocco, *Advances chem. Physics* , **5** (1963) 318.

3) C.T.O'Konski, *Determination of organic structures by physical methods*, **Vol. 2**, Chap. 11. Academic Press, New York, 1962.

4) C.H.Townes and B.P.Dailey, *J.Chem.Physics*. **17** (1949) 782.

5) F.A.Cotton and C.B.Harris, *Proc.Nat.Acad.Sci.USA*, **56** (1966) 12.

6) E.A.C.Lucken, *Trans.Faraday Soc.*, **57** (1961) 729.

7) J.M.Sichel and M.A.Whitehead, *Thoret.chim.Acta (Berl)*, **11** (1968) 263.

8) N.F.Ramsey, *Phys.Rev.*, **78**(1950)699.

9) N.F.Ramsey, *Phys.Rev.,* **86** (1952) 213.

10) S.Ando, I.Ando, A.Shoji and T.Ozaki, *J.Am.Chem.Soc.*, **110** (1988) 3380.

11) N.Asakawa, S.Kuroki, H.Kurosu, I.Ando, A.Shoji and T.Ozaki, *J.Am.Chem.Soc.*, **114** (1192) 3261.

12) S.Kuroki, S.Ando, I.Ando, A.Shoji, T.Ozaki and G.A.Webb, *J.Mol.Struct.*, **240** (1990) 19.

13) S.Kuroki, S.Ando, I.Ando, A.Shoji and T.Ozaki, *J.Mol.Struct.*, **245** (1991) 69.

14) M.J.S.Dewar and W.Thiel, *J.Am.Chem. Soc.*, **99** (1977) 4899, 4907.

15) M.J.S.Dewar, E.G. Zoebisch, E.F.Healy and J.J.P.Stewart, *J.Am.Chem.Soc.*, **107** (1985) 3902

16) (a) J.J.P.Stewart, *J.Cpmput.Chem.*, **10** (1989) 209.

(b) J.J.P.Stewart, *J.Cpmput.Chem.*, **10** (1989) 221.

17) L.E.McMurchie and E.R.Davidson, *J.Cpmput.Phys.*, **26** (1978) 218.

18) S.Ando, Doctoral Thesis, Department of Polymer Chemistry, Tokyo Institute of Technology (1988)

19) W.Wu, X.You and A.Dai, *Scientia Sincia (Series B)*, **31** (1988) 1048.

20) P.Gerber, *Helv.Phys.Acta*, **45** (1972) 655.

21) B.Rosenblum and A.H.Nethercot, *J.Phys.Chem.*, **27** (1957) 828.

22) O.Lumpkin and W.T.Dixon, *Chem.Phys.Lett*, **62** (1979) 139.

23) S.G.P.Brosnan, D.T.Edmonds and I.J.F.Poplett, *J.Magn.Reson*, **45** (1981) 451.

24) W.H.Flygar and J.T.Lowe, *J.Chem.Phys.*, **45** (1965) 3645.
25) O.Lumpkin and W.T.Dixon, *J.Chem.Phys.*, **71** (1979) 3550.

Chapter 6
Summary

In this dissertation, I am concerned with two kinds of NMR observable nuclei such as ^{15}N and ^{17}O associated with hydrogen-bonding in peptides and polypeptides. Using these nuclei, NMR studies on hydrogen-bonding structure in solid peptides and polypeptides have been done. The following is noted in each chapter.

In Chapter 2, in order to obtain and accumulate further knowledge about the nature of the hydrogen-bonding in peptides, ^{15}N CP/MAS NMR spectra of oligopeptides containing glycine residue were measured in the solid state. Further, in order to clarify the origin of the relationship between the ^{15}N chemical shift and the manner of hydrogen bond, the ^{15}N shielding and tensor components of the glycine amide nitrogen were calculated by using quantum-chemical method. From these results, it was found that the observed ^{15}N chemical shifts of amide nitrogen move upfield linearly with a decrease in the N-H bond length associated with the hydrogen bond length, and quantum chemical calculations explain reasonably such experimental results. Further, it was demonstrated that the ^{15}N shielding is applicable as a means for obtaining direct information about the nature of hydrogen bond in the solid state, in addition to the ^{13}C shielding of the carbonyl carbon associated with hydrogen-bonding.

In Chapter 3, the isotropic ^{15}N chemical shifts and individual components of ^{15}N chemical shift tensors of the glycine residue (Gly) in a variety of oligopeptides with tert-buthyloxycarbonyl(Boc) group in the terminal were measured. On the basis of these results, the relationship between hydrogen bond length, and isotropic chemical shifts and individual components of chemical shift tensors was discussed.

Further, to do a deep insight into the experimental results, the ^{15}N shieldings were calculated by using quantum chemical method. From these results, it was found that the observed isotropic ^{15}N chemical shift moves downfield with a decrease in the hydrogen bond length and the principal value of the σ_{33} component moves linearly downfield with a decrease in the hydrogen bond length. The quantum chemical calculation explains reasonably these experimental results. Further, quantum calculations show that the σ_{11} and σ_{22} components are related to not only the hydrogen bond length, but also the hydrogen bond angle. From these results, it can be said that the ^{15}N chemical shift of amide nitrogen provides useful information about the hydrogen bond length and the hydrogen bond angle.

In Chapter 4, high-resolution ^{17}O NMR spectra of solid polyglycine(PG)I, PGII, glycylglycine(GlyGly) and glycylglycine nitrate (GlyGly•HNO_3) were measured, in order to obtain three kinds of NMR parameters such as chemical shift(δ), quadrupolar coupling constant(e^2qQ/h) and asymmetric parameter(η_Q), and to understand the relationship between these NMR parameters and the hydrogen-bonding structure. From these observed carbonyl ^{17}O NMR spectra, it is found that the e^2qQ/h values decrease linearly with a decrease in the hydrogen bond length. This indicates that it is possible to determine the hydrogen bond length through the observation of e^2qQ/h values. It was found that there is difference in η_Q between the polypeptides and peptides. This may come from large difference in molecular packing between them. The chemical shift values in peptides and in polypeptides move upfield with a decrease in the hydrogen bond length. However, there is difference in the chemical shift value between peptides and polypeptides. This may come from difference in molecular packing between them. From these experimental findings,

it was demonstrated that ^{17}O NMR spectroscopy becomes a useful mean for elucidating the hydrogen-bonding structure in solid peptides and polypeptides.

In Chapter 5, quantum-chemical approach of calculating the quadrupolar coupling constants and the chemical shieldings will provide systematic information on the conformation and electronic state. The theoretical calculations of the electric field gradients of hydrogen-bonded carbonyl oxygen were successfully carried out by the FPT-MNDO-PM3 method. From these calculated results, it was found that the calculated e^2qQ/h value decreases with a decrease in the hydrogen bond length, and the chemical shielding values move upfield with a decrease in the hydrogen bond length. These calculations explain the experimental finding obtained in the preceding chapter. Further, the directions of the principal axes of the electric field gradient tensor and chemical shielding of the carbonyl oxygen were reasonably obtained by the FPT-MNDO-PM3 method.

Summing up, it was concluded that ^{15}N and ^{17}O NMR spectroscopy combined with quantum chemical calculation is a useful means for elucidating the hydrogen-bonding structure in solid peptides and polypeptides.

Acknowledgment

I gratefully wish to express my thanks to Professor I.Ando for many helpful discussions, suggestions and encouragement throughout this work.

I wish to express my gratitude to Dr. S.Ando, NTT Interdisciplinary Research laboratories, for valuable advice to quantum chemical calculation.

I acknowledge Professors A.Shoji and T.Ozaki, Gunma University, for giving me same samples and measurement of NMR.

I would like to thank Professor G.A.Webb, Surrey University of England, for useful suggestion to nitrogen NMR study.

I would like to thank Dr.T.Shimizu, the National Research Institute for Metals High Field Magnet Laboratory for the use of the high resolution magnet system.

I wish to thank Akihiro Takahashi, master course student of T.I.T, for making the spectrum simulation program with me.

I am indebted to Kaoru Tsuchiya and Masatoshi Kobayashi, master course students of T.I.T, for their assistance in writing this dissertation.

My thanks are also due to the staffs of Ando's laboratory. Among them are Dr.H.Yoshimizu, Dr.H.Yasunaga, Dr.H.Kurosu, Naoki Asakawa and Chiyoko Watanabe.

Finally I express my sincere gratitude to my parents, Kimiko and Atsusi Kuroki, for their hearty encouragement and support.

February 16, 1994

Shigeki Kuroki

黒木重樹